UNIVERSITY OF CALIFORNIA, SAN DIEGO

INTEGRATION OF CARTILAGE AND BONE THORUGH A CALCIFIED CARTILAGE INTERFACE TO FORM A FUNCTIONAL OSTEOCHONDRAL GRAFT

A dissertation submitted in partial satisfaction of the

requirements for the degree Doctor of Philosophy

in

Bioengineering

by

Jennifer Hwang

Committee in charge:

Professor Robert L. Sah, Chair
Professor William D. Bugbee
Professor Karen L. Christman
Professor Paul A. Price
Professor Shyni Varghese

2010

ProQuest LLC
789 East Eisenhower Parkway
P.O. Box 1346
Ann Arbor, MI 48106-1346

The dissertation of Jennifer Hwang is approved, and it is acceptable in quality and form for publication on microfilm and electronically:

_____

_____

_____

_____

_____

_____

Chair

University of California, San Diego

2010

TABLE OF CONTENTS

Signature Page ..... **iii**

Table of Contents ..... **iv**

List of Figures ..... **viii**

List of Tables ..... **x**

Acknowledgments ..... **xi**

Vita ..... **xv**

Abstract of the Dissertation ..... **xvii**

Chapter 1: Introduction **1**

1.1 General Introduction to the Dissertation 1

1.2 Composition and Structure of Articular Cartilage 5

1.3 The Zone of Calcified Cartilage 7

1.4 Articular Cartilage Defect Repair 10

1.5 Graft Fixation in Articular Cartilage Defect Repair 12

1.6 Osteochondral Tissue Engineering 14

1.7 Cartilage-Bone Integration for Osteochondral Tissue Engineering 17

1.8 Cartilage Calcification for Osteochondral Tissue Engineering 19

1.9 Cartilage-Bone Integration in Defect Repair 21

1.10 Acknowledgments 22

1.11 References 23

Chapter 2: Increased Hydraulic Conductance of Human Articular Cartilage and Subchondral Bone Plate with Progression of Osteoarthritis 31

2.1 Abstract 31

2.2 Introduction 33

2.3 Materials and Methods 37

2.4 Results 43

2.5 Discussion 49

2.6 Acknowledgments 59

2.7 References 60

Chapter 3: In Vitro Calcification of Immature Bovine Articular Cartilage: Formation of a Functional Zone of Calcified Cartilage 64

3.1 Abstract 64

3.2 Introduction 66

3.3 Materials and Methods 70

3.4 Results 75

3.5 Discussion 86

3.6 Acknowledgments 91

3.7 References 92

Chapter 4: Fetuin-Mediated *In Vitro* Calcification of Adult Bovine Articular Cartilage 96

4.1 Abstract 96

4.2 Introduction 98

4.3 Materials and Methods 102

4.4 Results 113

4.5 Discussion 126

4.6 Acknowledgments 132

4.7 References 133

Chapter 5: Fetuin-Mediated Calcification for Integration of Articular Cartilage to Bone to form a Functional Osteochondral Graft 137

5.1 Abstract 137

5.2 Introduction 139

5.3 Materials and Methods 143

5.4 Results 150

5.5 Discussion 161

5.6 Acknowledgments 165

5.7 References 166

Chapter 6: Conclusions 169

6.1 Summary of Findings 169

6.2 Discussion 172

6.3 Future Work 176

6.4 References 179

LIST OF FIGURES

Figure 1.1: Articular cartilage zonal composition and structure 6

Figure 1.2: The zone of calcified cartilage 9

Figure 1.3: Cartilage defects and treatments 13

Figure 1.4: Strategies in osteochondral tissue engineering 16

Figure 2.1: Schematic diagram of perfusion test setup and hydraulic conductance of osteochondral tissue and ScBP 42

Figure 2.2: Normal, partially eroded, or fully eroded osteochondral samples with or without articular cartilage removal 46

Figure 2.3: Typical vascular canals in normal ScBP, partially eroded ScBP, and fully eroded ScBP 47

Figure 2.4: Stereological measurements of subchondral bone plate structure 48

Figure 2.5: Schematic of osteochondral tissue and potential deleterious effects of increased ScBP permeability leading to increased fluid loss 55

Figure 3.1: Sample harvest for AC and GPC explants and experimental design 72

Figure 3.2: Macroscopic and microscopic views of AC and GPC 78

Figure 3.3: Deep region of AC, epiphyseal end of GPC, and metaphyseal end of GPC after incubation with 10 mM β-glycerophosphate 79

Figure 3.4: Indentation stiffness and $^{45}Ca^{++}$ uptake by AC and GPC 80

Figure 3.5: Equilibrium modulus, $^{45}Ca^{++}$ uptake, and biochemical content for AC and GPC 84

Figure 3.S1: Deep region of AC, epiphyseal end of GPC, and metaphyseal end of GPC at time of harvest 85

Figure 4.1: Schematic of model setup for mass transfer analysis of cartilage calcification 108

Figure 4.2: Calcium supernatant concentration for different starting concentrations without or with fetuin 114

Figure 4.3: Macroscopic staining of calcification on cartilage quarter-disks by Alizarin Red S 116

Figure 4.4: Alizarin Red histological staining of cartilage for calcium before and after calcification culture without and with fetuin..... 117

Figure 4.5: Calcium and GAG released and retained within cartilage samples as a function of starting ion concentrations and addition of fetuin 119

Figure 4.6: Toluidine Blue histological staining of cartilage for proteoglycan before and after calcification culture without and with fetuin..... 120

Figure 4.7: Live/Dead images of cartilage disk cross-sections after incubation in media without or with fetuin at different calcium and phosphate starting concentrations..... 122

Figure 4.8: Percentage cell viability in cartilage samples as a function of media starting concentration, fetuin and tissue region..... 123

Figure 4.9: Mass transfer simulation results for calcium concentration in supernatant and calcified cartilage thickness with time..... 125

Figure 5.1: Schematic of experimental methods and cartilage analysis..... 149

Figure 5.2: Average load-displacement curves from lap shear testing 151

Figure 5.3: Adhesive integrative strength of osteochondral constructs and calcium content of the cartilage component..... 152

Figure 5.4: MicroCT vertical cross-sections of intact osteochondral constructs and interface 155

Figure 5.5: Alizarin Red S staining for calcium on fractured cartilage surface..... 156

Figure 5.6: Histological staining of cartilage for calcification..... 158

Figure 5.7: Histological staining of cartilage with Toluidine Blue..... 159

Figure 5.8: Live/Dead of cartilage after composite culture..... 160

LIST OF TABLES

Table 2.1: Hydraulic permeability (k_p) (mm^2/[MPa·second]) of articular cartilage and subchondral bone plate 53

Table 3.1: Indentation stiffness and equilibrium modulus of AC and GPC, fresh and after 3 weeks of culture without or with β−glycerophosphate 83

Table 4.1: Experimental design with different media concentrations of calcium chloride and sodium phosphate, without or with addition of fetuin 104

Table 4.2: Key variables and parameters in the mass transfer analysis 109

Table 5.1: Experimental design with varying cartilage viability, maturity, trypsin digestion time, and media components 144

ACKNOWLEDGMENTS

There are many individuals whose support throughout the years has been invaluable to the completion of this thesis. To these people, I would like to express my deep gratitude and appreciation.

First and foremost, I would like to thank my advisor Dr. Robert Sah for his constant guidance and tireless efforts in pushing me to think critically and grow as a scientific researcher, and to communicate clearly (both in writing and through the use of schematic diagrams). It has been a privilege to be trained as a bioengineer by Dr. Sah, and I am certain that the skills and knowledge I have learned will be invaluable throughout my career and future endeavors.

I would also like to thank the members of my thesis committee, Dr. William Bugbee, Dr. Paul Price, Dr. Shyni Varghese, and Dr. Karen Christman. Dr. Bugbee provided helpful insight on clinical needs for cartilage and osteochondral defect repair. Dr. Price shared his expertise on calcification and provided input on experimental plans and methods instrumental to the work in Chapters 4 and 5.

I would like to acknowledge the funding sources that have made this work possible. The National Science Foundation Graduate Research Fellowship Program supported me through the first 3 years of my graduate studies, for which I am thankful. I would also like to acknowledge support from the National Institute of Health, Musculoskeletal Transplant Foundation, and Howard Hughes Medical Institute through the Professors Program Grant to UCSD for Dr. Robert L Sah.

I would like to acknowledge Touch Briefings, Inc. for permission to reprint Chapter 1, in part, from *US Musculoskeletal Review*. For their contributions, I would like to thank co-authors Simon Görtz, Dr. Robert Sah, and Dr. William Bugbee.

I would like to acknowledge John Wiley and Sons, Inc. for permission to reprint, in full, Chapter 2 which has been published in *Arthritis and Rheumatism*. For their contributions to Chapter 2, I would like to thank co-authors Dr. Won Bae, Wendy Shieu, Dr. Chad Lewis, Dr. William Bugbee and Dr. Robert Sah.

I would like to acknowledge SAGE Publications, Inc. for permission to reprint, in full, Chapter 3 which has been published OnlineFirst in *Cartilage*. For their contributions to Chapter 3, I would like to thank co-authors Espoir Kyubwa, Dr. Won Bae, Dr. William Bugbee, Dr. Koichi Masuda, and Dr. Robert Sah.

In addition, Chapters 4 and 5 are in preparation for submission. I would like to thank co-authors Andrea Pallante, Dr. Paul Price, and Dr. Robert Sah for their contributions to the work described in Chapter 4. I would also like to thank co-authors Esther Cory, Dr. Paul Price and Dr. Robert Sah for their contributions to the work described in Chapter 5.

I never cease to be amazed by how smoothly the CTE Lab runs, which would not be possible without the CTE staff and project scientists. The lab intranet site built and maintained by lab manager Van Wong is one the most organized and comprehensive sources of information I have used, and ever growing in functionality. I would like to thank Dr. Michele Temple-Wong and Dr. Albert Chen, who have provided invaluable training on biochemistry assays and mechanical testing of cartilage. I'd also like to thank Barb Schumacher for her help with histological techniques and for her support, scientific and otherwise. Finally, I'd like to thank

Johnny Du for dealing with all the behind-the-scenes work and for always providing snacks.

I would like to thank my mentors from my early days in the CTE lab, who introduced me to the world of cartilage research. Dr. Travis Klein was busy finishing his thesis as I was starting in the lab, but he still graciously took the time to mentor me in a tissue engineering rotation project that encouraged me to join the lab. Dr. Won Bae and Dr. Chad Lewis helped introduce me to working at the interface of cartilage and bone. Without their expertise and training me in 3-D imaging and perfusion testing techniques, this thesis might have turned out very differently.

During my time in the CTE lab, I have also had the opportunity to mentor several undergraduate and Master's students: Wendy Shieu, Espoir Kyubwa, and Jérôme Hollenstein. Wendy was my first undergraduate researcher and was a great help in the perfusion experiments. Espoir and Jérôme have stayed on as Master's and Ph.D. students, and together we make up the "osteochondral team." It has been a joy and a privilege to transition from teaching them to the role of working with them and learning from them as they develop their own thesis projects. I have truly appreciated their help and friendship, and I look forward to great things from them in the future.

The past and present graduate students of the CTE Lab are a group that I am proud and humbled to be a part of. To the older CTE grad student alumni, Drs. Tannin Schmidt, Kyle Jadin, Gayle Nugent-Derfus, Ken Gratz, Megan Blewis, and Nancy Hsieh-Bonassera, thank you for your inspiration and advice, and for all the good stories of past antics inside and outside of the lab. To the graduate student alumni near my time, Drs. Ben Wong and Greg Williams, you were my go-to's for all my little questions about statistics and lab work, so thank you for all your help in lab, but more than that, thanks for all the great times hanging out as friends. To Jennifer Antonacci,

who started in the lab with me and has become a close friend, thank you for helping to keep me sane with coffee breaks, campus runs, and other fun times. To the current graduate students, Eun Hee Han, Hoa Nguyen, Andrea Pallante, Bill McCarty, Elaine Chan, Brad Hansen, Alex Hui, Murray Grissom, and Felix Hsu, it has been a great experience working with you and getting to know you. Thank you for your friendship and conversations over happy hours, in the office pod, and in lab at really random times late at night and on weekends.

To my parents, Dr. Cherngye and Meiyun Hwang, thank you for giving me the freedom to study whatever I wanted, for trusting me to make the right decisions, and for always encouraging and supporting me in whatever path I chose. Any success I have is due in large part to you and the values you taught me. To my sister Geraldine, thank-you for being the best little sister ever! I can't wait to see what places you go and things you do.

I would especially like to thank my close friends, Monica Mo, Wen-Lin Tsai, Esther Chu, and Tanya Chu for being constant sources of support and encouragement. Thank you for always believing in me and keeping me going. I cherish our talks over coffee, over brunches, and over the phone. Most of all, thank you for giving me perspective on life and for keeping me sane, especially during the past 6 years.

Finally, I would like to thank my fiancé, Menzies Chen, whose unconditional love, encouragement, and humor has carried me through graduate school and especially through the last 3 months of this work. Without you, this dissertation would not have been possible. I am so lucky to have a partner in all aspects of life, and I can't wait to be your wife.

VITA

2004	B.S., Bioengineering University of California, Berkeley, Berkeley, California
2004-2010	Graduate Student Researcher Cartilage Tissue Engineering Laboratory University of California, San Diego, La Jolla, California
2007	M.S., Bioengineering University of California, San Diego, La Jolla, California
2010	Ph.D., Bioengineering University of California, San Diego, La Jolla, California

Journal Articles

Hwang J, Kyubwa EM, Bae WC, Bugbee WD, Masuda K, Sah RL. *In vitro* calcification of immature bovine cartilage: formation of a functional zone of calcified cartilage. *Cartilage* doi: 10.1177/1947603510369552 (published 10 May 2010).

Hwang J, Bae WC, Shieu W, Lewis CW, Bugbee WD, Sah RL. Increased hydraulic conductance of human articular cartilage and subchondral bone plate with progression of osteoarthritis. *Arthritis Rheum* 58:3831-42, 2008.

Hwang J, Gortz S, Sah RL, Bugbee WD. Osteochondral graft transfer – techniques, outcomes, and the future. *US Musculoskeletal Review* 3:75-80, 2009.

Bae WC, Wong VW, Hwang J, Antonacci JM, Nugent-Derfus GE, Blewis ME, Temple-Wong MM, Sah RL. Wear-lines and split-lines of human patellar cartilage: relation to tensile biomechanical properties. *Osteoarthritis Cartilage* 16:841-5, 2008.

Selected Abstracts

Kyubwa EM, Hwang J, Chen AC, Sah RL. Maturation-associated increase in intrinsic fracture toughness of the osteochondral interface. *Trans Orthop Res Soc*. 35:1727, 2010.

Hwang J, Kyubwa EM, Bae WC, Bugbee WD, Masuda K, Sah RL. *In vitro* calcification of immature cartilage: formation of a functional zone of calcified cartilage. *Trans Orthop Res Soc.* 34:1304, 2009.

Hwang J, Kyubwa EM, Bae WC, Bugbee WD, Masuda K, Sah RL. *In vitro* calcification of immature cartilage to form a functional zone of calcified cartilage. *Trans Tiss Eng Regen Med Intnl Soc North America*, 2008.

Hwang J, Bae WC, Shieu W, Lewis CW, Bugbee WD, Sah RL. Changes in hydraulic conductance of human subchondral bone plate with progression of osteoarthritis. *Trans Orthop Res Soc* 32:48, 2007.

Bae WC, Wong VW, Antonacci JM, Hwang J, Nugent-Derfus GE, Blewis ME, Temple-Wong MM, Sah RL. Biomechanical effects of splitlines and wear patterns in human patellar cartilage. *Trans Orthop Res Soc* 32:93, 2007.

Chawla K, Jadin KD, Schumacher BL, Han EH, Hwang J, Huynh NT, Bae WC, Lewis CL, Kitahara S, Masuda K, Sah RL. Stratification of cartilaginous tissue implants with labeled chondrocyte subpopulations: effects on early in vivo repair of articular defects. *Trans Orthop Res Soc* 31: 47, 2006.

ABSTRACT OF THE DISSERTATION

INTEGRATION OF CARTILAGE AND BONE
THROUGH A CALCIFIED CARTILAGE INTERFACE
TO FORM A FUNCTIONAL OSTEOCHONDRAL GRAFT

by

Jennifer Hwang

Doctor of Philosophy in Bioengineering
University of California, San Diego, 2010
Professor Robert L. Sah, Chair

Articular cartilage is a load-bearing tissue covering the ends of long bones that normally allows for painless motion of joints. Adult articular cartilage has limited capacity for self-repair when injured. Current surgical treatments for cartilage defects include the transplantation of fresh osteochondral tissue from autologous or allogeneic sources to restore the architecture and characteristics of native tissue at the defect site. Such treatments have a successful clinical history but are limited by tissue availability. Osteochondral tissue engineering aims to fabricate osteochondral grafts *in vitro* but faces the challenge of integrating the cartilaginous and osseous layers to form a mechanically functional unit. The native osteochondral interface consists of a zone of

calcified cartilage (ZCC) that anchors articular cartilage to subchondral bone through an interdigitated zone of intermediate stiffness. Thus, the overall goal of this dissertation was to form a functional osteochondral tissue graft *in vitro* by integrating articular cartilage to bone through a biomimetic transitional zone of calcified cartilage.

The ZCC at the human osteochondral interface was found to have increased hydraulic conductance, or ease of fluid transport, and undergo changes in thickness and vascularity with increasing stages of osteoarthritis, suggesting that the ZCC is a zone of active tissue remodeling during cartilage repair. Cartilage explants were used to investigate conditions for *in vitro* calcification of cartilage and the resulting functional biomechanical consequences of matrix calcification. The *in vitro* calcification of immature articular cartilage in medium supplemented with β-glycerophosphate was dependent on cell viability and occurred only in the deep zone, resulting in a local increase in mechanical stiffness. Calcification of mature cartilage occurred within 3 days in medium with supersaturated calcium and phosphate and was dependent on supplementation with fetuin, an abundant serum protein. Cartilage explants cultured atop devitalized bone underwent fetuin-mediated calcification in the zone adjacent to bone, thereby attaching cartilage to bone through a calcified cartilage interface and achieving integration strengths similar to that of native immature osteochondral tissue.

These studies demonstrate that calcification can be used to integrate cartilage and bone to form a mechanically functional osteochondral graft. Such methods can be useful to provide biological fixation of cartilaginous grafts to bone for the formation of osteochondral grafts suitable for the treatment of large defects or ultimately, for resurfacing damaged or osteoarthritic joints.

CHAPTER 1

INTRODUCTION

1.1 General Introduction to the Dissertation

Articular cartilage has limited capacity for self repair. Focal defects are common and often symptomatic, and if left untreated, can increase in size, leading to cartilage degeneration and wear, and progressing to osteoarthritis [76]. Surgical treatments for cartilage defects currently in common use include marrow stimulation techniques such as microfracture, autologous chondrocyte implantation, and osteochondral grafting using autologous or allogeneic tissue. Osteochondral grafting has a long and successful clinical history as a means of cartilage resurfacing and is the only current treatment that reintroduces structurally and functionally mature osteochondral tissue for the repair of articular cartilage defects.

Osteochondral tissue engineering has the potential to overcome current sourcing limitations of osteochondral grafts by fabricating engineered osteochondral grafts *in vitro* with structural and functional properties suitable for surgical transplantation and cartilage defect repair. The fabrication of engineered osteochondral grafts involves creating a composite graft with distinct but integrated cartilaginous and osseous components. Assembly of cartilaginous and osseous components into a single functionally integrated unit usually involves initial

mechanical fixation, followed by a period of biological remodeling to enhance integration. In native osteochondral tissue, the zone of calcified cartilage at the cartilage-bone interface anchors articular cartilage to subchondral bone through interdigitation at the cement line interface and facilitates load transfer between cartilage and bone [61, 65]. The intermediate stiffness of the ZCC may serve to reduce stress concentrations and resist fracture that would otherwise occur at the osteochondral interface due to the discontinuity in material stiffness of cartilage and bone. Including such a specialized interface structure as the ZCC between cartilage and bone layers of an engineered osteochondral graft may be important in forming a structurally and functionally mature osteochondral graft.

Thus, the overall goal of this dissertation was to form a functional osteochondral tissue graft with a biomimetic transitional zone of calcified cartilage at the interface of cartilage and bone, and thereby further the understanding of the function of a specialized ZCC interface structure in native and engineered osteochondral tissues. To achieve this, (1) fluid transport through osteochondral tissue and the ZCC structure were measured in normal and osteoarthritic human osteochondral tissue, (2) zonal variations in the *in vitro* calcification of immature bovine articular cartilage and resulting tissue stiffness were assessed, (3) *in vitro* biochemical calcification of mature bovine articular cartilage using fetuin and supersaturated concentrations of calcium and phosphate was assessed, and (4) local calcification of cartilage at the interface with bone was used to integrate cartilage and bone to form a functional osteochondral graft.

This chapter starts with a review of articular cartilage, the zone of calcified cartilage and current repair strategies for cartilage defects. The use of osteochondral grafts and advances in osteochondral tissue engineering are discussed, with a focus on

methods for cartilage calcification and the integration of cartilage and bone for osteochondral interface engineering.

Chapter 2, which is published in *Arthritis and Rheumatism* [36], describes the increase in hydraulic conductance, or ease of fluid flow, through human osteochondral tissue and subchondral bone plate with increasing stages of osteoarthritic erosion. Osteochondral cores from tissue donors with macroscopically normal appearance and cores from osteoarthritis patients with partial-thickness or full-thickness erosion to bone were perfusion-tested to determine the hydraulic conductance in their native state and after removal of uncalcified cartilage. Osteochondral tissue samples were analyzed by 3-D histology for ZCC and subchondral bone thickness and vascular canal density, as possible structural determinants of hydraulic conductance.

Chapter 3, which is in press in *Cartilage* [37], describes zonal variations in the *in vitro* calcification of immature bovine articular cartilage and the increase in tissue stiffness associated with calcification. Immature bovine articular cartilage and growth plate cartilage were harvested in strips preserving the full thickness and incubated up to 3 weeks in medium supplemented with β-glycerophosphate (β-GP) as a phosphate source. The effects of culture duration, cell viability, and β-GP on calcium accumulation, indentation stiffness, and compressive modulus of immature bovine articular cartilage and growth plate cartilage were determined.

Chapter 4 examines the *in vitro* calcification of mature bovine articular cartilage using medium boosted with calcium and phosphate and supplemented with fetuin, an abundant serum protein. Mature bovine articular cartilage disks were depleted of proteoglycan by enzymatic digestion and incubated in media with or without fetuin, boosted with various calcium chloride and sodium phosphate up to 10 mM each. After 3 days, cartilage disks were analyzed for cell viability, calcium

content and distribution of bound calcium in the cartilage by histology. A mass transfer model was developed to describe the thickness of the calcified zone formed as a function of time and of solution calcium concentration.

Chapter 5 evaluates whether local calcification of cartilage to form an engineered zone of calcified cartilage at the interface with bone can form an osteochondral graft with integration strength similar to native tissue. Immature and mature articular cartilage disks with proteoglycan depleted from the deep surface were cultured in apposition with devitalized trabecular bone. Intermittent compressive loading was applied and samples were incubated in control media or in calcifying media with or without fetuin. Resulting osteochondral composites were tested by lap-shear to measure integration strength, and post-failure cartilage was analyzed for tissue calcification.

Chapter 6 summarizes the findings of this dissertation and discusses future directions for this work.

1.2 Composition and Structure of Articular Cartilage

Articular cartilage is a connective tissue covering the ends of long bones that provides a low-friction, wear-resistant surface for smooth articulation and sustains compressive and shear loads in the joint. Cartilage is comprised of sparsely distributed cells, called chondrocytes, in a fluid-filled extracellular matrix. While fluid accounts for 65-80% of cartilage wet weight, the main components of the cartilage solid matrix are proteoglycans and collagen [12, 54]. Proteoglycans have a high density of negatively charged sulfated glycosaminoglycans which can generate high osmotic pressure to resist compressive loads [68]. The collagen network constrains the swelling pressure of the proteoglycans and provides tensile strength to the cartilage tissue [53]. The balance of proteoglycan and collagen, as well as the interaction between the fluid and solid components of cartilage, together provide the load-bearing function of articular cartilage [60].

Cartilage has a zonal structure, with varying cellular and matrix composition and organization with increasing depth from the articular surface. Cartilage can be divided into superficial, middle, and deep zones [34, 39]. The cell density is highest in the superficial zone and decreases with depth from the articular surface [68]. At the surface, chondrocytes are arranged in clusters, while in the deeper zones, chondrocytes are organized in columns [34, 39]. Proteoglycan content increases with depth from the articular surface, with a corresponding increase in compressive stiffness with depth [15, 54]. Collagen fibrils are oriented parallel to the cartilage at the surface, transition to an oblique orientation through the middle zone, and become perpendicular to the surface in the deep zone [17, 73]. The zonal variations in composition and structure result in the depth-dependent mechanical properties of cartilage.

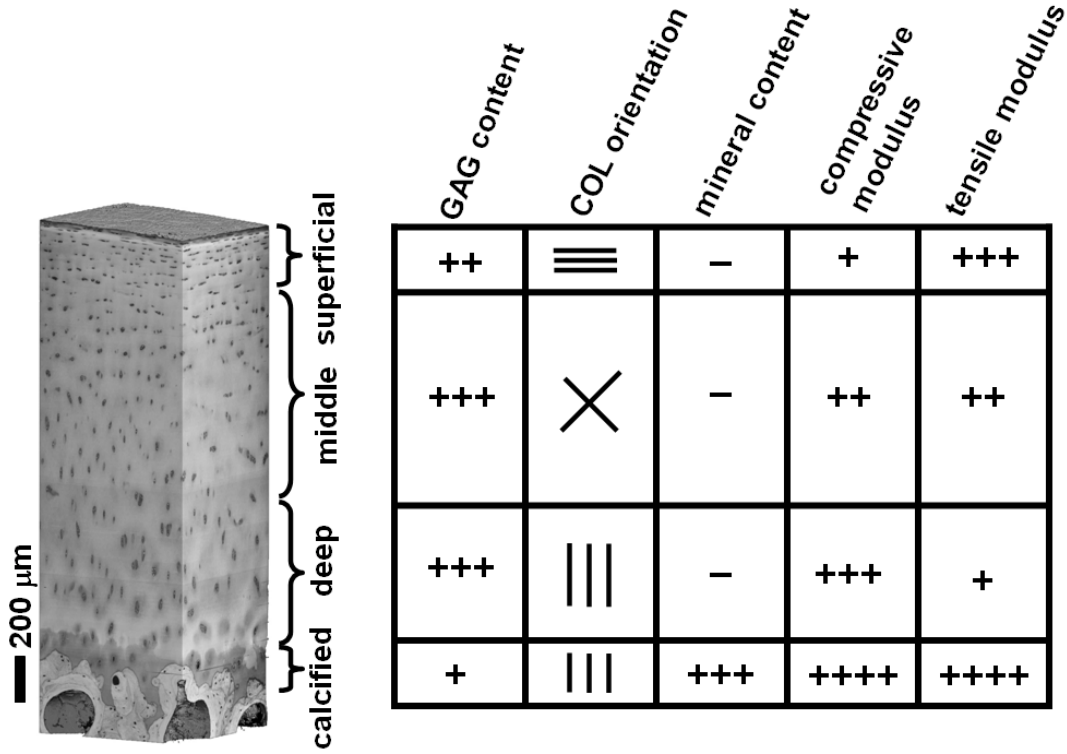

Figure 1.1: Articular cartilage zonal composition and structure. Cartilage can be divided into superficial, middle, deep, and calcified zones, which vary in cell and matrix organization and give rise to depth-dependent mechanical properties. Adapted from [4].

1.3 The Zone of Calcified Cartilage

Between normal articular cartilage and subchondral bone is the zone of calcified cartilage (ZCC), a mineralized transition zone with a thickness of 100-300μm [65]. The ZCC is bordered on one side by the tidemark, the gently undulating interface with uncalcified cartilage, and on the other side by the cement line, the highly interdigitated interface with bone. The ZCC is comprised of sparsely distributed chondrocytes expressing the hypertrophic phenotype, which are aligned in columns and enveloped in a calcified hyaline cartilage matrix [35, 49]. The hypertrophic chondrocytes secrete matrix vesicles, alkaline phosphatase and collagen X and are responsible for mineralizing the extracellular matrix [22, 34, 49]. The extracellular matrix of the ZCC contains collagen types II and X, proteoglycan, and carbonated hydroxyapatite. Collagen fibers in the ZCC are oriented perpendicular to the articular surface, with collagen II fibers crossing the tidemark but no fibers crossing the cement line interface [32, 69]. This disruption of fibers at the cement line suggests that cartilage and bone are attached only by mechanical interlocking due to interdigitation of the ZCC and bone [65]. Proteoglycan content in the ZCC matrix is ~50% lower than that of the uncalcified cartilage matrix [65]. Hydroxyapatite mineral is present continuously throughout the ZCC matrix with only small unmineralized regions around the cell columns [11, 73]. The ZCC contains carbonated hydroxyapatite crystals of similar size to those in bone, as well as similar mineral content, but is less stiff due to collagen-mineral packing structure different from that of bone [21, 27].

The ZCC serves the mechanical functions of anchoring articular cartilage to subchondral bone through interdigitation at the cement line interface and facilitating load transfer between cartilage and bone [61, 65]. The intermediate stiffness of the ZCC may serve to reduce stress concentrations that would otherwise occur at the

osteochondral interface due to the discontinuity in material stiffness of cartilage and bone [3, 61]. At the tidemark, the undulating geometric pattern and the collagen II fibrils crossing the interface may provide some resistance to shear loads [69]. High levels of shear stress occurring at the tidemark and cement line interfaces with joint loading are implicated in joint failure during fracture in the osteochondral region [10, 59]. In mature adult osteochondral tissue, delamination of cartilage tends to occur along the tidemark interface [59], while in adolescent osteochondral tissue without a well-defined ZCC, fracture tends to occur along an irregular plane in the region of the cement line and subchondral bone [57, 70]. The mature osteochondral junction is more able to resist the propagation of a crack and has a higher fracture toughness than immature tissue [10], suggesting that the ZCC structure at the osteochondral interface helps to resist crack propagation.

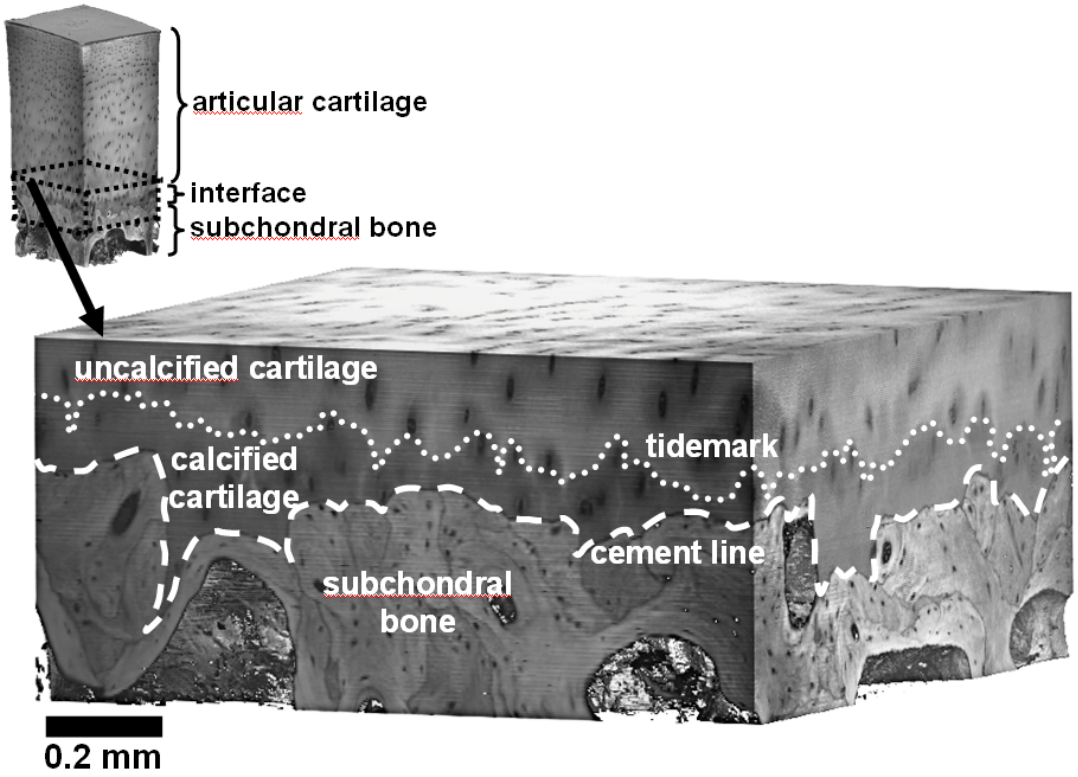

Figure 1.2: The zone of calcified cartilage provides attachment of articular cartilage to subchondral bone through interdigitation at the cement line interface. Adapted from [48]

1.4 Articular Cartilage Defect Repair

Articular cartilage has limited capacity for self repair. Defects in cartilage are common and often symptomatic. Arthroscopic studies of patients with symptomatic knees found that 19% had focal defects with areas ranging from <1 to 4 cm^2 [18, 31]. If left untreated, focal cartilage defects generally increase in size [16, 38, 87], contributing to exacerbation of symptoms and potentially leading to osteoarthritis [76]. Although the treatment threshold for surgical intervention varies, patients with symptomatic defects are generally considered for cartilage repair procedures. Surgical treatments for cartilage defects currently in common use include marrow stimulation techniques such as microfracture, autologous chondrocyte implantation and its variations, and osteochondral grafting using autologous or allogeneic tissue.

Microfracture involves creating perforations in the subchondral bone plate to induce bleeding and provide access of bone marrow to the defect [79]. This procedure is commonly considered as an initial treatment option due to its technical simplicity and short-term effectiveness [24]. However, it is limited to small, contained cartilage defects and generally results in fibrocartilaginous repair [25] with inferior biomechanical properties and wear characteristics compared to those of hyaline cartilage [50].

Autologous chondrocyte implantation (ACI) involves taking a biopsy from a non-weight bearing region of the patient's knee, isolating and expanding the chondrocytes in number, and implanting those chondrocytes into the defect under a periosteal patch [9]. Results from ACI have shown the presence of a hyaline-like repair tissue [66], although recent studies have not demonstrated a clear benefit of ACI over microfracture, based on functional outcomes and quality of repair tissue [45, 46]. Furthermore, complications from donor site morbidity and hypertrophy or

delamination of the periosteal patch can necessitate an additional operation in ~15% of patients [29, 30]. Variations on ACI include matrix-assisted ACI (MACI), in which the cultured chondrocytes are seeded in an artificial scaffold prior to implantation [6].

Transplantation of fresh osteochondral grafts involves transplanting structurally intact osteochondral tissue from autologous or allogeneic sources to restore the architecture and characteristics of native tissue at the defect site [7, 19]. Autologous osteochondral grafts are obtained from non-weight bearing regions of the patient's knee, while allogeneic grafts are obtained from knees of tissue donors in regions identical to the defect site. The chondrocytes within the cartilage of the graft are viable and functional, while the graft bone is eventually replaced by the patient's bone by creeping substitution [13]. Autologous osteochondral graft sources are advantageous due to immediate availability and nonantigenicity but are self-limited by lack of donor volume of suitable tissue quality [8]. Allogeneic osteochondral graft sources are advantageous for addressing large or multiple defects with a single graft that reproduces the joint anatomy, but are limited by scarcity of donor tissue and procurement issues [5].

1.5 Graft Fixation in Articular Cartilage Defect Repair

Early complications after implantation of chondrocytes or cartilaginous grafts often result from insufficient graft fixation to underlying bone or adjacent cartilage. Detachment and delamination of the periosteal patch occur in 5-7% of patients undergoing ACI [67]. Detachment of MACI grafts fixed to defects with fibrin glue occurred in 2 out of 16 cases in a clinical study [52]. Partial or complete delamination of grafts may cause locking or catching of the knee, leading to poor clinical outcomes and requiring graft retrieval [63]. Delamination of grafts may be due to graft adherence that is low compared to the detachment forces associated with joint articulation [20].

Graft fixation techniques vary depending on the type and biomechanical properties of the implant. In ACI, a flap harvested from the periosteum is sutured to the adjacent cartilage rim and sealed with fibrin glue to form a leakproof compartment for the cell suspension [9]. Scaffold-based cartilaginous grafts may be fixed to the defect through press-fit, fibrin glue, sutures to adjacent cartilage, or transosseous sutures to adjacent bone [44]. Gel-like cartilaginous grafts have also been press-fit into the defect [62]. Osteochondral grafts are stabilized by interference fit with host bone or by pins or screws, and subsequent osseous healing [75, 90].

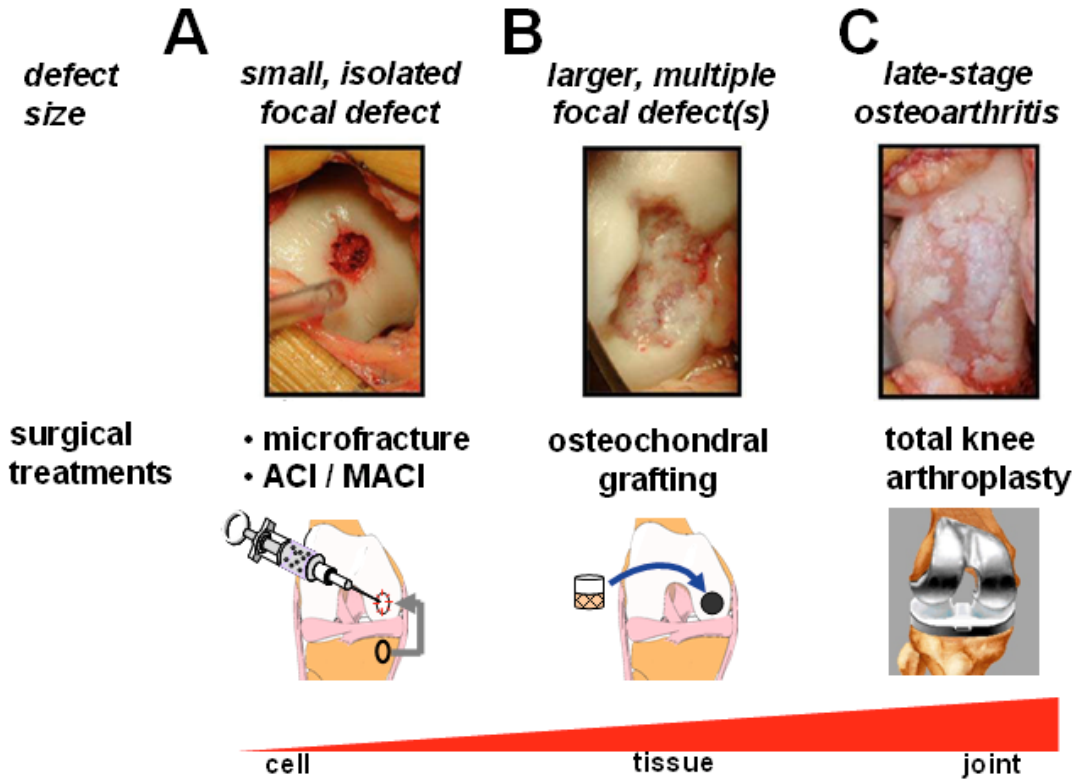

Figure 1.3: Cartilage defects and treatments. Surgical treatments vary depending on defect size. (**A**) Small isolated focal defects can be treated with microfracture or autologous chondrocyte implantation (ACI) while (**B**) large defects can be treated with osteochondral grafting (**C**) At late-stage osteoarthritis, the only surgical option for joint resurfacing is a total knee arthroplasty. Adapted from [89].

1.6 Osteochondral Tissue Engineering

Tissue engineering aims to create biological tissue substitutes that can restore, maintain, or improve the original tissue function [47]. Osteochondral tissue engineering aims to create engineered osteochondral grafts (eOCGs) with structural, functional, and remodeling properties suitable for surgical transplantation for cartilage and osteochondral defect repair, which can restore the normal biomechanical environment of the joint [58]. Like native osteochondral grafts, eOCGs would provide immediate load-bearing and structural support at the defect site, as well as long-term remodeling and regeneration, including integration at the graft-host bone and cartilage interfaces. In addition, eOCGs could be fabricated with anatomical size and shape to treat irregular, uncontained defects covering large areas of the joint to serve as a biological joint replacement.

The fabrication of eOCGs by osteochondral tissue engineering involves combining cells and scaffolds to create a composite graft with distinct but integrated cartilaginous and osseous components. Approaches to the fabrication of eOCGs can be distinguished by variations in cell source(s) and scaffold material(s) and design, as well as by different strategies for the assembly of cartilaginous and osseous components into a single unit [26, 51, 55]. Desirable features of cell sources for osteochondral tissue engineering include high proliferative capacity *ex vivo* for producing large numbers of cells, phenotypic stability for maintaining distinct cartilage and bone regions, and non-immunogenicity. Cell sources include autologous or allogeneic chondrocytes, mesenchymal stem cells, periosteal cells, or cell-free, which can be used alone or in combination for the cartilaginous and osseous layers [1, 23, 33, 42, 72, 77, 83, 84, 86]. Desirable features of material scaffolds for osteochondral tissue engineering are sufficient porosity for transport of nutrients and

waste, appropriate mechanical properties for load-bearing, non-toxicity, and non-immunogenicity. Scaffold materials used for eOCGs include natural polymers, such as collagen, alginate, agarose, and fibrin, synthetic polymers such as PEG, PLGA, and other variations, ceramics such as hydroxyapatite and other calcium phosphates, devitalized bone, and others [23, 33, 41, 56, 71].

Scaffold materials and design are often chosen to mimic the natural architecture and mechanical properties of their target tissue, such that they can differentially support formation of cartilage and bone in distinct but integrated layers. This has resulted in a trend in osteochondral tissue engineering of moving from single-phase homogenous scaffolds into biphasic scaffolds with different material types, porosities, and pore architectures. Examples of common differential features of biphasic scaffolds include using a larger pore size in the bone region (greater than 300 μm) to enhance vascularization [43] and a smaller pore size (less than 200 μm) for the cartilaginous portion [14, 58] as well as mineralization of the region intended for bone formation [28, 80], with the osteochondral interface consisting of either a gradual or abrupt change in these features. Alternatively, distinct scaffold types can be used for cartilaginous and osseous components [23, 33, 72], or a scaffold-free cartilaginous tissue can be used [42, 84, 86]. For these approaches, the method of integration between the cartilage and bone layers is a key design issue.

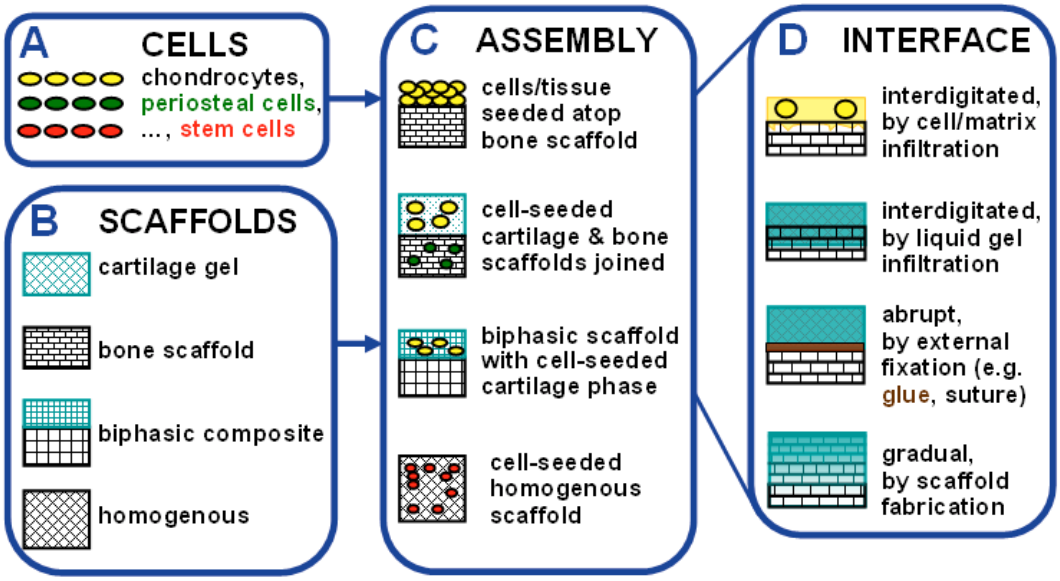

Figure 1.4: Strategies in osteochondral tissue engineering involve the combination of (**A**) different cell types with (**B**) different scaffolds, which can be (**C**) assembled in a number of ways to create a composite structure of cartilage and bone tissue, which may be (**D**) integrated through different types of interface structures.

1.7 Cartilage-Bone Integration for Osteochondral Tissue Engineering

Cartilage-bone integration is critical to the function of an engineered ostoechondral graft, particularly for withstanding the shear forces of joint articulation after graft implantation. In addition to sufficient initial fixation strength, it is important for the bonding between the cartilaginous and osseous layers of the graft to allow for biological remodeling to provide long-term integration *in vivo* at the osteochondral interface. Assembly of the cartilaginous and osseous components of an engineered osteochondral graft into a single functionally integrated unit often involves initial mechanical fixation followed by biological remodeling. Initial fixation may be attained through sutures [72], adhesives such as fibrin glue [23, 74], novel bioadhesives that bridge tissues with covalent chemical bonds [85], or mechanical interlocking such as that formed by hydrogel penetration into a porous substrate [14, 33, 40]. Alternatively, cells have been seeded directly onto a porous substrate without any additional mechanical fixation [84]. Following initial assembly, the composite may be cultured *in vitro* to enhance biologically-mediated fixation between the cartilaginous and osseous components. Such processes depend on factors including the maturity of cartilaginous tissue, transport properties of the osseous component, and the duration of composite culture [72, 82].

Integration between cartilaginous and osseous components has been measured structurally using percentage length interface in apposition [72], and functionally using tests of adhesive strength. Such mechanical tests include a push-out test, which measures the force required for a plunger to push a disk out from inside an annulus [64], and a peel-off test, which measures the force required to peel the cartilaginous layer off of the bone, in a configuration where the bony layer is fixed in place and the

cartilaginous layer is grasped at the edge and pulled perpendicular to the interface [74, 82].

Successful outcomes for osteochondral integration are often attributed to infiltration of chondrocytes and secretion of extracellular matrix into the osseous substrate to form a transition zone of apposed or interdigitated cartilaginous and osseous tissues. Immature cartilaginous constructs showed better integration with adjacent cartilage or bone compared to mature cartilaginous constructs or native cartilage [64, 72]. Integration by immature cartilaginous constructs occurred through cell proliferation and formation of new cartilaginous tissue at the interface, as opposed to mature cartilaginous constructs and native cartilage which integrated through secretion of extracellular matrix molecules [64, 74]. Osteochondral integration may also be improved by increasing transport properties through the osseous component to allow greater infiltration by cartilaginous tissue. Devitalized native bone showed better osteochondral integration than vital bone when cultured adjacent to cartilaginous constructs, which was attributed to the higher diffusivity of molecules in the devitalized bone structure [82].

1.8 Cartilage Calcification for Osteochondral Tissue Engineering

Calcification of cartilage at the interface between cartilage and bone in engineered osteochondral grafts mimics native osteochondral tissue by forming a transitional zone of calcified cartilage with intermediate stiffness. This may serve a similar mechanical function as the native ZCC of preventing high shear stresses at the interface between the cartilaginous and bony phases, and thereby improve the interfacial shear properties of the graft. Strategies used for the formation of a calcified cartilage transition zone *in vitro* have included using cell-mediated calcification, scaffold design, or a combination.

Cell-mediated calcification to form a zone of calcified cartilaginous tissue has been investigated using deep zone chondrocytes seeded atop a calcium polyphosphate bone substrate and incubated in medium with β-glycerophosphate (β-GP) as a phosphate source [2]. The mineral formed within the cartilaginous tissue was poorly crystalline hydroxyapatite, similar to the mineral in native ZCC, but the zone of calcification occurred slightly above the cartilaginous-bony interface, due to the inhibitory effects of the bone substrate degradation products on calcification [78]. Calcification of the cartilaginous tissue near the osteochondral interface resulted in modest increases in shear stiffness (a 3-fold increase to 12 N/mm) and peak load (2-fold increase to 2.2 N), compared to tissues incubated without β-GP [2]. Shear failure occurred at the cartilaginous-bony interface.

Scaffold-based designs to form a ZCC typically involve incorporating an interface phase between the cartilaginous and osseous layers, with an intermediate amount of mineralization and structural pre-integration between the cartilaginous and osseous scaffolds [28, 40, 80]. The structural pre-integration can be formed by an infiltration-based approach, in which the cartilaginous scaffold in liquid precursor

phase is solidified while partially impregnated into a solid osseous phase [40]. Alternatively, there is a liquid phase co-synthesis method, in which an unmineralized scaffold precursor suspension and a mineralized scaffold precursor suspension are diffused into each other while both still in liquid phase, and then freeze dried to make a multi-layered scaffold with an intermediate, interdigitated zone with a tidemark-like structure. Such osteochondral constructs have been demonstrated to withstand repeated compressive loads without interfacial delamination, but shear interfacial strength has not been measured [28].

Scaffold-based designs for ZCC formation have been demonstrated to support new cartilaginous and bone tissue formation while keeping cartilaginous and osseous tissue formation confined to their respective compartments [80]. It is foreseeable that scaffold-based and cell-mediated strategies for ZCC formation could be used in concert, such that a pre-integrated biphasic scaffold could help withstand implantation and early loading, while remodeling for long-term function could be facilitated by cells at the interface responding to the mineralized microenvironment and calcifying the matrix to form an engineered zone of calcified cartilage at the osteochondral interface.

1.9 Cartilage-Bone Integration in Defect Repair

After implantation of an eOCG into an osteochondral defect *in vivo*, the integrative remodeling of graft-host cartilage and bone interfaces are important for healing and long-term function of the graft. *In vivo* outcomes in animal models for eOCGs show encouraging results for osteochondral integration during defect repair. Press-fitting the eOCG into an osteochondral defect generally results in good graft fixation through interlocking of the implant bone with the host bone. Structural integration between graft cartilaginous and osseous components is inconsistent but may occur *in vivo* as early as 2-3 months post-implantation, either in an interdigitated structure formed through chondrocyte infiltration into an osseous substrate [88], or in an undulating structure resembling an immature tidemark between cartilaginous and osseous tissues [71, 81]. Further studies in load-bearing joints are needed to investigate the formation or maintenance *in vivo* of an engineered ZCC within an eOCG.

1.10 Acknowledgments

We would like to thank co-authors Dr. Simon Görtz, Dr. Robert L. Sah, and Dr. William D. Bugbee for their contributions to this work. We would also like to acknowledge Touch Briefings, Inc. for permission to reprint Chapter 1, in part, from *US Musculoskeletal Review*. This work was supported by the National Institute of Health and the Howard Hughes Medical Institute through the Professors Program Grant to UCSD for Dr. Robert L. Sah.

1.11 References

1. Alhadlaq A, Elisseeff JH, Hong L, Williams CG, Caplan AI, Sharma B, Kopher RA, Tomkoria S, Lennon DP, Lopez A, Mao JJ: Adult stem cell driven genesis of human-shaped articular condyle. *Ann Biomed Eng* 32:911-23, 2004.

2. Allan KS, Pilliar RM, Wang J, Grynpas MD, Kandel RA: Formation of biphasic constructs containing cartilage with a calcified zone interface. *Tissue Eng* 13:167-77, 2007.

3. Anderson DD, Brown TD, Radin EL: The influence of basal cartilage calcification on dynamic juxtaarticular stress transmission. *Clin Orthop Rel Res* 286:298-307, 1993.

4. Bae WC. Indentation testing of articular cartilage: biomechanics and efficacy [PhD Thesis]. La Jolla: University of California, San Diego; 2004.

5. Ball ST, Amiel D, Williams SK, Tontz W, Chen AC, Sah RL, Bugbee WD: The effects of storage media on fresh human osteochondral allografts. *Clin Orthop Relat Res* 418:246-52, 2004.

6. Bartlett W, Flanagan AM, Gooding CR, Skinner JA, Carrington RW, Briggs TW, Bentley G: Autologous chondrocyte implantation versus matrix-induced autologous chondrocyte implantation for osteochondral defects of the knee: A prospective, randomised study. *J Bone Joint Surg Br* 87:640-5, 2005.

7. Bobic V: Current methods of treating articular cartilage defects in the knee: an update on arthroscopic osteochondral autograft transplantation. *Arthroscopy* S10:14, 1998.

8. Bobic V, Morgan CD, Schmieding R, Burkhart SS: Method and apparatus for osteochondral autograft transplantation885,752, July 6 1999, 1999.

9. Brittberg M, Lindahl A, Nilsson A, Ohlsson C, Isaksson O, Peterson L: Treatment of deep cartilage defects in the knee with autologous chondrocyte transplantation. *N Engl J Med* 331:889-95, 1994.

10. Broom ND, Oloyede A, Flachsmann R, Hows M: Dynamic fracture characteristics of the osteochondral junction undergoing shear deformation. *Med Eng Phys* 18:396-404, 1996.

11. Brown RA, Blunn GW, Salisbury JR, Byers PD: Two patterns of calcification in primary (physeal) and secondary (epiphyseal) growth cartilage. *Clin Orthop Relat Res* 294:318-24, 1993.

12. Buckwalter JA, Mankin HJ: Articular cartilage. Part I: tissue design and chondrocyte-matrix interactions. *J Bone Joint Surg Am* 79-A:600-11, 1997.
13. Bugbee WD: Fresh osteochondral allografts. *J Knee Surg* 15:191-5, 2002.

14. Chang CH, Lin FH, Lin CC, Chou CH, Liu HC: Cartilage tissue engineering on the surface of a novel gelatin-calcium-phosphate biphasic scaffold in a double-chamber bioreactor. *J Biomed Mater Res B Appl Biomater* 71B:313-21, 2004.

15. Chen AC, Bae WC, Schinagl RM, Sah RL: Depth- and strain-dependent mechanical and electromechanical properties of full-thickness bovine articular cartilage in confined compression. *J Biomech* 34:1-12, 2001.

16. Cicuttini F, Ding C, Wluka A, Davis S, Ebeling PR, Jones G: Association of cartilage defects with loss of knee cartilage in healthy, middle-age adults: a prospective study. *Arthritis Rheum* 52:2033-9, 2005.

17. Clark JM: Variation of collagen fiber alignment in a joint surface: a scanning electron microscope study of the tibial plateau in dog, rabbit, and man. *J Orthop Res* 9:246-57, 1991.

18. Curl WW, Krome J, Gordon ES, Rushing J, Smith BP, Poehling GG: Cartilage injuries: a review of 31,516 knee arthroscopies. *Arthroscopy* 13:456-60, 1997.

19. Czitrom AA, Langer F, McKee N, Gross AE: Bone and cartilage allotransplantation. A review of 14 years of research and clinical studies. *Clin Orthop Relat Res*:141-5, 1986.

20. Driesang IM, Hunziker EB: Delamination rates of tissue flaps used in articular cartilage repair. *J Orthop Res* 18:909-11, 2001.

21. Ferguson VL, Bushby AJ, Boyde A: Nanomechanical properties and mineral concentration in articular calcified cartilage and subchondral bone. *J Anat* 203:191-202, 2003.

22. Gannon JM, Walker G, Fischer M, Carpenter R, Thompson RC, Jr., Oegema TR, Jr.: Localization of type X collagen in canine growth plate and adult canine articular cartilage. *J Orthop Res* 9:485-94, 1991.

23. Gao J, Dennis JE, Solchaga LA, Awadallah AS, Goldberg VM, Caplan AI: Tissue-engineered fabrication of an osteochondral composite graft using rat bone marrow-derived mesenchymal stem cells. *Tissue Eng* 7:363-71, 2001.

24. Gill TJ: The treatment of articular cartilage defects using microfracture and debridement. *Am J Knee Surg* 13:33-40, 2000.

25. Gill TJ, McCulloch PC, Glasson SS, Blanchet T, Morris EA: Chondral defect repair after the microfracture procedure. *Am J Sports Med* 33:680-5, 2005.
26. Grayson WL, Chao PH, Marolt D, Kaplan DL, Vunjak-Novakovic G: Engineering custom-designed osteochondral tissue grafts. *Trends Biotechnol* 26:181-9, 2008.

27. Gupta HS, Schratter S, Tesch W, Roschger P, Berzlanovich A, Schoeberl T, Klaushofer K, Fratzl P: Two different correlations between nanoindentation modulus and mineral content in the bone-cartilage interface. *J Struct Biol* 149:138-48, 2005.

28. Harley BA, Lynn AK, Wissner-Gross Z, Bonfield W, Yannas IV, Gibson LJ: Design of a multiphase osteochondral scaffold III: Fabrication of layered scaffolds with continuous interfaces. *J Biomed Mater Res A* 92:1078-93, 2010.

29. Henderson I, Gui J, Lavigne P: Autologous chondrocyte implantation: natural history of postimplantation periosteal hypertrophy and effects of repair-site debridement on outcome. *Arthroscopy* 22:1318-24 e1, 2006.

30. Henderson I, Tuy B, Oakes B: Reoperation after autologous chondrocyte implantation. Indications and findings. *J Bone Joint Surg Br* 86:205-11, 2004.

31. Hjelle K, Solheim E, Strand T, Muri R, Brittberg M: Articular cartilage defects in 1,000 knee arthroscopies. *Arthroscopy* 18:730-4, 2002.

32. Hough AJ, Banfield WG, Mottram FC, Sokoloff L: The osteochondral junction of mammalian joints. An ultrastructural and microanalytic study. *Lab Invest* 31:685-95, 1974.

33. Hung CT, Lima EG, Mauck RL, Taki E, LeRoux MA, Lu HH, Stark RG, Guo XE, Ateshian GA: Anatomically shaped osteochondral constructs for articular cartilage repair. *J Biomech* 36:1853-64, 2003.

34. Hunziker EB: Articular cartilage structure in humans and experimental animals. In: *Articular Cartilage and Osteoarthritis,* ed. by KE Kuettner, Schleyerbach R, Peyron JG, Hascall VC, Raven Press, New York, 1992, 183-99.

35. Hunziker EB, Quinn TM, Hauselmann HJ: Quantitative structural organization of normal adult human articular cartilage. *Osteoarthritis Cartilage* 10:564-72, 2002.

36. Hwang J, Bae WC, Shieu W, Lewis CW, Bugbee WD, Sah RL: Increased hydraulic conductance of human articular cartilage and subchondral bone plate with progression of osteoarthritis. *Arthritis Rheum* 58:3831-42, 2008.

37. Hwang J, Kyubwa EM, Bae WC, Bugbee WD, Masuda K, Sah RL: *In vitro* calcification of immature bovine articular cartilage: formation of a functional zone of calcified cartilage. *Cartilage*, 2010.

38. Jackson DW, Lalor PA, Aberman HM, Simon TM: Spontaneous repair of full-thickness defects of articular cartilage in a goat model. A preliminary study. *J Bone Joint Surg Am* 83-A:53-64, 2001.

39. Jadin KD, Wong BL, Bae WC, Li KW, Williamson AK, Schumacher BL, Price JH, Sah RL: Depth-varying density and organization of chondrocyte in immature and mature bovine articular cartilage assessed by 3-D imaging and analysis. *J Histochem Cytochem* 53:1109-19, 2005.

40. Jiang J, Tang A, Ateshian GA, Guo XE, Hung CT, Lu HH: Bioactive Stratified Polymer Ceramic-Hydrogel Scaffold for Integrative Osteochondral Repair. *Ann Biomed Eng*, 2010.

41. Kandel RA, Boyle J, Gibson G, Cruz T, Speagle M: In vitro formation of mineralized cartilagenous tissue by articular chondrocytes. *In Vitro Cell Dev Biol Anim* 33:174-81, 1997.

42. Kandel RA, Grynpas M, Pilliar R, Lee J, Wang J, Waldman S, Zalzal P, Hurtig M: Repair of osteochondral defects with biphasic cartilage-calcium polyphosphate constructs in a sheep model. *Biomaterials* 27:4120-31, 2006.

43. Karageorgiou V, Kaplan D: Porosity of 3D biomaterial scaffolds and osteogenesis. *Biomaterials* 26:5474-91, 2005.

44. Knecht S, Erggelet C, Endres M, Sittinger M, Kaps C, Stussi E: Mechanical testing of fixation techniques for scaffold-based tissue-engineered grafts. *J Biomed Mater Res B Appl Biomater* 83:50-7, 2007.

45. Knutsen G, Drogset JO, Engebretsen L, Grontvedt T, Isaksen V, Ludvigsen TC, Roberts S, Solheim E, Strand T, Johansen O: A randomized trial comparing autologous chondrocyte implantation with microfracture. Findings at five years. *J Bone Joint Surg Am* 89:2105-12, 2007.

46. Knutsen G, Engebretsen L, Ludvigsen TC, Drogset JO, Grontvedt T, Solheim E, Strand T, Roberts S, Isaksen V, Johansen O: Autologous chondrocyte implantation compared with microfracture in the knee. A randomized trial. *J Bone Joint Surg Am* 86-A:455-64, 2004.

47. Langer R, Vacanti JP: Tissue engineering. *Science* 260:920-6, 1993.

48. Lewis CW, Jadin KM, Wheeler JM, Bae WC, Sah RL: 3D morphology of adult human calcified cartilage. *Trans Orthop Res Soc,* 30:1466, 2005.

49. Lovell T, Eyre D: Unique biochemical characteristics of the calcified cartilage zone of articular cartilage. *Trans Orthop Res Soc,* Atlanta, GA, 1988.

50. Mandelbaum BR, Browne JE, Fu F, Micheli L, Mosely JB, Jr., Erggelet C, Minas T, Peterson L: Articular cartilage lesions of the knee. *Am J Sports Med* 26:853-61, 1998.

51. Mano JF, Reis RL: Osteochondral defects: present situation and tissue engineering approaches. *J Tissue Eng Regen Med* 1:261-73, 2007.

52. Marlovits S, Striessnig G, Kutscha-Lissberg F, Resinger C, Aldrian SM, Vecsei V, Trattnig S: Early postoperative adherence of matrix-induced autologous chondrocyte implantation for the treatment of full-thickness cartilage defects of the femoral condyle. *Knee Surg Sports Traumatol Arthrosc* 13:451-7, 2005.

53. Maroudas A: Balance between swelling pressure and collagen tension in normal and degenerate cartilage. *Nature* 260:808-9, 1976.

54. Maroudas A: Physico-chemical properties of articular cartilage. In: *Adult Articular Cartilage,* ed. by MAR Freeman, Pitman Medical, Tunbridge Wells, England, 1979, 215-90.

55. Martin I, Miot S, Barbero A, Jakob M, Wendt D: Osteochondral tissue engineering. *J Biomech* 40:750-65, 2007.

56. Masuda K, Sah RL, Hejna MJ, Thonar EJ-MA: A novel two-step method for the formation of tissue-engineered cartilage by mature bovine chondrocytes: the alginate-recovered-chondrocyte (ARC) method. *J Orthop Res* 21:139-48, 2003.

57. Matthewson MH, Dandy DJ: Osteochondral fractures of the lateral femoral condyle. A result of indirect violence to the knee. *J Bone Joint Surg Br* 60-B:199-202, 1978.

58. McMahon LA, O'Brien FJ, Prendergast PJ: Biomechanics and mechanobiology in osteochondral tissues. *Regen Med* 3:743-59, 2008.

59. Meachim G, Bentley G: Horizontal splitting in patellar articular cartilage. *Arthritis Rheum* 21:669-74, 1978.

60. Mow VC, Ratcliffe A: Structure and function of articular cartilage and meniscus. In: *Basic Orthopaedic Biomechanics,* ed. by VC Mow, Hayes WC, Raven Press, New York, 1997, 113-78.

61. Muller-Gerbl M, Schulte E, Putz R: The thickness of the calcified layer of articular cartilage: a function of the load supported? *J Anat* 154:103-11, 1987.

62. Nehrer S, Domayer S, Dorotka R, Schatz K, Bindreiter U, Kotz R: Three-year clinical outcome after chondrocyte transplantation using a hyaluronan matrix for cartilage repair. *Eur J Radiol* 57:3-8, 2006.

63. Nehrer S, Spector M, Minas T: Histologic analysis of tissue after failed cartilage repair procedures. *Clin Orthop Rel Res* 365:149-62, 1999.

64. Obradovic B, Martin I, Padera RF, Treppo S, Freed LE, Vunjak-Novakovic G: Integration of engineered cartilage. *J Orthop Res* 19:1089-97, 2001.

65. Oegema T, Jr., Carpenter R, Hofmeister F, Thompson RC, Jr.: The interaction of the zone of calcified cartilage and subchondral bone in osteoarthritis. *Microsc Res Tech* 37:324-32, 1997.

66. Peterson L, Brittberg M, Kiviranta I, Akerlund EL, Lindahl A: Autologous chondrocyte transplantation. Biomechanics and long-term durability. *Am J Sports Med* 30:2-12, 2002.

67. Peterson L, Minas T, Brittberg M, Nilsson A, Sjogren-Jansson E, Lindahl A: Two- to 9-year outcome after autologous chondrocyte transplantation of the knee. *Clin Orthop Rel Res* 374:212-34, 2000.

68. Poole AR, Kojima T, Yasuda T, Mwale F, Kobayashi M, Laverty S: Composition and structure of articular cartilage: a template for tissue repair. *Clin Orthop Rel Res*:S26-33., 2001.

69. Redler I, Mow VC, Zimny ML, Mansell J: The ultrastructure and biomechanical significance of the tidemark of articular cartilage. *Clin Orthop Rel Res* 112:357-62, 1975.

70. Rosenberg NJ: Osteochondral fractures of the lateral femoral condyle. *J Bone Joint Surg Am* 46-A:1013-26, 1964.

71. Schaefer D, Martin I, Jundt G, Seidel J, Heberer M, Grodzinsky A, Bergin I, Vunjak-Novakovic G, Freed LE: Tissue-engineered composites for the repair of large osteochondral defects. *Arthritis Rheum* 46:2524-34, 2002.

72. Schaefer D, Martin I, Shastri P, Padera RF, Langer R, Freed LE, Vunjak-Novakovic G: In vitro generation of osteochondral composites. *Biomaterials* 21:2599-606, 2000.

73. Schenk RK, Eggli PS, Hunziker EB: Articular cartilage morphology. In: *Articular Cartilage Biochemistry,* ed. by K Kuettner, Schleyerbach R, Hascall VC, Raven Press, New York, 1986, 3-22.

74. Scotti C, Wirz D, Wolf F, Schaefer DJ, Burgin V, Daniels AU, Valderrabano V, Candrian C, Jakob M, Martin I, Barbero A: Engineering human cell-based, functionally integrated osteochondral grafts by biological bonding of engineered cartilage tissues to bony scaffolds. *Biomaterials* 31:2252-9, 2010.

75. Shasha N, Krywulak S, Backstein D, Pressman A, Gross AE: Long-term follow-up of fresh tibial osteochondral allografts for failed tibial plateau fractures. *J Bone Joint Surg Am* 85-A Suppl 2:33-9, 2003.

76. Shelbourne KD, Jari S, Gray T: Outcome of untreated traumatic articular cartilage defects of the knee: a natural history study. *J Bone Joint Surg Am* 85-A Suppl 2:8-16, 2003.

77. Sherwood J, Riley S, Palazzolo R, Brown S, Monkhouse D, Coates M, Griffith L, Landeen L, Ratcliffe A: A three-dimensional osteochondral composite scaffold for articular cartilage repair. *Biomaterials* 23:4739-51, 2002.

78. St-Pierre J-P, Pilliar RM, Grynpas MD, Kandel RA: Calcification of cartilage formed *in vitro* on calcium polyphosphate bone substitutes is regulated by inorganic polyphosphate. *Acta Biomater*, 2010.

79. Steadman JR, Rodkey WG, Rodrigo JJ: Microfracture: surgical technique and rehabilitation to treat chondral defects. *Clin Orthop Rel Res*:362-9, 2001.

80. Tampieri A, Sandri M, Landi E, Pressato D, Francioli S, Quarto R, Martin I: Design of graded biomimetic osteochondral composite scaffolds. *Biomaterials* 29:3539-46, 2008.

81. Tanaka T, Komaki H, Chazono M, Fujii K: Use of a biphasic graft constructed with chondrocytes overlying a beta-tricalcium phosphate block in the treatment of rabbit osteochondral defects. *Tissue Eng* 11:331-9, 2005.

82. Tognana E, Chen F, Padera RF, Leddy HA, Christensen SE, Guilak F, Vunjak-Novakovic G, Freed LE: Adjacent tissues (cartilage, bone) affect the functional integration of engineered calf cartilage in vitro. *Osteoarthritis Cartilage* 13:129-38, 2005.

83. Tuli R, Nandi S, Li WJ, Tuli S, Huang X, Manner PA, Laquerriere P, Noth U, Hall DJ, Tuan RS: Human Mesenchymal Progenitor Cell-Based Tissue Engineering of a Single-Unit Osteochondral Construct. *Tissue Eng* 10:1169-79, 2004.

84. Waldman SD, Grynpas MD, Pilliar RM, Kandel RA: Characterization of cartilagenous tissue formed on calcium polyphosphate substrates in vitro. *J Biomed Mater Res* 62:323-30, 2002.

85. Wang DA, Varghese S, Sharma B, Strehin I, Fermanian S, Gorham J, Fairbrother DH, Cascio B, Elisseeff JH: Multifunctional chondroitin sulphate for cartilage tissue-biomaterial integration. *Nat Mater* 6:385-92, 2007.

86. Wang X, Grogan SP, Rieser F, Winkelmann V, Maquet V, LaBerge M, Mainil-Varlet P: Tissue engineering of biphasic cartilage constructs using various biodegradable scaffolds: an in vitro study. *Biomaterials* 25:3681-8, 2004.

87. Wang Y, Ding C, Wluka AE, Davis S, Ebeling PR, Jones G, Cicuttini FM: Factors affecting progression of knee cartilage defects in normal subjects over 2 years. *Rheumatology (Oxford)* 45:79-84, 2006.

88. Weng Y, Cao Y, Silva CA, Vacanti MP, Vacanti CA: Tissue-engineered composites of bone and cartilage for mandible condylar reconstruction. *J Oral Maxillofac Surg* 59:185-90, 2001.

89. Williams GM, Chan EF, Temple-Wong MM, Bae WC, Masuda K, Bugbee WD, Sah RL: Shape, loading, and motion in the bioengineering design, fabrication, and testing of personalized synovial joints. *J Biomech* 43:156-65, 2010.

90. Williams SK, Amiel D, Ball ST, Allen RT, Tontz WL, Jr., Emmerson BC, Badlani NM, Emery SC, Haghighi P, Bugbee WD: Analysis of cartilage tissue on a cellular level in fresh osteochondral allograft retrievals. *Am J Sports Med* 35:2022-32, 2007.

CHAPTER 2

INCREASED HYDRAULIC CONDUCTANCE OF HUMAN ARTICULAR CARTILAGE AND SUBCHONDRAL BONE PLATE WITH PROGRESSION OF OSTEOARTHRITIS

2.1 Abstract

Objective: Osteoarthritis (OA) is characterized by progressive degeneration of articular cartilage and remodeling of the subchondral bone plate (ScBP), comprised of calcified cartilage (CC) and underlying subchondral bone (ScB). CC remodeling due to upward invasion by vascular canals or to CC erosion may contribute to biomechanical alteration of the osteochondral (OC) tissue and its ScBP component. The study hypothesis was that hydraulic conductance of OC tissue and ScBP increases with structural changes indicative of increasing stages of OA.

Methods: OC cores were harvested from knees of cadaveric tissue donors and from discarded fragments of OA knee surgery patients. Tissue donor cores were macroscopically normal, and OA cores had partial- or full-thickness erosion to bone. Cores were perfusion-tested to determine the hydraulic conductance, or ease of fluid

flow, in their native state and after enzymatic removal of cartilage. Adjacent portions were analyzed by 3-D histology for CC, ScB, and ScBP thickness and vascular canal density.

Results: The hydraulic conductances of native OC tissue and ScBP were higher (2700- and 3-fold) in fully eroded samples than normal samples. The CC layer was thicker (1.5-fold) in partially eroded samples than normal samples, but thinner and incomplete in fully eroded samples. ScBP vascularity was altered with increasing stages of OA.

Conclusion: During joint loading, increased hydraulic conductance of the OC tissue and ScBP could have deleterious biomechanical consequences for cartilage. Increased fluid exudation from overlying and opposing cartilage, increased fluid depressurization, and increased cartilage tissue strains could lead to chondrocyte death and cartilage damage.

2.2 Introduction

Articular cartilage is a low-friction, load-bearing material joined to the subchondral bone plate at the ends of long bones that form a synovial joint. During joint loading, pressurization of interstitial fluid within cartilage protects it from high compressive strains [32, 46]. The ability of cartilage to support load through interstitial fluid pressurization is dependent on its low hydraulic permeability. Hydraulic permeability describes the ease of fluid flow through a material, which for articular cartilage is governed by the extracellular matrix. Degenerative changes in cartilage that occur with osteoarthritis (OA) have been correlated with increased hydraulic permeability of cartilage [3, 7, 42]. However, hydraulic permeability has been determined only for cartilage slices separated from the subchondral bone, not for full-thickness osteochondral tissue. Although fluid transport and resistance to fluid flow through osteochondral tissue is normally governed by cartilage, the contribution of the subchondral bone plate (ScBP) boundary may become increasingly important as the cartilage is eroded with the progression of OA.

In OA, progressive degeneration of the articular cartilage matrix is associated with remodeling of the ScBP. While cartilage decreases in thickness and mechanical integrity with the progression of OA, subchondral bone increases in thickness and stiffness, undergoes accelerated turnover [8], and exhibits altered trabecular architecture [11, 22, 44] and cysts [25]. Although it is clear that progression of OA involves structural and mechanical changes in both cartilage and bone, it is unknown

if such changes are associated with altered fluid transport characteristics of the osteochondral tissue.

While the ease of fluid flow through cartilage is traditionally described by hydraulic permeability, it is useful to describe the ease of fluid flow through osteochondral tissue and ScBP by the related structural property of hydraulic conductance. Since hydraulic conductance describes flow through a structure rather than a material, it can be used to characterize ease of fluid flow through irregular structures, such as osteochondral tissue with cartilage erosion or the undulating CC layer of ScBP. Thus, the hydraulic conductance can include the contribution from ScBP in determining fluid flow through an osteochondral structure, including how that role may change with erosion of cartilage in OA.

Although hydraulic permeability has been measured for cartilage [30], cortical bone [21], and cancellous bone [38], the fluid transport properties of the zone of calcified cartilage (CC) at the osteochondral interface remain unknown. In studies of cartilage nutrition, the CC has been considered an impermeable barrier to material transport from the subchondral bone, particularly after maturation of the joint [31]. However, *in vivo* MRI studies have observed penetration by intravenous $Gd(DTPA)^{2-}$ across the osteochondral interface into the deep regions of human articular cartilage [6]. Furthermore, at the osteochondral interface of the intervertebral disc studied *ex vivo*, fluid flows between the marrow cavity and the cartilaginous disc through vascular channels [5]. This suggests that vascular channels in the ScBP may contribute to the fluid flow through, and hydraulic conductance of, the osteochondral interface.

The ScBP is the underlying support structure for articular cartilage in synovial joints. The ScBP begins at the tidemark, which separates uncalcified cartilage from CC, and consists of both the CC layer and the underlying subchondral bone (ScB). Calcified cartilage is composed of hypertrophic chondrocytes enveloped in a calcified matrix and is vascular [12, 13], whereas articular cartilage is normally avascular. The CC layer attaches cartilage to ScB [19, 39] and provides a transitional zone of intermediate stiffness, reducing stress concentrations at the cartilage-bone interface [34]. Below the calcified cartilage is the cement line or ossification front which marks the beginning of the porous and vascular ScB

The CC layer may play a critical role in OA pathogenesis by mediating interactions between cartilage and bone. Calcified cartilage becomes “activated” in OA, increasing in thickness with the formation of new zones of CC, duplications of the tidemark, and vascular invasion into the tidemark [15, 39, 40]. Vascular invasion in the initiation or development of OA has been speculated to occur through microcracks that extend between the bone marrow space and the CC after repeated physiological loading [36, 45]. The vascular canals in the CC may affect the fluid pressurization load-bearing behavior of the articular cartilage by affecting the hydraulic permeability of the underlying ScBP. Alteration of fluid flow across the cartilage-bone interface could affect the mechanical and chemical environment in ways that promote the progression of OA.

The hypothesis of this study was that the hydraulic conductance of osteochondral tissue and ScBP increases with structural changes indicative of increasing stages of OA. The objectives of this study were to determine, for the human

medial femoral condyle with different grades of OA erosion: [1] the hydraulic conductance for osteochondral tissue before and after removal of cartilage, and [2] the thickness and vascularity of the CC and ScBP, as possible structural determinants of hydraulic conductance of ScBP

2.3 Materials and Methods

Sample Harvest. Osteochondral cores (9mm diameter) were harvested from the medial femoral condyles of cadaveric tissue bank donors and discarded knee fragments from total knee replacement surgery patients with Institutional Review Board approval. Each core was obtained from a different donor, and adjacent osteochondral fragments were taken for histology. Tissue bank donor cores were macroscopically normal (n=12, age 24±3 years), and OA cores were graded by visual inspection as having partial erosion of cartilage (n=15, age 71±3 years) or full erosion of cartilage with exposure of bone (n=16, age 71±2 years).

Experimental Design. Cores from normal, partially eroded, and fully eroded ScBP were perfusion-tested first in the intact state at harvest and again after removal of cartilage by papain (Sigma-Aldrich, St Louis, MO). To prepare samples, an Isomet low-speed saw (Buehler, Lake Bluff, IL) was used to trim the bone side of cores to a ScBP thickness of 5mm, leaving the cartilage intact. Core diameter was measured with digital calipers, and all samples were perfusion-tested. Next, uncalcified cartilage was enzymatically removed from all cores by papain digestion (125 μg/mL papain, 0.005 *M* cysteine HCL, 0.1 *M* sodium phosphate, pH 6.2) at 60ºC for 18-24h [13]. Marrow was removed from papain-digested cores by incubation in an ultrasonic bath in saline for 2-5h followed by rinsing via perfusion of 50mL saline through the core in each direction. After rinsing, samples were perfusion-tested again. Additional 9mm-diameter cores (n=3) of normal and partially eroded ScBP were used to assess the effect of papain digestion on hydraulic conductance of bone. Uncalcified cartilage was

removed from these samples by mechanical debridement with a curette to isolate ScBP, followed by trimming and marrow removal. Samples were perfusion tested for hydraulic conductance, papain-digested, and retested.

Perfusion Testing. Darcy's Law was used to estimate the hydraulic conductance constant, c, using a least squares fit of linear fluid velocity, U, vs. pressure drop across the sample, ΔP. Darcy's Law describes how easily fluid flows through a porous solid and is expressed as:

$$\mathbf{U = \frac{Q}{A} = \frac{k_p \Delta P}{h} = c \Delta P} \quad (1)$$

where U is the linear flow rate, with dimensions of [m/s], Q is the volumetric flow rate, with dimensions of [m^3/s] and A is the sample cross-sectional area in the direction of flow, with dimensions of [m^2]. Ease of fluid flow through a structure can be described by c, the hydraulic conductance with dimensions of [m/(Pa·s)], or by k_p, the hydraulic permeability with dimensions of [m^2/(Pa·s)], and h, the sample thickness with dimensions of [m]. For ScBP, c was assessed because the undulating CC layer has an irregular thickness, making it difficult to identify a value for h to allow calculation of k_p. Thus, ease of fluid flow through samples was characterized as a hydraulic conductance constant for short-term perfusion, c^{2h} for OC samples and $c^{0.5h}$ for ScBP samples (representing equilibrium values).

Each sample was inserted into Tygon tubing (Cole-Parmer, Vernon Hills, IL), sealed circumferentially, and tested for hydraulic conductance (Figure 1A). Phosphate-buffered saline (PBS) was perfused through each sample at constant flow rates controlled by a syringe pump (Harvard PHD-2000; Harvard Apparatus,

Holliston, MA), and pressure drop across the sample was measured using a low-range pressure transducer (ΔP = 0-55 kPa) (Validyne DP-45, Validyne, Northridge, CA). Different flow rates were used for OC and ScBP cores to keep pressures within the range of the transducer. OC samples were perfused for 2h at flow rates, U, of 0.0013 mm/s and 0.0026 mm/s (or equivalent Q, 0.083 mm^3/s and 0.17 mm^3/s, normalized to A, 64 mm^2). ScBP samples were perfused for 0.5h at flow rates starting from 0.026 mm/s and increased in increments of 0.65 mm/s up to 3.9 mm/s. The pressure drop across the sample at each flow rate was measured, averaging readings over 5s at 2 Hz. Samples were tested both with flow outwards from the joint (from cartilage to bone) and inwards into the joint (from bone to cartilage). Conductance estimates from different flow directions were reproducible (-16% to +20%) and averaged for each sample. Conductance estimates were also reproducible within the same sample in repeated measurements. Thus, three trials per sample per flow direction were used to obtain a best-fit conductance estimate for each sample using a least squares analysis (typical $r^2 = 0.98$).

Histology. Osteochondral fragments were taken adjacent to each core site; one was left intact and the other was papain-digested along with the core. Paired samples were fixed in 4% paraformaldehyde in PBS, pH 7.4, 4˚C for 3 days and then decalcified in 15% EDTA, pH 8.5, 37˚C for 3 weeks. For 3D histology, samples (n = 3) were cut to ~3 mm^3 blocks and fluorescently stained with 0.1% Eosin-Y (pH 5.0) for 12-16h, embedded in Spurr resin, and imaged at $(2.24\ \mu m)^3$ voxel resolution with a Nikon (Tokyo, Japan) E600 fluorescence microscope [20]. Three-dimensional image datasets were visualized using RESView 3.0 software (Resolution Sciences Corporation, Corte

Madera, CA), and 2D cross-sections were exported for qualitative viewing and stereological analysis of structural features using Adobe Photoshop (Adobe Systems, Inc., San Jose, CA) and ImageJ (NIH, Bethesda, MD).

Stereological measurements. CC and ScB thickness: The thickness of the CC and ScB was measured by averaging individual thickness measurements from histological sections of a control tissue volume. Ten random 2D cross-sections uniformly spaced by 0.1 mm were exported for a volume of tissue $(1\ mm)^2 \times 2$ mm deep encompassing the osteochondral interface for each sample. On each vertical (1 mm × 2 mm) cross-section, a grid of 4 lines (each 0.2 mm apart) was overlaid on the image with the lines normal to the tissue surface. The thickness of the CC and ScB was measured along each of the 4 lines for a total of 40 individual measurements across all 10 cross-sections and averaged to produce one CC and one ScB thickness for each sample. The CC thickness was defined as the distance between the tidemark and the cement line, and the ScB thickness was defined as the distance between the cement line and the bottom edge of the cortical bone plate, or the boundary between the solid bone matrix and the large void space associated with trabecular bone porosity. ScBP thickness was the sum of the CC and ScB thicknesses. In OA partially eroded samples where multiple tidemarks were present, the CC thickness was measured between the lowest tidemark (closest to the bone) and the cement line. Vascular canal density: The number of vessels per cross-sectional area was counted within the same tissue volume used for the thickness measurements. Fifty vertical 2D sections (1 mm x 2 mm) uniformly spaced 0.02 mm apart were exported from the tissue volume. Vessels were defined as void space sheathed by bone that started from the subchondral bone space

and ended within the CC or beyond the CC into the cartilage deep zone (in partially eroded samples) or up to the bony ScBP surface (in fully eroded samples). Larger vessels appearing in multiple neighboring sections were counted only once.

Statistics. Data are presented as mean ± SEM. Conductance data were $\log_{10}$ transformed to improve homoscedasticity [18]. Log_{10} transformed data were confirmed to be normally distributed by the Anderson-Darling test ($P < 0.01$) [1]. To assess the effect of erosion and papain digestion on conductance, a repeated-measures ANOVA was used with a fixed factor of the degree of OA erosion (normal, partial, full) and with repeated measures for before and after digestion. Post-hoc comparisons were performed using unpaired t-tests between each group and its three relevant comparison groups (1 to compare before vs. after papain digestion, 2 to compare normal vs. partially eroded vs. fully eroded). For these t-tests, significance was adjusted ($P < 0.05 / 3$). To assess structural changes in thickness and vascularity, a repeated measures ANOVA was used with a fixed factor of the degree of OA erosion and with repeated measures for paired samples with and without papain digestion. Tukey post-hoc comparisons were used with $P < 0.05$ considered significant.

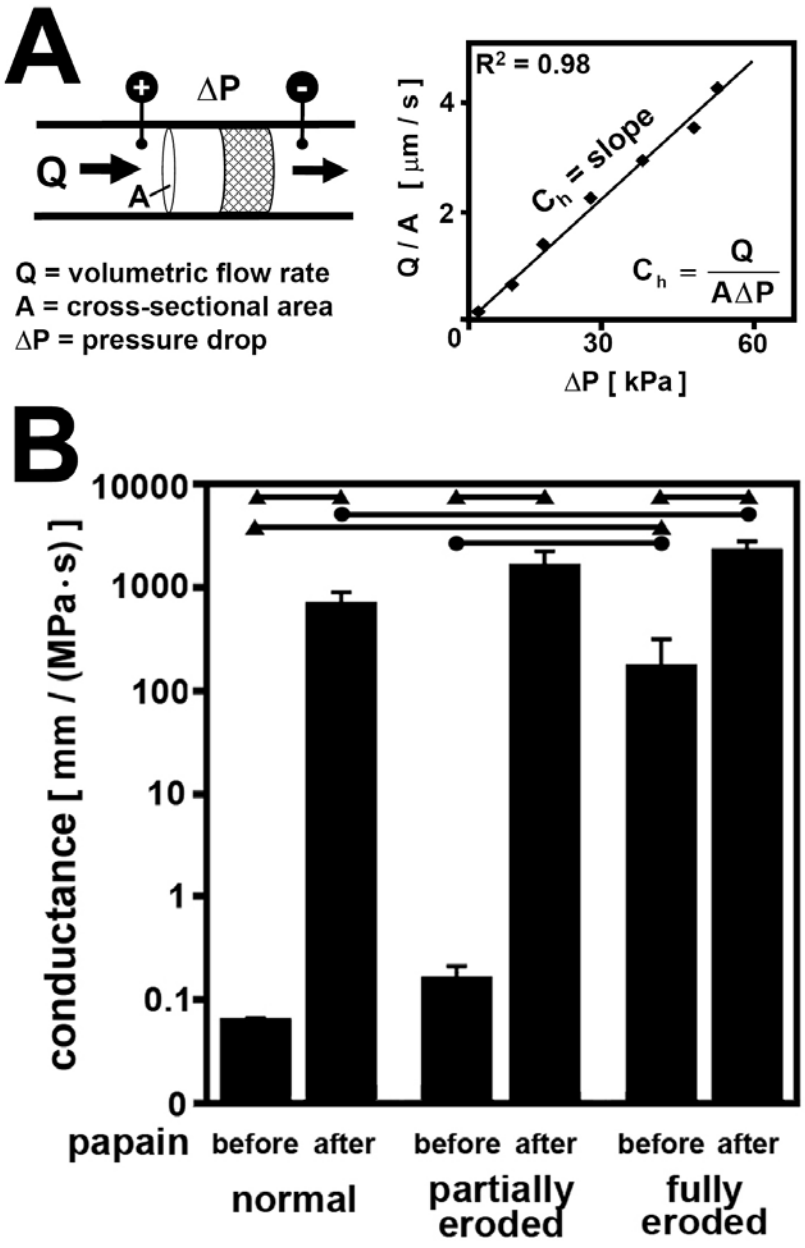

Figure 2.1: (**A**) Schematic diagram of perfusion test setup and representative Darcy plot to estimate hydraulic conductance constant, c. (**B**) Effect of OA erosion and papain digestion on hydraulic conductance of osteochondral tissue and ScBP. Conductance values after 2h perfusion of normal, partially eroded, and fully eroded osteochondral tissue before and after removal of cartilage by papain digestion. ● = $p<0.013$; ▲ = $p<0.0033$.

2.4 Results

Hydraulic conductance. Hydraulic conductance was found to be dependent on both OA erosion and papain digestion. With increasing severity of OA erosion, the hydraulic conductance of osteochondral samples and ScBP increased significantly ($P < 0.01$) (Figure 1B). The effect of OA erosion on conductance was evident both in the native state and after cartilage removal in ScBP samples. Osteochondral samples in their native state increased in hydraulic conductance from 0.065 mm/(MPa·s) for normal cartilage and 0.16 mm/(MPa·s) for partially eroded cartilage to 176 mm/(MPa·s) for fully eroded cartilage down to exposed bone. There was a 2700-fold increase in conductance from the normal to the fully eroded samples ($P < 0.0033$), and a 1000-fold increase from the partially eroded to the fully eroded samples ($P < 0.017$). Similar trends were evident after papain digestion of all samples to remove cartilage and isolate the ScBP. ScBP conductance followed an increasing trend from 702 mm/(MPa·s) for normal ScBP to 1673 mm/(MPa·s) for partially eroded ScBP to 2316 mm/(MPa·s) for fully eroded ScBP. There was a significant 3-fold increase between hydraulic conductance of normal and fully eroded ScBP ($P < 0.017$).

After removal of uncalcified cartilage by papain digestion, hydraulic conductance increased significantly for all grades of samples (Figure 1) ($P < 0.001$). Hydraulic conductance of normal and partially eroded OC samples increased 10800-fold ($P < 0.0033$) and 10500-fold ($P < 0.0033$), respectively, while hydraulic conductance of fully eroded samples increased 13-fold ($P < 0.0033$). For normal and

partially eroded ScBP samples isolated by mechanical debridement, ScBP hydraulic conductance increased 2-fold ($P < 0.05$) after papain digestion.

Histology. 3D histology showed differences in CC and ScBP structure associated with degrees of degeneration. CC was histologically distinct from surrounding tissues in all groups. In normal and partially eroded samples, the CC layer bordered both the overlying uncalcified cartilage with a gently undulating tidemark and the underlying subchondral bone with a highly interdigitated cement line (Figures 2A, B, D, E). In fully eroded samples, the CC was an incomplete layer, appearing in irregular pockets at the smooth bony surface (Figure 2C).

OA samples with partial-thickness erosion of cartilage exhibited fibrillated cartilage, multiple tidemarks, and a thickened CC layer (Figure 2B, E). Papain digestion removed uncalcified cartilage but appeared to preserve the entire CC below the lowest tidemark (Figures 2D, E). OA samples with full-thickness erosion of cartilage with exposure of bone had a smooth bony surface and a thick, dense ScBP (Figures 2C, F), with an incomplete CC layer present in irregular pockets at the surface (Figure 2C). Papain digestion appeared to open up more void space and channels through the ScBP (Figure 2F).

Vascularity was present in normal ScBP as well as OA partial- and full-thickness erosion ScBP, but differed in appearance. In normal ScBP, vascular canals were most commonly seen as long finger-like protrusions sheathed by bone originating from the marrow space and ending within the CC (Figure 3A). In partially eroded ScBP, vascular canals appeared greater in size and number, either ending in the CC or protruding above the CC into deep zone cartilage nearing the duplicate

tidemark (Figure 3B). In fully eroded ScBP, vascularity appeared as large, interconnected void spaces or channels starting from within the thickened bone plate and ending at the smooth, bony surface (Figures 2F, 3C).

Stereological measurements. CC and ScB thickness varied with the degree of OA erosion but were not altered by papain digestion. Papain digestion did not have an effect on CC thickness ($P = 0.46$) or ScB thickness ($P = 0.41$), which was consistent with qualitative histological observations (Figure 4A). The grade of OA erosion did have a significant effect on both CC thickness ($P < 0.01$) and ScB thickness ($P < 0.01$). The CC thickness in partially eroded samples was 157 μm, ~1.5-fold greater than normal ($P < 0.01$), while the CC thickness in fully eroded samples was 54 μm, ~2-fold less than normal ($P < 0.01$) and ~3-fold less than in the partially eroded samples ($P < 0.001$). The ScB thickness of fully eroded samples was 911 μm, ~2-fold greater than that of both normal ($P < 0.01$) and partially eroded samples ($P < 0.01$).

The density of vessels penetrating into the CC layer or ScBP surface varied with the degree of OA erosion but was not affected by papain digestion. Papain digestion did not have a significant effect on the density of vessels penetrating into or beyond the CC ($P = 0.27$) (Figure 4B). The grade of OA erosion did have a significant effect on density of vessels ($P < 0.01$), displaying a similar trend to the one seen for CC thickness. Partially eroded ScBP tended to have the greatest density of vessels penetrating the CC, with 19 vessels per mm^2

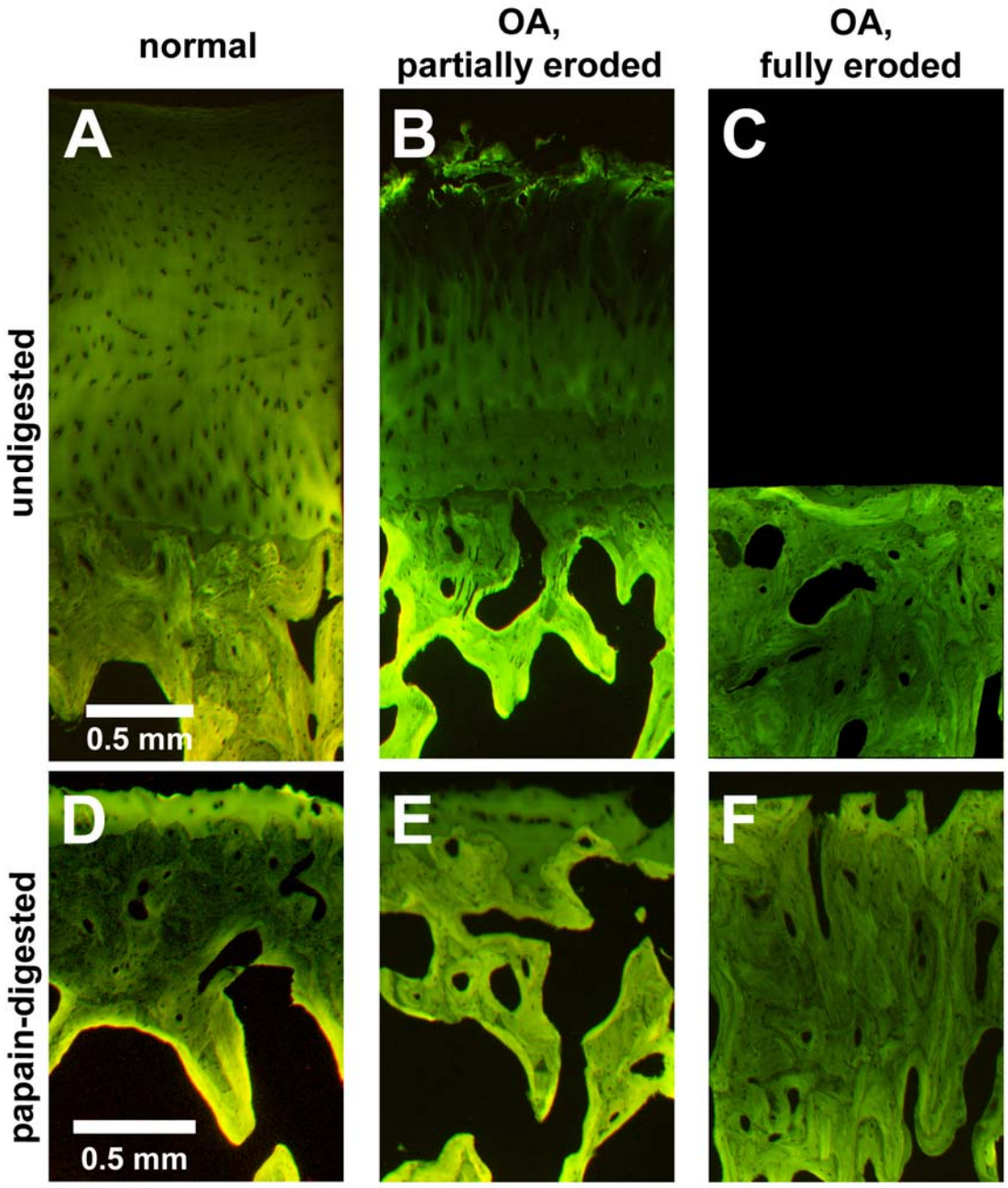

Figure 2.2: Normal (**A, D**), partially eroded (**B, E**), or fully eroded (**C, F**) osteochondral samples without (**A, B, C**) and with (**D, E, F**) articular cartilage removal by papain digestion.

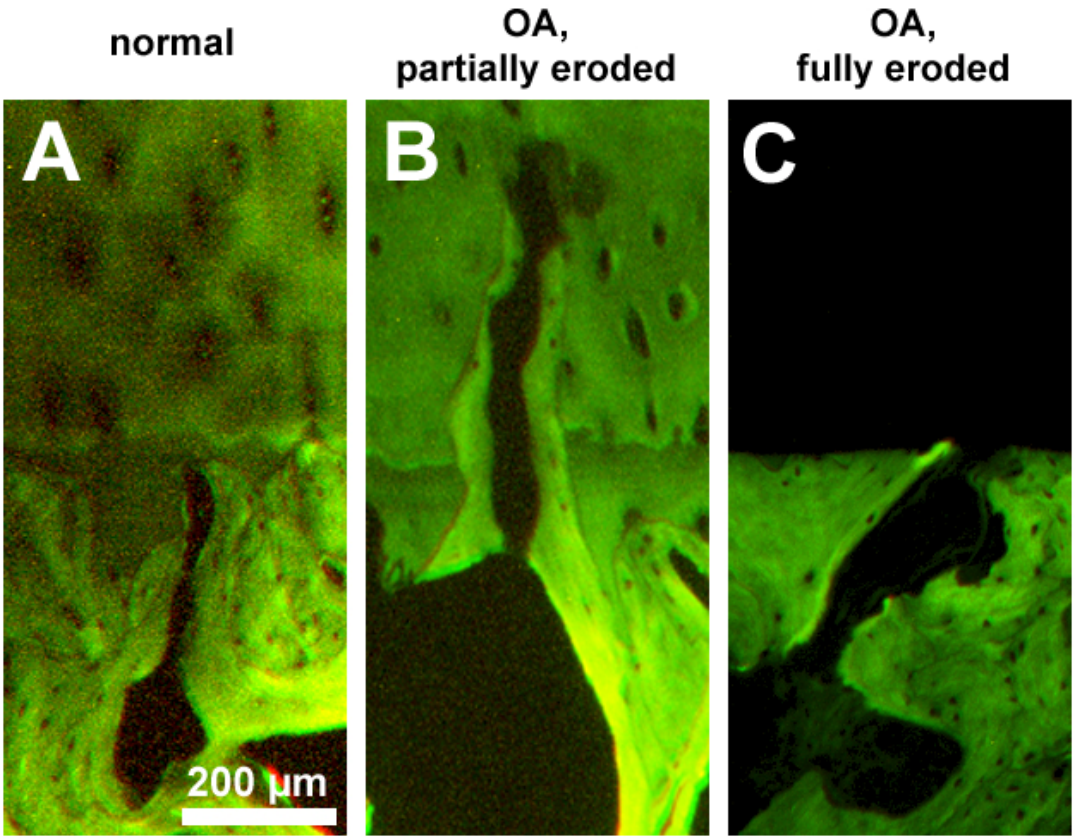

Figure 2.3: Typical vascular canals penetrating (**A**) into calcified cartilage in normal ScBP, (**B**) into deep zone cartilage in partially eroded ScBP, and (**C**) to the surface of fully eroded ScBP.

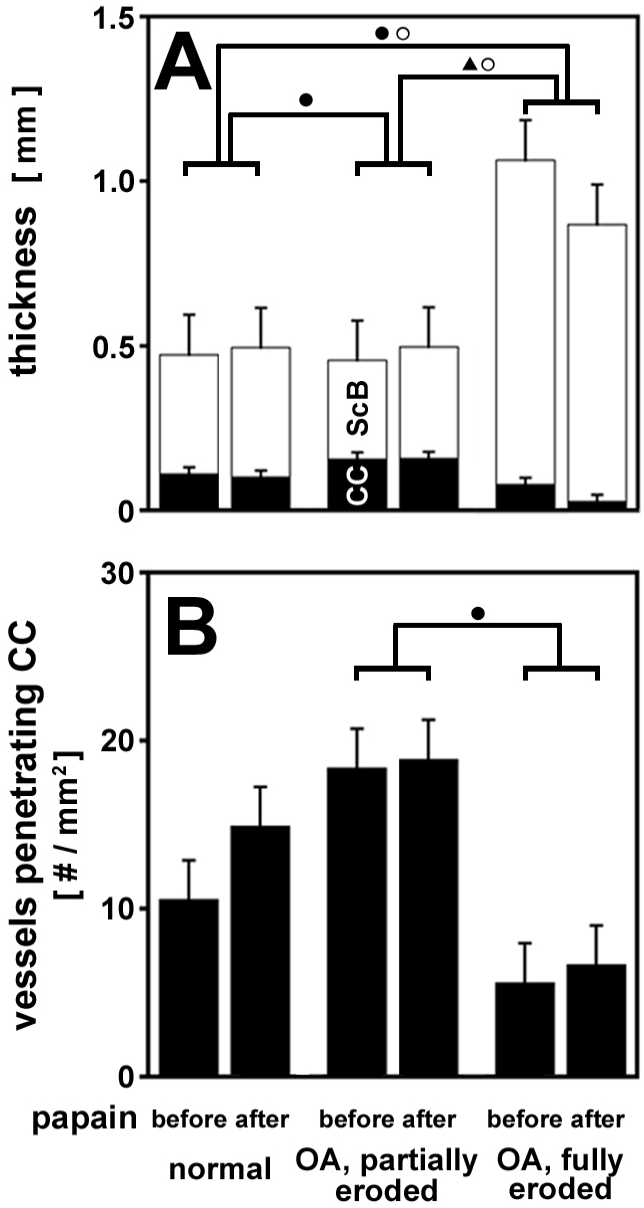

Figure 2.4: Stereological measurements of subchondral bone plate structure. (**A**) Thickness of calcified cartilage (black) and underlying subchondral bone (white). Total height of each column is ScBP thickness. ●, $p<0.01$; ▲, $p<0.001$. (**B**) Number of vessels penetrating the CC/bone interface per cross-sectional area for normal, partially eroded and fully eroded osteochondral samples before and after cartilage removal by papain digestion. ●, $p<0.01$.

2.5 Discussion

The results described here indicate that hydraulic conductance of both osteochondral tissue and the isolated ScBP is increased with increasing stage of OA cartilage erosion, in association with structural changes in CC and ScB thickness and vascularity. Increased hydraulic conductance allows for greater ease of interstitial fluid flow through the osteochondral tissue and ScBP. Compared to normal OC tissue and ScBP, partially-eroded OC tissue and ScBP exhibited no significant difference in hydraulic conductance (Figure 1). However, structural changes were evident in partially eroded ScBP, with increased CC thickness (1.5-fold), a trend for increased density of vascular canals penetrating the CC, and larger vascular canals (Figures 2AB, 3AB, 4). Compared to normal tissues, fully-eroded OC tissue and ScBP exhibited a marked increase (2700-fold and 3-fold, respectively) in hydraulic conductance (Figure 1). Structural changes were also evident in fully eroded ScBP, with the appearance of discontinuities in CC, increased ScB thickness (2-fold), decreased density of vascular canals penetrating the ScBP surface, and larger void spaces within the ScBP (Figures 2BC, 3BC, 4). In the progression from normal OC tissue into the partially- and fully-eroded stages of OA, changes in CC thickness and vascularity occur together with increases in hydraulic conductance and ScB thickness. These results suggest that the CC structural and vascular remodeling that occurs with OA contributes to increased ease of fluid flow across the osteochondral structure, a factor which may play a role in advancing OA degeneration (Figure 5).

The ScBP was isolated from OC tissue with a method that may have affected the hydraulic conductance results. In human ScBP preparations, papain digestion selectively removes uncalcified cartilage down to the tidemark while maintaining CC thickness and contour but not creating perforations through the ScBP [13]. Such ScBP preparations are devoid not only of cartilage but also of marrow and soft tissue linings of vascular canals, which could participate in modulating fluid transport across the ScBP. Papain digestion may also remove proteins such as collagen from bone, which could affect the ScBP hydraulic conductance. Papain digestion of normal and partially eroded ScBP (which had been isolated mechanically) increased conductance 2-fold, whereas papain digestion of fully eroded samples increased conductance ~13-fold (Figure 1B). Thus, the estimate of hydraulic conductance of ScBP, as performed in the current study with papain digestion, is likely to be higher than ScBP conductance *in vivo*. Nevertheless, papain digestion was useful as a repeatable, non-destructive method for removing uncalcified cartilage while preserving CC structure.

The two-hour hydraulic conductance constant (c^{2h}) evaluated in the present study is an upper bound estimate of the overall conductance of full-thickness OC tissue. Hydraulic conductance of OC tissue is determined by the low fluid permeability of the cartilage matrix, which dominates the fluid pressurization behavior and resistance to flow. As fluid enters the cartilage and flows from the superficial towards the deep zone, it exerts drag forces to pull the solid matrix with it. The drag forces result in matrix compaction, which decreases porosity and permeability within the tissue in a depth-varying, non-uniform manner [10, 28, 37]. A new steady-state is reached when the matrix consolidation and fluid flow through the tissue are balanced,

maintaining a constant pressure across the tissue. In the present study, perfusion flow time was standardized to 2 hours, as a physiologically relevant period of loading, and to allow calculation of c^{2h}. At 2h, full-thickness OC tissue would not be fully compacted, and c^{2h} is higher than that at steady-state (c^{SS}). For normal OC tissue, c^{2h} is greater than c^{SS} by ~5-fold (data not shown). For porous, permeable materials with a stiff solid matrix, such as ScBP, the effect of flow-dependent matrix consolidation is negligible, so steady-state is reached on a shorter time scale; for ScBP, $c^{0.5h}$ and c^{SS} were similar (data not shown).

The differences in permeability and structure between normal and OA articular cartilage and ScBP extend the findings of previous studies. The present study extends permeability measurements, traditionally made on isolated cartilage and bone tissues, by directly analyzing the full thickness of articular cartilage still attached to ScBP, providing an overall conductance for the osteochondral unit. Previous measurements of hydraulic permeability on cartilage sections elucidated variations in zonal properties [29] and may be influenced by alterations in matrix organization and water content due to detachment from the underlying CC [23, 30]. The c^{2h} and $c^{0.5h}$ of normal osteochondral tissue and ScBP determined in the present study can be converted into corresponding apparent hydraulic permeability (k_p) values using average thicknesses for cartilage and ScBP, allowing comparison to previous studies (Table 1). The apparent k_p of normal cartilage attached to ScBP in the present study was greater than values from literature for normal cartilage [17, 30, 32]. This can be attributed in part to the 2-hour perfusion time, which did not allow the full-thickness cartilage to reach steady-state hydrostatic pressurization and associated matrix

compaction, resulting in a higher apparent permeability and precluding direct comparison to literature values of k_p, which reflect steady-state. The k_p of normal ScBP found in the current study, which reached steady-state on a shorter time scale (<0.5hr), was within the range of values reported for normal cortical and cancellous bone (Table 1) [26, 38, 41].

The trend for a small increase in hydraulic conductance of OA OC tissue is consistent with slight increases in hydraulic permeability of OA articular cartilage reported in previous studies [3, 7, 42]. Increased hydraulic conductance of OC tissue occurring with OA may be due primarily to decreased cartilage thickness, increased hydraulic permeability of the remaining OA cartilage, or a combination of both. However, in the current study, hydraulic conductance of partially eroded OC tissue was not significantly different from normal despite cartilage thickness being 30% lower. Since fluid pressurization is normally maintained by the low hydraulic permeability of deep zone cartilage [10, 29, 43], the overall hydraulic conductance of OC tissue may remain close to normal for cases of partial erosion where the deep zone remains intact. For OC tissue with full-thickness erosion of cartilage, the relatively high hydraulic conductance may be determined by any residual cartilage in the ScBP.

Table 2.1: Hydraulic permeability (k_p) (mm^2/[MPa·second]) of articular cartilage and subchondral bone plate. Values are from the current study and others, where noted.

Tissue/type	k_p	Average thickness, mm	Ref.
Cartilage			
Normal	0.0001–0.002	0.3–0.8	1, 11, 32
Cartilage plus ScBP			
Normal	0.15	2.5	Present study
OA, partially eroded*	0.27	1.8	Present study
Cortical bone			
Normal (canine)	40–80	0.5–1.0	33, 34
ScBP			
Normal	90	0.47	Present study
OA, partially eroded	140	0.46	Present study
OA, fully eroded	190	1.1	Present study
ScBP, papain-digested			
Normal	350	0.49	Present study
OA, partially eroded	830	0.50	Present study
OA, fully eroded	2,010	0.87	Present study
Cancellous bone			
Normal	20,000–8,000,000	1.0	13, 33

* OA = osteoarthritis; ScBP = subchondral bone plate.

Increased hydraulic conductance of osteochondral tissue and the ScBP could have deleterious biomechanical consequences for cartilage during joint loading (Figure 5). Normally, articular cartilage is able to support joint loads through interstitial fluid pressurization due to its low hydraulic conductance (Figure 5A). Fluid pressurization in cartilage plays a major role in providing load support for a prolonged duration after contact, preventing the solid matrix from deforming to an equilibrium strain state [4]. The duration of load support by fluid pressurization can be characterized using a time constant to reach equilibrium that depends on factors affecting the rate of fluid loss from cartilage, including the radial path length, compressive modulus, and hydraulic permeability [2]. For normal human cartilage with contact radius, a, of 10 mm, compressive modulus, H_A, of 0.5 MPa and k_p of 2×10^{-15} $m^4/(N\cdot s)$, the characteristic time constant, $a^2/(H_A\cdot k_p)$, is ~28 hrs, thus protecting cartilage for long durations of load. In OA, increased fluid loss from cartilage during joint loading may occur due to fluid exudation into the underlying ScBP, causing shorter times to equilibrium and potentially leading to large deformations and accelerated cartilage degeneration (Figure 5B).

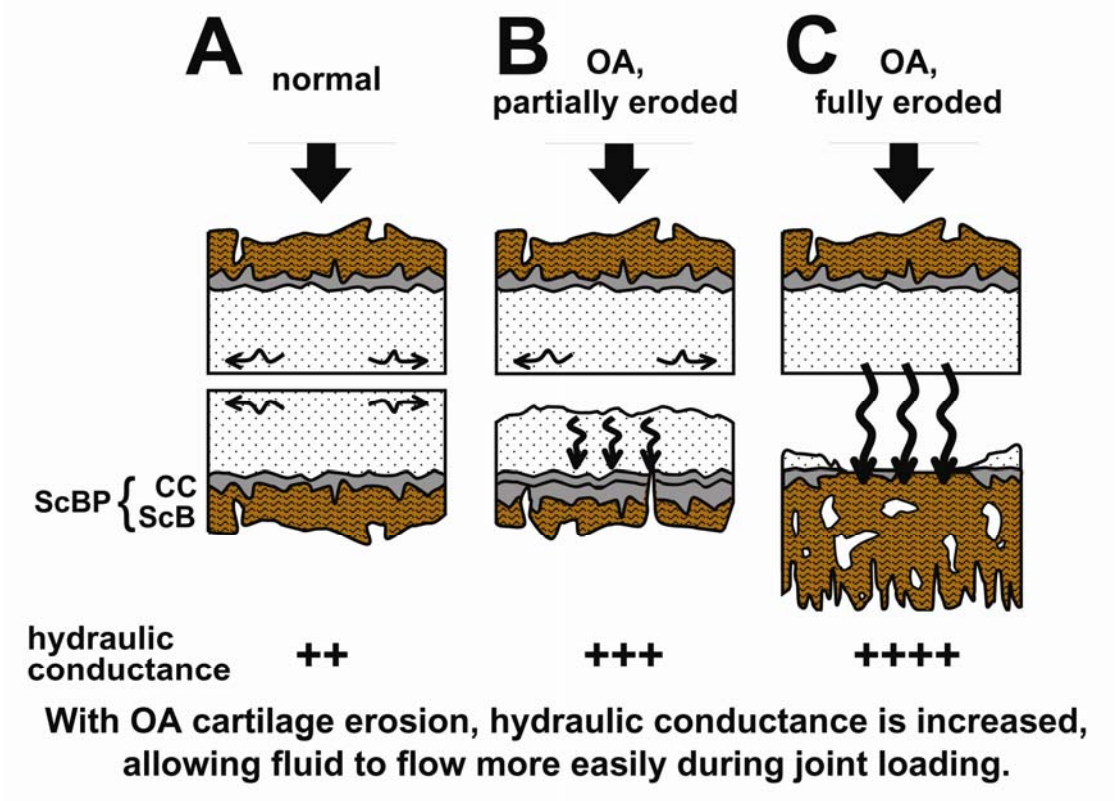

Figure 2.5: Schematic of normal (**A**), partially eroded (**B**), and fully eroded (**C**) osteochondral tissue and potential deleterious effects of increased ScBP permeability leading to increased fluid loss. Wavy arrows indicate fluid flow within cartilage and also fluid loss from from overlying (**B**) and opposing (**C**) articular cartilage during loading. Plus signs indicate magnitude of osteochondral and ScBP hydraulic conductance..

For full-thickness cartilage erosion with exposed ScBP, the articular cartilage of the opposing joint surface may be damaged through fluid exudation from its superficial zone into and through the eburnated and permeable joint surface (Figure 5C). The depth of the opposing cartilage that undergoes fluid depressurization and concomitant tissue consolidation would depend on the time characteristics of loading. The characteristic time to equilibrium for the opposing cartilage, using confined compression analysis of normal human cartilage with 2 mm thickness, is ~1 hr [24]. At the relatively high physiological frequency of gait (0.5 Hz), the characteristic depth of fluid depressurization extends ~40 μm from the articular surface. With a prolonged loading duration typical of standing, e.g. for periods of 15 min (0.001 Hz), the fluid depressurization extends ~1 mm from the surface[17]. Even for a short loading duration of 2 min and a conservative contact stress of 0.5 MPa, the opposing cartilage surface would experience a deformation of ~0.2mm [24], which could lead to localized cell death, as when the superficial zone is compressed against a porous platen *in vitro* [35]. Thus, the biomechanical consequences for increased ScBP permeability in OA may contribute to overlying cartilage degeneration as well as the spreading of OA onto the opposing joint surface.

In the normal joint, the CC interface may function as a zone of intermediate hydraulic permeability between articular cartilage and subchondral bone, similar to its role as a zone of intermediate stiffness for the transfer of mechanical loads. Although the CC layer in mature joints has previously been considered impermeable [14, 31], this perception may have been due to low rates of solute diffusion and convection into the adjacent cartilage deep zone rather than low hydraulic permeability of the CC

layer itself. In the present study, eburnated ScBP with eroded CC had higher hydraulic conductance than normal ScBP with intact CC, in spite of the greater ScB thickness and density from eburnation which would be expected to decrease conductance. Thus, an intact CC layer appears to be more permeable to fluid than articular cartilage but less permeable than cortical bone, making it a zone of intermediate permeability between deep zone cartilage and ScB in the normal osteochondral junction. With the onset of OA, the relative permeabilities of cartilage, CC and ScB in the osteochondral junction may be altered, which may disrupt the homeostasis of the osteochondral unit and affect progression of the disease.

OA ScBP may undergo additional structural changes due to the intrusion of fluid into eroded or permeable areas, including the development of cartilaginous pockets and bone marrow lesions. Hydraulic conductance of fully eroded ScBP increased 10-fold along with the appearance of void pockets and channels after papain digestion, consistent with residual cartilage within the ScBP. Cartilaginous pockets in OA joints with exposed bone have been documented both within and at the surface of the ScBP and may participate in the repair process [27, 33, 47]. The void areas may also represent bone cysts or bone marrow lesions found in sclerotic bone which are associated with pain in OA [9, 16]. Bone cysts may arise from intrusion of pressurized fluid into bone at the joint surface, as suggested by openings between cysts and the joint cavity and their rounded morphology [25].

The increase in hydraulic conductance of osteochondral tissue and ScBP in OA allows more direct fluid movement between cartilage and bone compared to the normal joint. Fluid movement can, in turn, act as a mechanical signal to cells and

enhance the transport of diffusible factors, processes that may mediate the crosstalk between cartilage and bone. In OA, altered boundary conditions at the osteochondral interface may disrupt the mechanical and chemical interactions between the microenvironments of cartilage and bone, which may affect tissue homeostasis and cell physiology. Understanding how altered boundary conditions affect the mechanical and chemical interactions between cartilage and bone will lead to a more complete picture of the multi-tissue pathogenesis of OA.

2.6 Acknowledgments

We would like to thank co-authors Won C. Bae, Wendy Shieu, Dr. Chad W. Lewis, Dr. William D. Bugbee, and Dr. Robert L. Sah for their contributions to this work. We would like to acknowledge John Wiley and Sons, Inc. for permission to reprint, in full, Chapter 2 which has been published in *Arthritis and Rheumatism*. This work was supported by the National Institute of Health, National Science Foundation, Musculoskeletal Transplant Foundation, and the Howard Hughes Medical Institute through the Professors Program Grant to UCSD for Dr. Robert L. Sah.

2.7 References

1. Anderson TW, Darling DA: Asymptotic theory of certain "goodness of fit" criteria based on stochastic processes. *Ann Math Statist* 23:193-212, 1952.

2. Armstrong CG, Lai WM, Mow VC: An analysis of the unconfined compression of articular cartilage. *J Biomech Eng* 106:165-73, 1984.

3. Armstrong CG, Mow VC: Variations in the intrinsic mechanical properties of human articular cartilage with age, degeneration, and water content. *J Bone Joint Surg Am* 64-A:88-94, 1982.

4. Ateshian GA, Lai WM, Zhu WB, Mow VC: An asymptotic solution for the contact of two biphasic cartilage layers. *J Biomech* 27:1347-60, 1994.

5. Ayotte DC, Ito K, Tepic S: Direction-dependent resistance to flow in the endplate of the intervertebral disc: an ex vivo study. *J Orthop Res* 19:1073-7, 2001.

6. Bashir A, Gray ML, Boutin R, Burstein D: In vivo imaging of GAG in articular cartilage using delayed Gd(DTPA)2- enhanced MRI. *Radiology* 205:551-8, 1997.

7. Brocklehurst R, Bayliss MT, Maroudas A, Coysh HL, Freeman MA, Revell PA, Ali SY: The composition of normal and osteoarthritic articular cartilage from human knee joints. With special reference to unicompartmental replacement and osteotomy of the knee. *J Bone Joint Surg Am* 66:95-106, 1984.

8. Burr DB: The importance of subchondral bone in osteoarthrosis. *Curr Opin Rheumatol* 10:256-62, 1998.

9. Carrino JA, Blum J, Parellada JA, Schweitzer ME, Morrison WB: MRI of bone marrow edema-like signal in the pathogenesis of subchondral cysts. *Osteoarthritis Cartilage* 14:1081-5, 2006.

10. Chen AC, Bae WC, Schinagl RM, Sah RL: Depth- and strain-dependent mechanical and electromechanical properties of full-thickness bovine articular cartilage in confined compression. *J Biomech* 34:1-12, 2001.

11. Christensen P, Kjaer J, Melsen F, Nielsen HE, Sneppen O, Vang PS: The subchondral bone of the proximal tibial epiphysis in osteoarthritis of the knee. *Acta Orthop Scand* 53:889-95, 1982.

12. Clark JM: The structure of vascular channels in the subchondral plate. *J Anat* 171:105-15, 1990.

13. Clark JM, Huber JD: The structure of the human subchondral plate. *J Bone Joint Surg Br* 72:866-73, 1990.

14. Collins DH. The Pathology of Articular and Spinal Disease. London: Arnold; 1949.

15. Dequeker J, Mokassa L, Aerssens J, Boonen S: Bone density and local growth factors in generalized osteoarthritis. *Microsc Res Tech* 37:358-71, 1997.

16. Felson DT, Chaisson CE, Hill CL, Totterman SM, Gale ME, Skinner KM, Kazis L, Gale DR: The association of bone marrow lesions with pain in knee osteoarthritis. *Ann Intern Med* 134:541-9, 2001.

17. Frank EH, Grodzinsky AJ: Cartilage electromechanics-II. A continuum model of cartilage electrokinetics and correlation with experiments. *J Biomech* 20:629-39, 1987.

18. Glantz SA. Primer of Biostatistics. 3rd ed. San Francisco, CA: McGraw-Hill, Inc.; 1992.

19. Green WT, Jr., Martin GN, Eanes ED, Sokoloff L: Microradiographic study of the calcified layer of articular cartilage. *Arch Pathol* 90:151-8, 1970.

20. Jadin KD, Wong BL, Bae WC, Li KW, Williamson AK, Schumacher BL, Price JH, Sah RL: Depth-varying density and organization of chondrocyte in immature and mature bovine articular cartilage assessed by 3-D imaging and analysis. *J Histochem Cytochem* 53:1109-19, 2005.

21. Johnson M, Katz JL: Some new developments in the rheology of bone. *Biorheology Suppl* 1:169-74, 1984.

22. Kamibayashi L, Wyss UP, Cooke TD, Zee B: Trabecular microstructure in the medial condyle of the proximal tibia of patients with knee osteoarthritis. *Bone* 17:27-35, 1995.

23. Keinan-Adamsky K, Shinar H, Navon G: The effect of detachment of the articular cartilage from its calcified zone on the cartilage microstructure, assessed by 2H-spectroscopic double quantum filtered MRI. *J Orthop Res* 23:109-17, 2005.

24. Kwan MK, Lai WM, Mow VC: Fundamentals of fluid transport through cartilage in compression. *Ann Biomed Eng* 12:537-58, 1984.

25. Landells JW: The bone cysts of osteoarthritis. *J Bone Joint Surg Br* 35-B:643-9, 1953.

26. Li GP, Bronk JT, An KN, Kelly PJ: Permeability of cortical bone of canine tibiae. *Microvasc Res* 34:302-10, 1987.

27. Mankin HJ: The reaction of articular cartilage to injury and osteoarthritis (Part II). *N Engl J Med* 291:1335-40, 1974.

28. Mansour JM, Mow VC: The permeability of articular cartilage under compressive strain and at high pressures. *J Bone Joint Surg Am* 58-A:509-16, 1976.

29. Maroudas A: Physicochemical properties of cartilage in the light of ion exchange theory. *Biophys J* 8:575-95, 1968.

30. Maroudas A, Bullough P: Permeability of articular cartilage. *Nature* 219:1260-1, 1968.

31. Maroudas A, Bullough P, Swanson SA, Freeman MA: The permeability of articular cartilage. *J Bone Joint Surg Br* 50:166-77, 1968.

32. McCutchen CW: The frictional properties of animal joints. *Wear* 5:1-17, 1962.

33. Meachim G, Osborne GV: Repair at the femoral articular surface in osteo-arthritis of the hip. *J Pathol* 102:1-8, 1970.

34. Mente PL, Lewis JL: Elastic modulus of calcified cartilage is an order of magnitude less than that of subchondral bone. *J Orthop Res* 12:637-47, 1994.

35. Milentijevic D, Torzilli PA: Influence of stress rate on water loss, matrix deformation and chondrocyte viability in impacted articular cartilage. *J Biomech* 38:493-502, 2005.

36. Mori S, Harruff R, Burr DB: Microcracks in articular calcified cartilage of human femoral heads. *Arch Pathol Lab Med* 117:196-8, 1993.

37. Mow VC, Holmes MH, Lai WM: Fluid transport and mechanical properties of articular cartilage: a review. *J Biomech* 17:377-94, 1984.

38. Nauman EA, Fong KE, Keaveny TM: Dependence of intertrabecular permeability on flow direction and anatomic site. *Ann Biomed Eng* 27:517-24, 1999.

39. Oegema T, Jr., Carpenter R, Hofmeister F, Thompson RC, Jr.: The interaction of the zone of calcified cartilage and subchondral bone in osteoarthritis. *Microsc Res Tech* 37:324-32, 1997.

40. Oettmeier R, Abendroth K, Oettmeier S: Analyses of the tidemark on human femoral heads. II. Tidemark changes in osteoarthrosis--a histological and

histomorphometric study in non-decalcified preparations. *Acta Morphol Hung* 37:169-80, 1989.

41. Sander EA, Nauman EA: Permeability of musculoskeletal tissues and scaffolding materials: experimental results and theoretical predictions. *Crit Rev Biomed Eng* 31:1-26, 2003.

42. Setton LA, Mow VC, Muller FJ, Pita JC, Howell DS: Mechanical properties of canine articular cartilage are significantly altered following transection of the anterior cruciate ligament. *J Orthop Res* 12:451-63, 1994.

43. Setton LA, Zhu W, Mow VC: The biphasic poroviscoelastic behavior of articular cartilage: role of the surface zone in governing the compressive behavior. *J Biomech* 26:581-92, 1993.

44. Shimizu M, Tsuji H, Matsui H, Katoh Y, Sano A: Morphometric analysis of subchondral bone of the tibial condyle in osteoarthrosis. *Clin Orthop Relat Res*:229-39, 1993.

45. Sokoloff L: Microcracks in the calcified layer of articular cartilage. *Arch Pathol Lab Med* 117:191-5, 1993.

46. Soltz MA, Ateshian GA: Experimental verification and theoretical prediction of cartilage interstitial fluid pressurization at an impermeable contact interface in confined compression. *J Biomech* 31:927-34, 1998.

47. Zhang D, Johnson LJ, Hsu HP, Spector M: Cartilaginous deposits in subchondral bone in regions of exposed bone in osteoarthritis of the human knee: Histomorphometric study of PRG4 distribution in osteoarthritic cartilage. *J Orthop Res*, 2007.

CHAPTER 3

IN VITRO CALCIFICATION OF IMMATURE BOVINE ARTICULAR CARTILAGE: FORMATION OF A FUNCTIONAL ZONE OF CALCIFIED CARTILAGE

3.1 Abstract

Objective: The zone of calcified cartilage (ZCC) anchors articular cartilage (AC) to subchondral bone through a layer of intermediate stiffness. The regulation and functional consequences of cartilage calcification may vary with depth from the articular surface. The hypothesis of this study was that the *in vitro* calcification of immature AC occurs selectively in the deep region and is associated with a local increase in stiffness.

Methods: AC and growth plate cartilage (GPC) from calves were incubated in DMEM, 1% FBS, 100μg/mL ascorbate, and ±10mM ß-glycerophosphate (ßGP) for up to 3 weeks. To assess the time course and effects of cell viability and ßGP, full-depth strips of AC and GPC were analyzed by histology, indentation, and $^{45}Ca^{++}$ uptake. To assess the effect of tissue zone, disks harvested from surface and deep zone AC and

from reserve and hypertrophic zone of GPC were incubated independently and analyzed by compression and for $^{45}Ca^{++}$ uptake and biochemical components.

Results: The deep ~20% of immature AC calcified within 3 weeks, with calcification dependent on cell viability and ßGP. Mineral was deposited continuously around cells in AC but only between cell columns in GPC. The deep zone of AC exhibited a compressive modulus of 0.53 MPa after ßGP-induced calcification, ~4-fold stiffer than AC incubated without ßGP.

Conclusions: Cartilage explants exhibit inherent zone-specific calcification processes, resulting in an increase in stiffness associated with cartilage calcification. Such properties may be useful for engineering a biomimetic ZCC tissue to integrate cartilaginous tissue to bone, thereby forming a mechanically functional osteochondral unit.

3.2 Introduction

The zone of calcified cartilage (ZCC) is a specialized structure at the native osteochondral junction that functions as a biomechanical connection between articular cartilage and underlying subchondral bone [35, 36]. The ZCC is 100-300 μm thick and is bound on one side by the tidemark, the gently undulating interface with uncalcified cartilage, and on the other side by the cement line, the highly interdigitated interface with subchondral bone. The intermediate stiffness of the ZCC can facilitate load transfer at the interface between cartilage and bone by reducing stress concentrations that would otherwise occur from the discontinuity in material stiffness of cartilage and bone [3, 35]. The ZCC is comprised of chondrocytes expressing the hypertrophic phenotype, which are enveloped in a calcified hyaline matrix [22, 30].

The native ZCC is formed through the calcification of immature articular cartilage matrix during postnatal development. During postnatal growth, chondrocytes near the articular surface proliferate gradually while forming new cartilage [21, 31]. Concomitantly, chondrocytes in the deep region near the subchondral bone also proliferate and form new cartilage, some of which becomes calcified and is resorbed and replaced by ingrowing bone advancing toward the articular surface [31, 36]. This process of new cartilage formation and resorption slows after puberty and achieves a steady-state with skeletal maturity [29]. In the mature skeleton, deep zone AC is joined to the underlying bone through the ZCC, with the ZCC normally persisting throughout adulthood. Studying calcification of cartilage in immature AC that does not yet have a fully formed ZCC may provide insight into the factors involved in

balancing bone ingrowth with the maturation of the calcified cartilage matrix into the ZCC.

Calcification of articular cartilage may occur through a mechanism similar to that in the terminal stages of endochondral ossification of growth plate cartilage (GPC) during long bone growth. Growth plate chondrocytes progressively differentiate while transitioning from the resting zone to the proliferative, and hypertrophic zones, eventually undergoing apoptosis with matrix calcification, vascular invasion, and bone ingrowth and remodeling [6, 16]. In the lower hypertrophic zone, calcification initiates in the territorial matrix close to chondrocytes and spreads throughout the matrix of the longitudinal septa between columns of lower hypertrophic chondrocytes [19].

The coordinated expression of inhibitory and stimulatory factors by cells in different tissue zones [20] may be involved in the regulation of cartilage calcification to form the ZCC. Chondrocytes isolated from the deep zone of immature AC readily calcify during *in vitro* culture, stimulated by factors such as BMPs, thyroid hormone, and organic phosphate [23, 25, 37, 41]. Chondrocytes from the superficial zone secrete soluble factors that can inhibit mineralization by deep zone chondrocytes during *in vitro* co-culture [23], but it remains unclear how readily such factors would be transported from the superficial zone to the deep zone through the cartilage matrix *in vivo*. Using cartilage explants sectioned vertically to preserve full-thickness zonal structure or sectioned horizontally to separate zones and disrupt zonal cross-talk, the effects of the superficial zone on matrix calcification of deep zone AC can be assessed within the transport limitations of the normal tissue environment. Cartilage explant

cultures can expand upon chondrocyte cultures by analyzing how calcification is coordinated with remodeling of the existing extracellular matrix. Cartilage explants have been used to study matrix remodeling for integrative repair between cartilage surfaces [1] and may also be useful for studying the relationship between matrix calcification and mechanical function.

The mechanical properties of cartilage may be affected by the extent of its mineralization. For compact bone, the Young's modulus in tension has a strong positive relationship with mineral content even for bones with different porosities and structures [14], and Young's modulus may increase substantially with even a relatively small increase in mineral content [13]. For calcified cartilage, the nanoindentation modulus is positively related to the local mineral content, although lower for calcified cartilage than for subchondral bone for the same mineral content [17, 18]. The culture of cartilage explants *in vitro* has been useful to elucidate the mechanisms and consequences of cartilage cell and matrix metabolism as related to proteoglycan depletion in osteoarthritis and the balance between proteoglycan and collagen metabolism during growth [4, 26]. Previous cultures of explants have focused on the regions near the articular surface; those extending to the deep layers may elucidate the composition-metabolism-function relationships between progressive mineralization of cartilage, mineral content, and mechanical properties of a calcified cartilage matrix.

The hypothesis of this study was that the *in vitro* calcification of immature articular cartilage (AC) occurs only in the deep zone and is associated with a local increase in mechanical stiffness. The objectives of this study were to determine the

effects of (1) culture duration, (2) cell viability and medium supplementation with ß-glycerophosphate, and (3) separation of surface and deep zone cartilage on the *in vitro* calcification of immature bovine AC.

3.3 Materials and Methods

Experimental Design (Fig. 1). Experiment 1: The zonal variation and time course of *in vitro* calcification were assessed by comparing groups analyzed fresh and after 1, 2, or 3 weeks of incubation in medium with addition of ß-glycerophosphate (ßGP). Cartilage strips encompassing the full zonal structure (n = 6-8) were assessed by histology, indentation, and $^{45}Ca^{++}$ uptake. Experiment. 2: The effects of cell viability and ßGP on *in vitro* calcification were analyzed by killing cells prior to incubation with ßGP, along with live cartilage strips incubated with or without ßGP for 3 weeks. Samples (n = 6-8) were analyzed by histology, indentation and $^{45}Ca^{++}$ uptake. Experiment 3: The effect of zone on *in vitro* calcification was assessed by separate incubation of surface and deep zone cartilage for 3 weeks with or without ßGP. Samples (n = 6-10) were analyzed fresh and after culture by unconfined compression, $^{45}Ca^{++}$ uptake, and assays for sulfated glycosaminoglycan (GAG), collagen, and DNA content. Immature bovine growth plate cartilage (GPC) was used as a positive control tissue for calcification in all experiments.

Cartilage Explant Preparation and Culture (Fig. 1A). For AC, full-thickness cartilage blocks were harvested from the patellofemoral groove of 1-3 week-old calf (8 animals). For GPC, cartilage blocks were harvested from the distal radius of third-trimester fetal calf from the region between the epiphyseal bone and the metaphyseal bone [9] (7 animals). GPC was harvested from fetal calf because at this age the distal radius growth plate was still sufficiently thick (~3 mm) to enable parallel harvest procedures and experiments with AC samples. For Experiments 1 and 2, AC and GPC

blocks were sectioned and cut into strips preserving full zonal structure ($5\times1\times1$ mm^3 for AC, $3\times1\times1.7$ mm^3 for GPC). For Experiment 2, some strips were frozen at -80°C for 4h and thawed prior to culture. Loss of cell viability was confirmed using the Live/Dead Viability/Cytotoxicity Kit (Invitrogen, Carlsbad, CA). For Experiment 3, full-thickness cartilage blocks were cut into 1-mm-thick sequential transverse slices (parallel to the cartilage-bone interface for AC or to the metaphyseal bone for GPC), resulting in 5 slices for AC and 3 slices for GPC. From the top and bottom slices, disks (3 mm diameter) were punched. Samples were incubated in medium consisting of DMEM with 1% fetal bovine serum, ascorbic acid (100 μg/mL), 0.5 μCi/mL $^{45}Ca^{++}$, antibiotics, amino acids, and HEPES buffer solution at 37°C and 5% CO_2. After 3 days, some cultures were supplemented with the addition of 10 mM ßGP. Medium was changed every 3 days until sample termination.

Histology. Upon termination, samples were fixed in 4% paraformaldehyde in phosphate buffered saline (PBS) (pH 7.0) for 18h, embedded in OCT, and sectioned at 8 μm-thickness undecalcified using a cryostat. To assess cell and tissue morphology, sections were stained with hematoxylin and eosin. To localize calcification, sections were stained with 2% Alizarin Red S (pH 4.2) for 2 minutes [32].

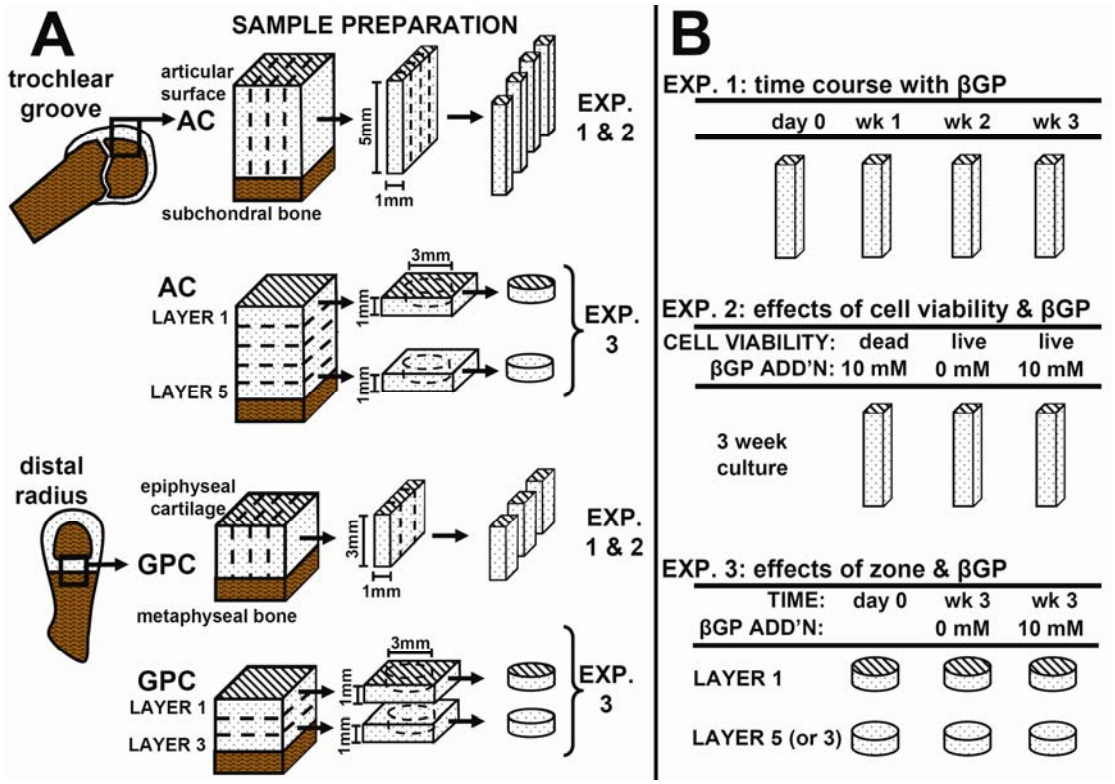

Figure 3.1: Sample harvest for AC and GPC explants (**A**) and experimental design (**B**)

Biomechanics. Indentation: Each sample strip was subjected to short-duration indentation testing. Using a benchtop mechanical tester (Mach-1^{TM} V500, BioSyntech Canada, Montreal) fitted with a flat-ended indenter tip (0.4 mm diameter) as described previously [5], indentation was performed to a depth of 0.2 mm at a rate of 0.1 mm/s at sites spaced 0.25 mm apart down the centerline of each sample. Indentation load-displacement curves were approximately linear (R^2 = 0.96), and the indentation stiffness at each site was obtained by dividing the peak load by the indentation depth. To normalize for strip length, samples were binned into 5 segments or layers, each encompassing 20% of the total strip length, and stiffness values within each layer were averaged. Compression: Sample disks were subjected to radially-unconfined compression between an impermeable stainless steel post and test chamber bottom surface attached to a mechanical spectrometer (Dynastat, IMASS, Accord, MA), using a loading configuration and setup similar to that described previously [11]. Briefly, sample disks were subjected to static compression at amplitudes of 15%, 30% and 45% of the uncompressed thickness, and equilibrium stress-strain data were used to estimate, using least-squares analysis, the equilibrium modulus, E.

Biochemistry. Sample strips in Experiments 1 and 2 were cut into segments of equal length (5 segments for AC or 3 segments for GPC) to allow separate biochemical analysis of different tissue layers. The number of layers was chosen to correspond to the initial length of the strips (5 mm for AC, 3 mm for GPC), and layer 1 was defined to start from the articular surface for AC and from the epiphysis for GPC. Sample strip layers and whole disks from Experiment 3 were solubilized by digestion with proteinase K (Roche Diagnostics, Indianapolis, IN) in 5% EDTA at 60°C for 18 h.

Portions of the sample digests were mixed with EcoLume scintillation fluid and assessed for calcium uptake by scintillation counting for incorporated $^{45}Ca^{++}$ radioactivity using a LKB/Wallac RackBeta 1214 Liquid Scintillation Counter, which has been correlated with total mineral accumulation [8, 39]. A portion of radio-labeled medium (with known calcium concentration) was analyzed for $^{45}Ca^{++}$ radioactivity in order to estimate a conversion factor between counts and absolute calcium content. For Experiment 3, portions of the sample tissue digest were analyzed to quantify content of sulfated GAG [15], hydroxyproline [40], and DNA [33]. DNA was converted to cell number using a conversion constant of 7.7 pg DNA per cell [28] and hydroxyproline was converted to collagen by assuming a mass ratio of collagen:hydroxyproline equal to 7.25:1 [38].

Statistics. Data are presented as mean ± SEM and were log-10 transformed for statistical analysis. In Experiments 1 & 2, ANOVA was used to assess effects with a fixed factor of tissue layer (1-5 for AC, 1-3 for GPC) and a repeated factor of culture duration (0, 1, 2, or 3 weeks) or culture condition (dead tissue with ßGP, live tissue with no ßGP, live tissue with ßGP). In Experiment 3, ANOVA was used to assess effects with a fixed factor of tissue layer (1 or 5 for AC, 1 or 3 for GPC) and repeated factor of culture condition (freshly isolated, culture with no ßGP, culture with ßGP). The relationship between equilibrium modulus and calcium, water, GAG, and collagen content in Experiment 3 was analyzed using linear regression. Tukey's post-hoc comparisons were used, with P values less than 0.05 considered significant.

3.4 Results

Experiment 1: Time course with ßGP. During the 3-week culture period, AC and GPC samples developed an orange-brown pigmentation which appeared during the culture period in regions of calcification (**Fig. 2A.iv.a, B.iv.a**). In AC, the orange-brown coloration was evident in the deep region of samples by week 2 and remained in the deep ~25% of tissue. In GPC, the orange-brown pigmentation appeared on both the metaphyseal and epiphyseal ends during week 1 of culture and advanced towards the middle to cover about ~50% of the sample area by week 3. The source of the pigmentation is unclear but is not associated with tissue fixation.

Histological staining with H&E and Alizarin Red S showed different calcification patterns for AC and GPC (Fig. 2, 3, S1). In AC, enlarged chondrocytes and calcified matrix were localized to the deep ~25% of AC. Chondrocytes appeared to be randomly organized **(Fig. 2A.iv.d, 3A)** with Alizarin Red-stained matrix completely surrounding the cells **(Fig. 2A.iv.e, 3B)**. For GPC, there was a different pattern of calcification for the epiphyseal and metaphyseal ends. At the epiphyseal side, the organization of cells and mineral was similar to deep AC **(Fig. 2B.iv.b, 2B.iv.c, 3CD)**, while at the metaphyseal side, the chondrocytes were stacked in columns **(Fig. 2B.iv.d, 3E)** with Alizarin Red-stained matrix between cell columns **(Fig. 2B.iv.e, 3F)**.

Indentation stiffness was dependent on culture duration for both AC and GPC ($P < 0.01$), with a significant interaction with tissue layer for AC ($P < 0.005$) but not for GPC ($P = 0.07$) **(Fig 4AB) (Table 1).** For AC, the indentation stiffness of layer 5

(deep 20%) at week 3 was 2.9 N/mm, 4-fold higher than its stiffness at week 1 ($P < 0.05$). For GPC, the indentation stiffness of layer 3 at week 3 was 1.1 N/mm, 3-fold higher than at week 1 ($P < 0.05$).

Ca^{++} uptake was dependent on culture duration for both AC and GPC ($P < 0.001$), with a significant interaction with tissue layer for AC ($P < 0.001$) **(Fig 4CD)**. For AC, Ca^{++} uptake by layer 5 increased 6-fold from 1.2 μmol to 6.6 μmol Ca^{++} between week 1 and 3 ($P < 0.01$). Similarly, Ca^{++} uptake by layer 3 of GPC increased from 1.2 μmol to 6.7 μmol Ca^{++} between week 1 and 3 ($P < 0.05$).

Experiment 2: Effects of cell viability and βGP. The effects of cell viability and βGP were evident in the macroscopic appearance of AC and GPC samples. Dead AC samples did not change in appearance from time of harvest (**Fig. 2A.ii.a**), whereas AC with no βGP had some orange pigmentation at the deep edge that did not extend into the tissue (**Fig. 2A.iii.a**). For GPC, both dead samples and samples with no βGP developed orange pigmentation on the epiphyseal and metaphyseal edges that did not extend into the tissue (**Fig. 2B.ii.a, 2B.iii.a**). Histological staining revealed similar cell and mineral organization as described in Experiment 1.

Indentation stiffness was dependent on cell viability and βGP for AC ($P < 0.01$) with a significant interaction with tissue layer ($P <0.01$) **(Fig. 4EF) (Table 1)**. The stiffness of layer 5 of AC was ~3-fold lower for dead samples and samples without βGP than for samples with βGP ($P <0.05$) **(Fig. 4E)**. Indentation stiffness of GPC layers 1 and 3 followed a similar trend **(Fig 4F)**.

Ca^{++} uptake was dependent on cell viability and βGP for AC ($P < 0.001$) and for GPC ($P < 0.001$), with a significant interaction with tissue layer for AC ($P < 0.001$) **(Fig. 4GH)**. Ca^{++} uptake by layer 5 of AC was 10-fold lower for dead samples and samples with no βGP than for samples with βGP ($P < 0.05$) **(Fig. 4G)**. Ca^{++} uptake by GPC layers 1 and 3 followed a similar trend **(Fig. 4H)**.

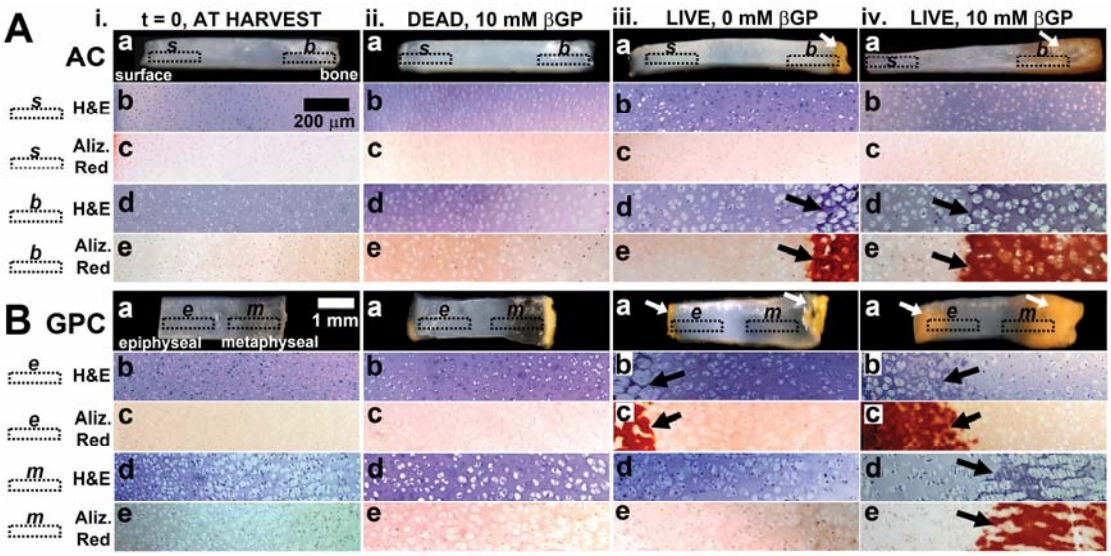

Figure 3.2: Macroscopic and microscopic views of AC (**A**) and GPC (**B**), fresh (**i**) and after 3wk incubation of dead tissue in medium supplemented with 10 mM β-glycerophosphate (**ii**), live tissue in medium with 0mM β-glycerophosphate (**iii**), and live tissue with 10 mM β-glycerophosphate (**iv**). Micrographs are of regions indicated: *s, b, e, m*. Arrows indicate areas of calcification..

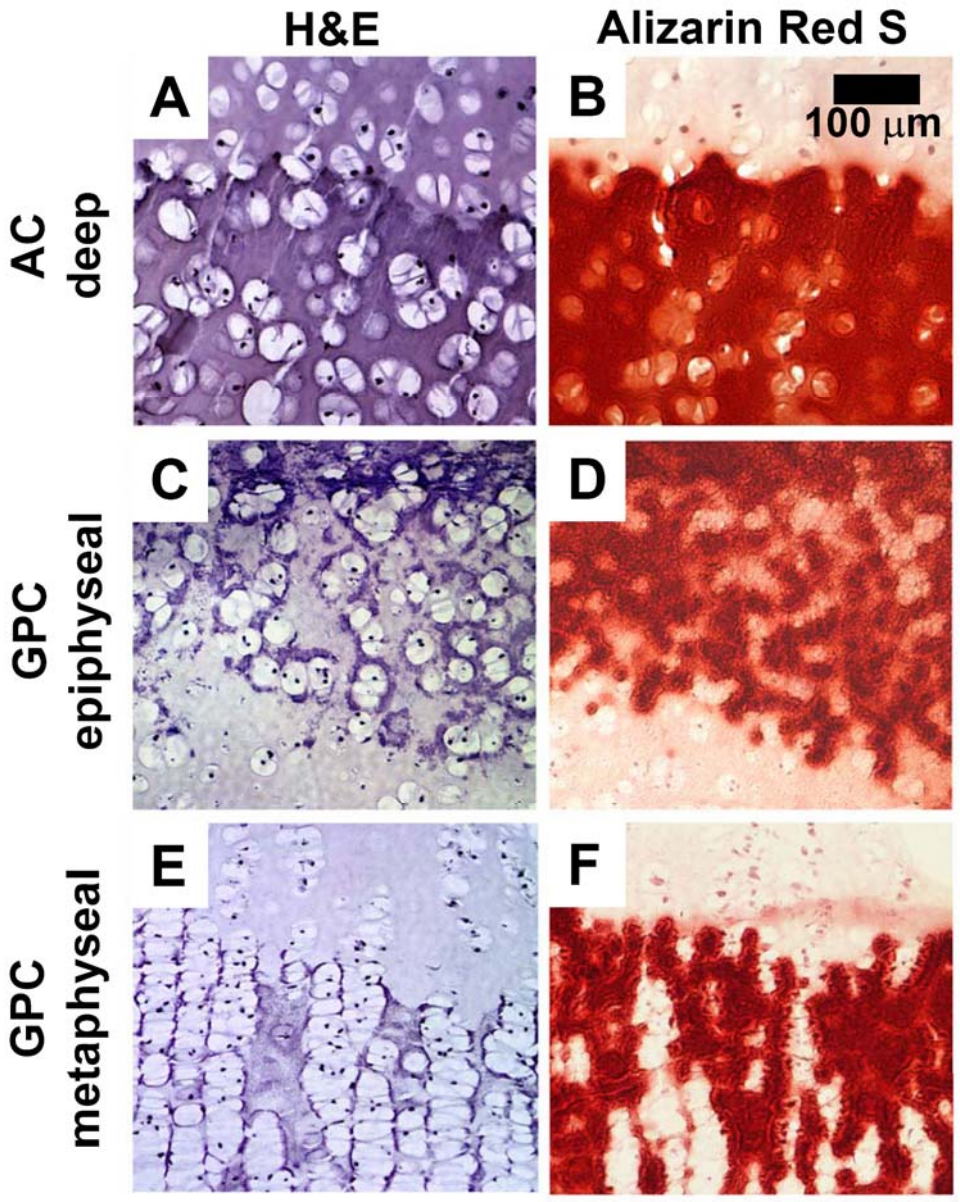

Figure 3.3: Deep region of AC (A, B), epiphyseal end of GPC (C, D), and metaphyseal end of GPC (E, F) after incubation in medium supplemented with 10 mM β-glycerophosphate for 3 weeks. Sections are stained with Hematoxylin & Eosin (A, C, E) or Alizarin Red S (B, D, F).

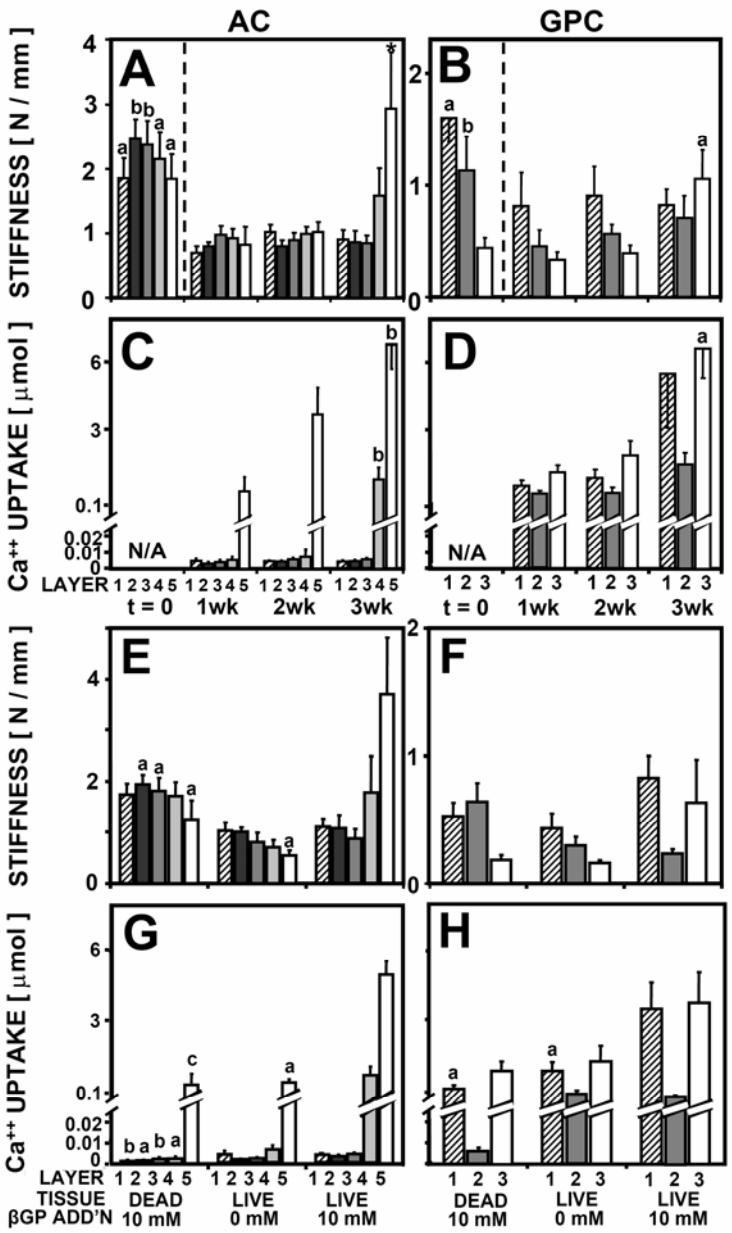

Figure 3.4: Indentation stiffness (**A, B, E, F**) and $^{45}Ca^{++}$ uptake (**C, D, G, H**) by AC (**A, C, E, G**) and GPC (**B, D, F, H**) as a function of tissue layer and culture duration up to 3 weeks, n = 6-8 (**A-D**) and as a function of tissue layer, cell viability, and media supplementation with βGP after incubation for 3 weeks, n = 6-8 (**E-H**). Significant differences from t=1wk (**A-D**) or from live tissue with 10 mM βGP addition (**E-H**) are indicated by a ($p<0.05$), b ($p<0.01$), c ($p<0.001$).

Experiment 3: Effects of zone and βGP. The effects of tissue zone and βGP were evident in the macroscopic appearance of AC and GPC disks. Disks from AC layer 5 and from GPC incubated with βGP became orange-brown in color, while disks from AC layer 1 remained white and glossy.Samples incubated with no βGP did not change in appearance from time of harvest.

The equilibrium unconfined compressive modulus was dependent on βGP for both AC ($P < 0.01$) and GPC ($P < 0.001$), with an interaction with tissue zone for AC ($P < 0.01$) **(Fig. 5AB) (Table 1).** For layer 1 of AC, βGP did not affect the modulus, which was ~0.1 MPa either with or without βGP. For layer 5 of AC, samples with βGP had a modulus of 0.53 MPa, 9-fold higher than samples without βGP ($P < 0.001$). For GPC, both layer 1 and 3 had a higher modulus with βGP.

Ca^{++} uptake was dependent on βGP for both AC ($P < 0.001$) and GPC ($P <0.001$), with an interaction with tissue zone for AC ($P < 0.01$) **(Fig. 5CD)**. Ca^{++} uptake results followed similar trends as described in Experiments 1 and 2.

Water content was dependent on βGP for AC ($P < 0.001$) and GPC ($P <0.001$), with an interaction with tissue zone for AC ($P < 0.05$) **(Fig. 5EF)**. For AC samples, layer 5 AC with βGP had 5% lower water content than samples without βGP ($P < 0.05$), but there was no difference for layer 1. Water content of both layers 1 and 3 GPC decreased with βGP ($P < 0.001$). Biochemical content, including GAG, collagen, and cell number, did not change with βGP for AC or GPC (**Fig, 5GHIJKL)**. GAG, collagen, and cell content were higher in layer 1 of GPC than in layer 3 ($P < 0.05$).

The equilibrium modulus correlated positively with Ca^{++} content for AC ($P < 0.001$, $R^2 = 0.70$) and for GPC ($P < 0.01$, $R^2 = 0.30$) and correlated negatively with water content for AC ($P < 0.01$, $R^2 = 0.18$) and for GPC ($P < 0.001$, $R^2 = 0.44$). For fresh samples and samples incubated without βGP, equilibrium modulus correlated positively with collagen content for AC ($P < 0.001$, $R^2 = 0.49$) and with both GAG and collagen content for GPC ($P < 0.001$, $R^2 = 0.71$).

Table 3.1: Indentation stiffness and equilibrium modulus of AC and GPC, fresh and after 3 weeks of culture with either no β-glycerophosphate (βGP) or 10 mM βGP.

		Indentation Stiffness (N/mm)			Equilibrium Modulus (MPa)		
Tissue	Layer	Fresh	0 mM βGP	10 mM βGP	Fresh	0 mM βGP	10 mM βGP
Articular cartilage	1	1.85	1.03	0.91	0.24	0.12	0.13
	2	2.46	1.00	0.86	—	—	—
	3	2.37	0.80	0.87	—	—	—
	4	2.15	0.71	1.58	—	—	—
	5	1.84	0.55	2.93	0.33	0.057	0.53
Growth plate cartilage	1	1.60	0.44	0.82	0.23	0.064	0.64
	2	1.13	0.29	0.71	—	—	—
	3	0.44	0.16	1.05	0.035	0.006	0.16

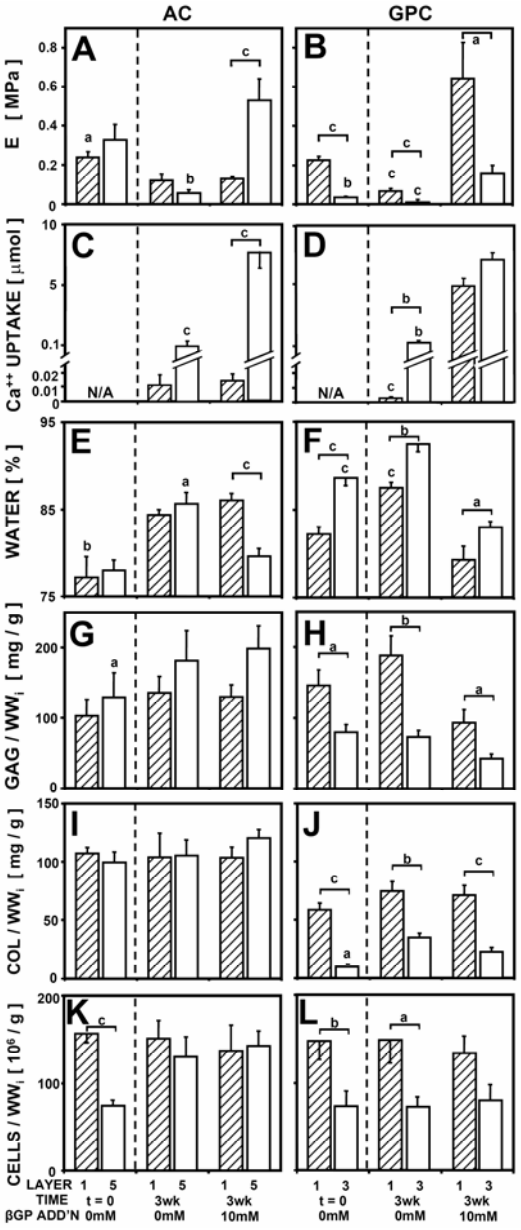

Figure 3.5: Equilibrium modulus (**A, B**), $^{45}Ca^{++}$ uptake (**C, D**), water content (**E, F**), GAG content (**G, H**), collagen content (**I, J**), and cell number (**K, L**) for AC (**A, C, E, G, I, K**) and GPC (**B, D, F, H, J, L**), as a function of tissue layer and media supplementation with βGP, n = 6-10. Significant differences from tissue with 10 mM βGP or between tissue layers 1 and 5 (or 3) are indicated by a ($p<0.05$), b ($p<0.01$), c ($p<0.001$).

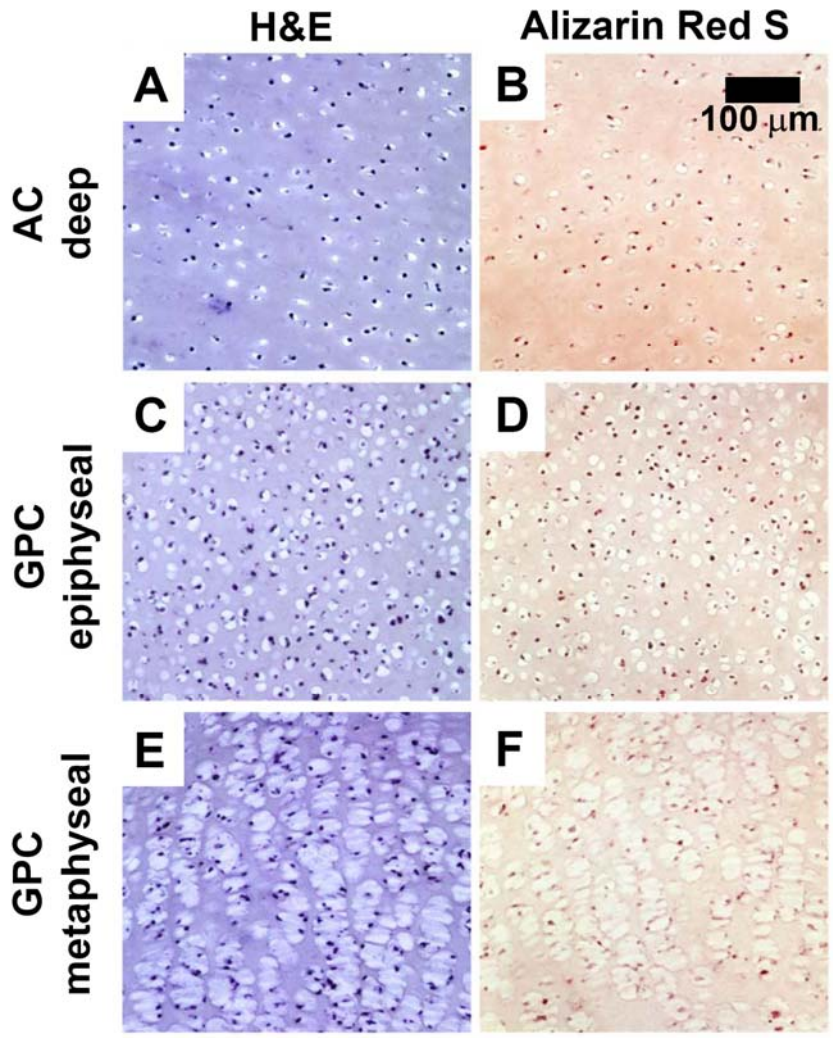

Figure 3.S1: Deep region of AC (**A, B**), epiphyseal end of GPC (**C, D**), and metaphyseal end of GPC (**E, F**) at time of harvest. Sections are stained with Hematoxylin & Eosin (**A, C, E**) or Alizarin Red S (**B, D, F**).

3.5 Discussion

The results presented here indicate that the deep ~20% of immature AC can undergo calcification within 3 weeks of *in vitro* explant culture, with functional biomechanical consequences related to the extent of calcification as governed by cell viability and medium supplementation with βGP as a phosphate source. Compared to fresh tissue, incubation of cartilage in medium without βGP resulted in lower tissue stiffness and compressive modulus for all tissue zones, whereas incubation in media with βGP resulted in calcification and markedly higher tissue stiffness and modulus (2-fold higher than fresh tissue and 4-fold higher than tissue incubated without βGP) in specific regions of AC and GPC. The regions of cartilage that calcified *in vitro* were the 1 mm of AC adjacent to the subchondral bone (layer 5) and 1 mm from each end of GPC adjacent to the epiphyseal and metaphyseal bone (layers 1 and 3). Zonal variations in calcification were maintained whether zones were incubated together as intact tissue (Experiments 1 and 2) or incubated separately (Experiment 3). Calcification patterns in AC and GPC had a distinct structure of mineral organization around cells, consistent with their expected *in vivo* phenotypes. In the deep immature AC, mineral was deposited around cells, similar to the organization seen in epiphyseal GPC but different from metaphyseal GPC, in which mineral was deposited primarily between cell columns. Such structure-metabolism-function relationships have implications for the mechanisms and consequences of native cartilage maturation, as well as strategies for tissue engineering to establish the ZCC.

The results of the study reflect, in part, various parameters chosen for study in explant culture, including the use of β-GP as a phosphate source in the calcifying medium to modulate mineral deposition in the cartilage matrix. Medium supplementation with 10 mM βGP has been commonly used in studies of osteoblast cultures to promote calcium phosphate deposition *in vitro* [12], with βGP acting as a source of phosphate due to its efficient hydrolysis by the alkaline phosphatase secreted by cells and present in serum [12, 27]. In cultures of cells such as osteoblasts, the use of βGP exceeding 2 mM may result in supraphysiological levels of medium phosphate (compared to physiological levels of 1.0-1.5 mM phosphate and ~3 mM organic phosphate) [12], leading to non-specific precipitation of mineral *in vitro*. In the present study, the low serum concentration (1%) and a relatively low rate of alkaline phosphatase secretion by chondrocytes within cartilage explants, along with the hindered transport of macromolecules within cartilage, may have maintained a physiological process of mineral precipitation in the cartilage matrix.

The calcified cartilage formed *in vitro* from deep immature AC had an equilibrium modulus of 0.53 MPa in unconfined compression, 4-fold higher than the modulus for cartilaginous calcified tissue formed *in vitro* by AC deep zone chondrocytes in a previous study [2]. The higher stiffness of calcified explants may be due to higher Ca^{++} content as well as higher collagen content from using the native matrix rather than building a new cartilaginous matrix. The equilibrium modulus of calcified metaphyseal GPC was 0.16 MPa, 3-fold lower than calcified deep zone AC despite having similar Ca^{++} uptake. This can be attributed to the lower collagen and GAG content in the GPC matrix compared to the AC. The stiffness of *in vitro*

mineralized explants in the present study was still lower than that of native ZCC in bovine femur, which has an elastic modulus of 320 MPa estimated in three-point bending [34].

The selective *in vitro* calcification of immature deep zone AC over 3 weeks is consistent with previous studies and extends those findings by providing a tissue-level view of *in vitro* calcification. The calcification of the deep 20% of AC explants *in vitro* in the presence of βGP supports previous findings that deep zone articular chondrocytes cultured in monolayer or at high density mineralize under stimulatory conditions, while superficial zone chondrocytes can resist mineralization [23, 25, 42]. Unlike monolayer chondrocyte cultures, which are subject to dedifferentiation [7] and may have effects on cell hypertrophy and mineralization, explant cultures maintain the chondrocyte phenotype since the cells remain within their native extracellular matrix. In the present study, the surface region (layer 1) of AC resisted mineralization in the presence of βGP, but did not inhibit mineralization of the deep zone when incubated together as intact full-thickness samples. Further investigation is needed to determine whether any inhibitory factors were secreted by the superficial zone chondrocytes and whether such factors were unable to inhibit mineralization in the deep zone due to hindered transport through the cartilage matrix.

In the present study, incubation of deep zone AC for 3 weeks in medium with βGP resulted in a Ca^{++} content of 7.1 μmol per disk, or 8.4 wt% Ca^{++}. This is similar to the Ca^{++} content of 9.1 wt% found for the ZCC of 9-month-old bovine [24], but lower than the 21 wt% in the ZCC of a 2-year-old bovine [30] and the 24 wt% in ZCC of mature human patella [43]. In mineralizing chondrocyte cultures, deep zone

chondrocytes can form mineral deposits within 1 day after addition of calcification medium, with progressive mineralization and accumulation of up to 6.5 wt% Ca^{++} content after 8 weeks of culture [23, 25]. Incubation of AC explants for longer times *in vitro* may result in mineral content approaching levels found in native mature ZCC.

The form of mineral deposited in the deep layer of immature AC explants and in GPC explants remains to be established. The calcification endpoint measures of $^{45}Ca^{++}$ uptake and Alizarin Red S staining were chosen to provide complementary information; however, they do not differentiate between different mineral phases, since they are both indices of calcium bound in the cartilage matrix. It remains to be determined whether the deposited mineral was comprised of amorphous calcium deposits or a more mature phase such as hydroxyapatite.

The use of young animals in the present study may have affected the type of calcified cartilage matrix that was formed. In immature AC where the ZCC has not yet developed, full-thickness AC explants include the articular epiphyseal complex cartilage, which normally becomes replaced by bone to expand the secondary ossification center and provide radial growth [10]. Thus, the calcification of deep immature AC in the present study is not necessarily equivalent to the formation of mature ZCC *in vivo*, which is likely a late event in the terminal differentiation of chondrocytes deriving from the superficial zone [21]. The use of immature AC may serve as a model to study transplantation of engineered cartilaginous tissues, which would likely resemble immature cartilage in terms of cellularity and matrix content and may respond similarly to *in vitro* stimuli as immature AC. In addition, the calcification of immature cartilage matrix *in vitro* could be applicable to form a ZCC-

like tissue that can be functionally equivalent to the native ZCC in an engineered osteochondral graft.

The modulated increase in stiffness associated with tissue calcification may be useful for tissue engineering methods to create a ZCC-like tissue to facilitate the biomimetic attachment of a cartilaginous tissue to a bony substrate. Anchoring cartilaginous tissue to bone is an important step toward the ultimate goal of fabricating a large osteochondral graft capable of withstanding physiological joint articulation soon after implantation. The *in vitro* culture of AC explants is useful not only for providing insight into critical biological questions in the development of the native osteochondral interface, but also for designing methods to integrate the cartilage-bone interface in chondral and osteochondral graft treatments for damaged cartilage or osteoarthritis.

3.6 Acknowledgments

We would like to thank co-authors Espoir M. Kyubwa, Drs. Won C. Bae, William D. Bugbee, Koichi Masuda, and Robert L. Sah for their contributions to this work. We would like to acknowledge SAGE Publications, Inc. for permission to reprint, in full, Chapter 3 which has been published OnlineFirst in *Cartilage*. This work was supported by the National Institute of Health and the Howard Hughes Medical Institute through the Professors Program Grant to UCSD for Dr. Robert L. Sah.

3.7 References

1. Ahsan T, Lottman LM, Harwood FL, Amiel D, Sah RL: Integrative cartilage repair: inhibition by beta-aminoproprionitrile. *J Orthop Res* 17:850-7, 1999.

2. Allan KS, Pilliar RM, Wang J, Grynpas MD, Kandel RA: Formation of biphasic constructs containing cartilage with a calcified zone interface. *Tissue Eng* 13:167-77, 2007.

3. Anderson DD, Brown TD, Radin EL: The influence of basal cartilage calcification on dynamic juxtaarticular stress transmission. *Clin Orthop Rel Res* 286:298-307, 1993.

4. Asanbaeva A, Masuda K, Thonar EJ, Klisch SM, Sah RL: Mechanisms of cartilage growth: modulation of balance between proteoglycan and collagen in vitro using chondroitinase ABC. *Arthritis Rheum* 56:188-98, 2007.

5. Bae WC, Schumacher BL, Sah RL: Indentation probing of human articular cartilage: effect on chondrocyte viability. *Osteoarthritis Cartilage* 15:9-18, 2007.

6. Ballock RT, O'Keefe RJ: The biology of the growth plate. *J Bone Joint Surg Am* 85-A:715-26, 2003.

7. Benya PD, Shaffer JD: Dedifferentiated chondrocytes reexpress the differentiated collagen phenotype when cultured in agarose gels. *Cell* 30:215-24, 1982.

8. Boskey AL, Stiner D, Doty SB, Binderman I, Leboy P: Studies of mineralization in tissue culture: optimal conditions for cartilage calcification. *Bone Miner* 16:11-36, 1992.

9. Boustany NN, Gray ML, Black AC, Hunziker EB: Correlation between synthetic activity and glycosaminoglycan concentration in epiphyseal cartilage raises questions about the regulatory role of interstitial pH. *J Orthop Res* 13:733-9, 1995.

10. Carlson CS, Hilley HD, Henrikson CK: Ultrastructure of normal epiphyseal cartilage of the articular-epiphyseal cartilage complex in growing swine. *Am J Vet Res* 46:306-13, 1985.

11. Chen AC, Bae WC, Schinagl RM, Sah RL: Depth- and strain-dependent mechanical and electromechanical properties of full-thickness bovine articular cartilage in confined compression. *J Biomech* 34:1-12, 2001.

12. Chung CH, Golub EE, Forbes E, Tokuoka T, Shapiro IM: Mechanism of action of beta-glycerophosphate on bone cell mineralization. *Calcif Tissue Int* 51:305-11, 1992.

13. Currey J. Collagen and the Mechanical Properties of Bone and Calcified Cartilage. 1st ed. New York, NY: Springer; 2008.

14. Currey JD: The effect of porosity and mineral content on the Young's modulus of elasticity of compact bone. *J Biomech* 21:131-9, 1988.

15. Farndale RW, Buttle DJ, Barrett AJ: Improved quantitation and discrimination of sulphated glycosaminoglycans by use of dimethylmethylene blue. *Biochim Biophys Acta* 883:173-7, 1986.

16. Farnum CE, Wilsman NJ: Determination of proliferative characteristics of growth plate chondrocytes by labeling with bromodeoxyuridine. *Calcif Tissue Int* 52:110-9, 1993.

17. Ferguson VL, Bushby AJ, Boyde A: Nanomechanical properties and mineral concentration in articular calcified cartilage and subchondral bone. *J Anat* 203:191-202, 2003.

18. Gupta HS, Schratter S, Tesch W, Roschger P, Berzlanovich A, Schoeberl T, Klaushofer K, Fratzl P: Two different correlations between nanoindentation modulus and mineral content in the bone-cartilage interface. *J Struct Biol* 149:138-48, 2005.

19. Hall BK, Newman S. Cartilage: Molecular Aspects: CRC Press; 1991.

20. Huitema LF, Vaandrager AB: What triggers cell-mediated mineralization? *Front Biosci* 12:2631-45, 2007.

21. Hunziker EB, Kapfinger E, Geiss J: The structural architecture of adult mammalian articular cartilage evolves by a synchronized process of tissue resorption and neoformation during postnatal development. *Osteoarthritis Cartilage* 15:403-13, 2007.

22. Hunziker EB, Quinn TM, Hauselmann HJ: Quantitative structural organization of normal adult human articular cartilage. *Osteoarthritis Cartilage* 10:564-72, 2002.

23. Jiang J, Leong NL, Mung JC, Hidaka C, Lu HH: Interaction between zonal populations of articular chondrocytes suppresses chondrocyte mineralization and this process is mediated by PTHrP. *Osteoarthritis Cartilage* 16:70-82, 2008.

24. Kandel R, Hurtig M, Grynpas M: Characterization of the mineral in calcified articular cartilagenous tissue formed in vitro. *Tissue Eng* 5:25-34, 1999.

25. Kandel RA, Boyle J, Gibson G, Cruz T, Speagle M: In vitro formation of mineralized cartilagenous tissue by articular chondrocytes. *In Vitro Cell Dev Biol Anim* 33:174-81, 1997.

26. Kempson GE, Tuke MA, Dingle JT, Barrett AJ, Horsfield PH: The effects of proteolytic enzymes on the mechanical properties of adult human articular cartilage. *Biochim Biophys Acta* 428:741-60, 1976.

27. Khouja HI, Bevington A, Kemp GJ, Russell RG: Calcium and orthophosphate deposits in vitro do not imply osteoblast-mediated mineralization: mineralization by betaglycerophosphate in the absence of osteoblasts. *Bone* 11:385-91, 1990.

28. Kim YJ, Sah RLY, Doong JYH, Grodzinsky AJ: Fluorometric assay of DNA in cartilage explants using Hoechst 33258. *Anal Biochem* 174:168-76, 1988.

29. Lane LB, Bullough PG: Age-related changes in the thickness of the calcified zone and the number of tidemarks in adult human articular cartilage. *J Bone Joint Surg Br* 62:372-5, 1980.

30. Lovell T, Eyre D: Unique biochemical characteristics of the calcified cartilage zone of articular cartilage. *Trans Orthop Res Soc,* Atlanta, GA, 1988.

31. Mankin HJ: Localization of tritiated thymidine in articular cartilage of rabbits. I. growth in immature cartilage. *J Bone Joint Surg Am* 44-A:682-98, 1962.

32. McGee-Russell S: Histochemical methods for calcium. *J Histochem Cytochem* 6:22-42, 1958.

33. McGowan KB, Kurtis MS, Lottman LM, Watson D, Sah RL: Biochemical quantification of DNA in human articular and septal cartilage using PicoGreen and Hoechst 33258. *Osteoarthritis Cartilage* 10:580-7, 2002.

34. Mente PL, Lewis JL: Elastic modulus of calcified cartilage is an order of magnitude less than that of subchondral bone. *J Orthop Res* 12:637-47, 1994.

35. Muller-Gerbl M, Schulte E, Putz R: The thickness of the calcified layer of articular cartilage: a function of the load supported? *J Anat* 154:103-11, 1987.

36. Oegema T, Jr., Carpenter R, Hofmeister F, Thompson RC, Jr.: The interaction of the zone of calcified cartilage and subchondral bone in osteoarthritis. *Microsc Res Tech* 37:324-32, 1997.

37. Oyajobi BO, Frazer A, Hollander AP, Graveley RM, Xu C, Houghton A, Hatton PV, Russell RG, Stringer BM: Expression of type X collagen and matrix calcification in three-dimensional cultures of immortalized temperature-sensitive

chondrocytes derived from adult human articular cartilage. *J Bone Miner Res* 13:432-42, 1998.

38. Pal S, Tang L-H, Choi H, Habermann E, Rosenberg L, Roughley P, Poole AR: Structural changes during development in bovine fetal epiphyseal cartilage. *Collagen Rel Res* 1:151-76, 1981.

39. Pourmand EP, Binderman I, Doty SB, Kudryashov V, Boskey AL: Chondrocyte apoptosis is not essential for cartilage calcification: evidence from an in vitro avian model. *J Cell Biochem* 100:43-57, 2007.

40. Woessner JF: The determination of hydroxyproline in tissue and protein samples containing small proportions of this imino acid. *Arch Biochem Biophys* 93:440-7, 1961.

41. Wu LN, Ishikawa Y, Genge BR, Wuthier RE: Chondrocytes isolated from tibial dyschondroplasia lesions and articular cartilage revert to a growth plate-like phenotype when cultured in vitro. *J Cell Physiol* 202:167-77, 2005.

42. Zizak I, Roschger P, Paris O, Misof BM, Berzlanovich A, Bernstorff S, Amenitsch H, Klaushofer K, Fratzl P: Characteristics of mineral particles in the human bone/cartilage interface. *J Struct Biol* 141:208-17, 2003.

CHAPTER 4

FETUIN-MEDIATED *IN VITRO* CALCIFICATION OF ADULT BOVINE ARTICULAR CARTILAGE

4.1 Abstract

Objective: To assess the effect of calcium and phosphate concentration and the effect of fetuin on the extent of *in vitro* calcification and cell viability in adult bovine articular cartilage, and to use mass transfer analysis to describe the calcification of cartilage.

Methods: Mature bovine articular cartilage disks were digested with trypsin to remove proteoglycan and incubated in media with calcium chloride ($CaCl_2$) and sodium phosphate (NaH_2PO_4) at physiological levels of 1.8 mM $CaCl_2$ and 2.0 mM NaH_2PO_4, and at supersaturated levels of 5.0 mM each, 7.5 mM each, and 10 mM each, with or without fetuin, for 3 days. The concentration of supernatant calcium in each media was monitored over the culture period. Cartilage disks were analyzed for calcium content, glycosaminoglycan content, cell viability, and localization of bound calcium in the cartilage tissue by histology. A mass transfer model was set up to describe the thickness of the calcified cartilage zone formed at cartilage edges, based on calcium concentration in solution and time.

Results: Calcification of cartilage was evident by 3 days of culture in media with $CaCl_2$ and NaH_2PO_4 starting concentrations of 5 mM and above, dependent on the presence of fetuin in the media. Calcification was highest for samples incubated in media with 7.5 mM starting $CaCl_2$ and NaH_2PO_4 concentrations, which accumulated ~250 μg/cm^2 of calcium, 9 times higher than samples without fetuin. Fetuin helped maintain high supernatant calcium concentration in the media at about half of starting concentration, whereas in media without fetuin, calcium fell to <2 mM within the first 24 h, with formation of precipitate outside of cartilage. Cell viability decreased by ~20 % on tissue edges compared to the bulk for samples incubated in media that promotes calcification. Cartilage exhibited calcification on tissue edges, with a calcified zone thickness of ~30-100 μm by histological analysis, consistent with predictions from the mass transfer analysis.

Discussion: Biomimetic calcification of cartilage mediated by fetuin and accelerated by high concentrations of $CaCl_2$ and NaH_2PO_4 is a feasible strategy to form an engineered zone of calcified cartilage with a thickness of ~30-100 μm at cartilage tissue edges. Such a strategy may be useful for tissue engineering a zone of calcified cartilage-like tissue to facilitate the attachment of cartilaginous tissue to bone and formation of osteochondral grafts able to withstand physiological joint articulation soon after implantation.

4.2 Introduction

The zone of calcified cartilage is a specialized structure at the osteochondral junction that is ~100-300μm in thickness [34] and anchors articular cartilage to underlying subchondral bone. The ZCC is bound on one side by the tidemark, the gently undulating interface with deep zone articular cartilage, and on the other side by the cement line, the highly interdigitated interface with bone. The ZCC is comprised of sparsely distributed chondrocytes expressing the hypertrophic phenotype, which are aligned in columns and enveloped in a calcified matrix [12, 17, 18, 27]. The extracellular matrix of the ZCC contains collagen types II and X, proteoglycan, and hydroxyapatite. Hydroxyapatite mineral is present throughout the ZCC matrix, with small uncalcified regions around the cell columns [6, 40]. The ZCC mineral has carbonated hydroxyapatite crystals of size similar to those found in bone, with mineral particle orientation aligned perpendicular to the interface in the cartilage and parallel to the interface in bone [43]. The ZCC has similar mineral content as bone of 20-24% by dry weight, but is less stiff, probably due to different collagen-mineral packing structure [11, 15]. Thus, the ZCC is a zone of intermediate stiffness between articular cartilage and subchondral bone.

The formation of the native ZCC *in vivo* occurs during postnatal development before reaching skeletal maturity through the calcification of immature AC matrix. Chondrocytes in the deep zone of immature cartilage near the subchondral bone proliferate and form new cartilage matrix, some of which is calcified and becomes resorbed and replaced by the ingrowing front of subchondral bone advancing toward the articular surface [28, 34].This process of new cartilage formation and resorption achieves a steady state with skeletal maturity [23]. In mature osteochondral tissue, the deep zone of articular cartilage is joined to the underlying bone through the

specialized ZCC interface structure, which normally persists throughout adulthood. During osteoarthritis, the ZCC may undergo remodeling to form multiple zones of calcification and move upwards into the cartilage [35]. Besides the formation of the ZCC and the late stages of endochondral ossification in growth plate cartilage during bone development, cartilage does not normally calcify. However, under appropriate conditions, mineralization of cartilage can be induced *in vitro*, with different possible mechanisms for the initiation and growth of mineral in cartilage.

Mechanisms of cartilage calcification involve modifications in matrix composition and achieving high concentrations of calcium and phosphate within a confined space, ultimately resulting in nucleation of mineral onto an organic matrix. Local increases in phosphate concentration can be mediated by alkaline phosphatase, an enzyme which cleaves phospho-compounds to inorganic phosphate and is highly expressed by hypertrophic chondrocytes and other mineralizing cells. Since the physiological organic phosphate substrate is unknown, some *in vitro* studies of calcification use β-glycerophosphate (β-GP) as an organic phosphate source [19, 21]. Initiation of calcification after the local increase in calcium and phosphate may occur within matrix vesicles, which are secreted by mineralizing cells and can concentrate calcium and phosphate to nucleate mineral crystals. Once the crystal is large enough, it can rupture the membrane of the matrix vesicle and contribute to the calcified matrix [1]. Calcification of cartilage *in vitro* can be achieved over extended periods in culture in the appropriate conditions. In a cartilage explant model, incubation of deep zone mmature articular cartilage in media supplemented with 10 mM β-GP resulted in accumulation of 285 μg of calcium, or 8.4 wt% over three weeks [19].

Mineralization may also be regulated by non-collagenous proteins which include proteoglycans, glycoproteins, the gla-containing proteins, and serum

associated proteins, including fetuin [16]. Fetuin is a 48 kDa glycoprotein that is synthesized in the liver and found in high concentrations in mammalian serum and bone. Fetuin binds strongly to apatite and inhibits its growth and precipitation in serum. Purified bovine fetuin has been shown to inhibit the growth and precipitation of a calcium phosphate mineral phase *in vitro* from supersaturated solutions of calcium and phosphate by the formation of a large fetuin-mineral complex [38, 41]. Fetuin is the essential component in serum for the serum-induced mineralization of collagen I fibrils, and can mineralize fibrils alone in a buffered solution of 5mM calcium and 5 mM phosphate [39]. The fetuin-mediated calcification mechanism is based on the nucleation of calcium phosphate mineral from a metastable supersaturated solution and selective crystal growth in the space where fetuin is excluded. Therefore, a matrix can undergo fetuin-mediated calcification if it can exclude fetuin based on size. Fetuin-mediated calcification has localized calcification to the inside of collagen I fibrils from bone and tendon, as well as synthetic matrices with similar size exclusion characteristics to collagen fibrils [39].

The removal of proteoglycan may enhance cartilage calcification. In the growth plate, the onset of mineralization is associated with a decrease in proteoglycan matrix content [26]. Proteoglycans have also been shown to be effective inhibitors of hydroxyapatite formation *in vitro*. Proteoglycans are highly charged and can bind calcium ions and restrict solute motility, which may be a barrier to hydroxyapatite nucleation and growth. Additionally, it is likely that the physical size and highly branched conformation of the proteoglycan aggregate interfere sterically with the growth of hydroxyapatite crystals. The removal of GAG would reduce this steric effect and increase the diffusivity of the cartilage matrix. *In vitro* studies suggest that removal of GAG subunits is necessary for calcification to take place [4]. Treatment of

cartilage explants with trypsin removes tissue proteoglycan without markedly affecting cell content or viability [25], and the existing collagen II network in the cartilage matrix should remain unaffected.

Analytical models of calcium phosphate crystallization have been useful for characterizing the kinetics of hydroxyapatite precipitation from metastable supersaturated solutions [20]. Kinetic models of hydroxyapatite growth typically use a hydroxyapatite seed material, which results in the formation of highly crystalline stoichiometic hydroxyapatite without formation of a precursor phase [22]. Such models have found the rate of hydroxyapatite formation to be first order with respect to calcium and phosphate concentration, with the rate of hydroxyapatite formation being a function of the degree of solution supersaturation. Models for the mineralization of bone osteons and tooth enamel have described precipitation of hydroxyapatite using mass transport of calcium and phosphate ions through a diffusion layer [24, 32]. Mass transfer analysis may be useful for describing the precipitation of hydroxyapatite in cartilage in metastable supersaturated solutions of calcium and phosphate.

The hypothesis of this study was that calcification of trypsin-treated adult articular cartilage in medium containing metastable supersaturated calcium and phosphate concentrations up to 10 mM is dependent on fetuin and increases with increasing concentrations of calcium and phosphate. The objectives of this study were (1) to assess the effect of calcium and phosphate concentrations and the effect of fetuin on the extent of *in vitro* calcification and cell viability in adult bovine articular cartilage, and (2) to use mass transfer analysis to describe the chemical calcification of cartilage.

4.3 Materials and Methods

Cartilage harvest and trypsin digestion. Osteochondral blocks were harvested from the patella of adult bovine knee (3 animals). From each block, the superficial slice (0.2-0.3mm thick for adult) was removed, and the next slice (1mm thick) was harvested as middle zone tissue. Cartilage disks were punched using disposable dermal punches with 4mm diameter. Calf cartilage disks were incubated 4 hours, at 37°C and 5% CO_2 on a nutator, in 25 tissue volumes of complete medium DMEM+ (DMEM, 10mM HEPES, 0.1 mM nonessential amino acids, 0.4 mM L-proline, 2 mM L-glutamine, 100 U/ml penicillin, 100 μg/ml streptomycin, 0.25 μg/ml amphotericin), with 10 μg/ml trypsin. To stop the digestion, samples were rinsed with DMEM+ with 20% FBS three times for 10 minutes each.

Cartilage calcification culture. Cartilage disks (n=5-6) were incubated individually in an excess of medium (2000 times tissue volume) to ensure that calcification of cartilage would not be limited by lack of calcium and phosphate ions in solution. Eight different media solutions were made from DMEM+ with 100 μg/ml ascorbate, to make media of final concentrations of 1.8 mM $CaCl_2$ and 2.0 mM NaH_2PO_4, 5.0 mM $CaCl_2$ and 5.0 mM NaH_2PO_4, 7.5 mM $CaCl_2$ and 7.5 mM NaH_2PO_4, and 10 mM $CaCl_2$ and 10 mM NaH_2PO_4, at pH 7.3. Media solutions were prepared using a procedure designed to achieve the near instantaneous mixing of calcium and phosphate in order to ensure that subsequent mineral formation occurred by homogenous nucleation , as described previously [39]. Each media was made without fetuin and with addition of 0.1 mM (5mg/ml) of bovine fetuin (Sigma-Aldrich, St.

Louis, MO) (Table 4.1). Samples were incubated for 3 days (72h) at at 37°C and 5% CO_2 on a nutator, and aliquots of media were taken from each sample 3 times each day (at 0h, 3h, and 9h) and assayed for calcium concentration using the o-cresophthalein complexone calcium assay. At the end of the termination period, cartilage disks were cut into quarters for subsequent endpoint analysis. One quarter-disk was used to assess calcium content, one quarter for Live/Dead and Alizarin Red S staining, one quarter for the DMMB assay for glycosaminoglycan (GAG) content, and the last quarter-disk was used for histology.

O-cresolphthalein complexone assay for calcium. Cartilage quarter-disks were incubated in 1 N HCl for 24 h at 110°C to extract calcium and hydrolyze cartilage. The acid was evaporated and samples were reconstituted in deionized water before colorimetrically assaying for calcium content using cresolphthalein complexone, as described previously [39]. Calcium content was normalized to disk surface area. Aliquots from calcification media were centrifuged to sediment the precipitate, and only the supernatant solution was assayed.

Table 4.1: Experimental design with different media concentrations of calcium chloride and sodium phosphate, without or with addition of fetuin

$CaCl_2$ final [mM]	NaH_2PO_4 final [mM]	fetuin
1.8	2.0	–
		+
5.0	5.0	–
		+
7.5	7.5	–
		+
10	10	–
		+

Live/Dead staining and quantitative analysis. To assess cell viability, cartilage quarter-disks were incubated in a solution of calcein AM and ethidium homodimer-1 for 20 minutes at room termperature. Images of live cells and dead cells were obtained for the vertical profile of the disk cross-section by fluorescence photomicroscopy. The images were processed to count live and dead cells using a custom MATLAB program as previously described [36]. Briefly, images were processed by filtering to reduce noise and thresholded with size criteria (greater than 40 μm^2 for live cells and 15 μm^2 for dead cells) to identify cells. Cell viability was calculated as the percentage of live cells divided by the total cells, and was determined for the overall cartilage thickness, for the cartilage edges (15% of sample thickness from top and bottom), and for the bulk cartilage (middle 70%).

Alizarin Red S stain. For macroscopic visualization of calcification, cartilage quarter-disks were incubated at room temperature in a staining solution of 0.0015% wt: vol Alizarin Red S in 0.5% KOH for 24 h. Samples were destained in 0.05% KOH for 24 h, and photographed, as described previously [39].

DMMB assay for GAG. Cartilage quarter-disks were digested with proteinase K (Roche Diagnostics, Indianapolis, IN) overnight and portions were analyzed for sulfated GAG as a measure of proteoglycan content using the DMMB assay [10].

Histological staining with Alizarin Red S and Toluidine Blue. Cartilage quarter-disks were fixed in 4% paraformaldehyde in PBS overnight, embedded in OCT, and tissue cross-sections were obtained at 5 μm thickness using a cryostat. Sections were stained with 2% Alizarin Red S at pH 4.2 for 2 minutes [33]or with 0.04% Toluidine blue in acetate buffer at pH 4.0 for 10 minutes.

Statistics. To assess difference in supernatant calcium, ANOVA was used with a fixed factor of fetuin (±) and repeated factor of culture time. To assess differences in calcium and GAG content, ANOVA was used with fixed factors of medium calcium concentration (1.8, 5.0, 7.5, or 10 mM) and fetuin (±). To assess differences in cell viability, ANOVA was used with fixed factors of starting calcium concentration and fetuin, and a repeated factor of tissue region (overall, middle, edge). Tukey's post-hoc comparisons were used, with *P* values less than 0.05 considered significant. Data are presented as mean ± SEM

Mass transfer analysis of cartilage calcification. A pseudo-steady state diffusion problem for calcium mass transfer was set up to represent the calcification of cartilage during incubation in calcifying solution. The problem setup is presented in Figure 4.1, and the key variables and parameters are listed in Table 4.2. Calcium ions in solution diffuse from the cartilage surface into the tissue and react at the interface of calcified cartilage (CC) and uncalcified cartilage (UC), $x = \delta$, to form hydroxyapatite, $Ca_{10}(PO_4)_6(OH)_2$, by the chemical reaction:

$$10\ Ca^{2+} + 6\ H_2PO_4^- + 14\ OH^- \rightarrow Ca_{10}(PO_4)_6(OH)_2 + 12\ H_2O \qquad (1)$$

The rate of hydroxyapatite formation was assumed to be controlled by the rate of diffusion of calcium through the CC layer to reach the boundary with UC, where the reaction occurs very rapidly so that free calcium concentration is zero. It was assumed that the reaction to form hydroxyapatite occurs only at the CC-UC interface, which acts as a sink for free calcium mass transfer. The solution was assumed to be well-mixed and to undergo exponential decay of free calcium concentration in the solution, due to the formation of mineral precipitate in the solution outside of cartilage. Fetuin

in the solution results in a different decay constant for free calcium. Finally, it was assumed that the rate of CC formation is slow enough so that at a given CC thickness δ, there is no accumulation of reactants or products within the CC layer. However, the thickness of the CC layer increases with time, making this a pseudo-steady-state process. The mass transfer analysis was used to predict the thickness of the CC layer, δ, as a function of time.

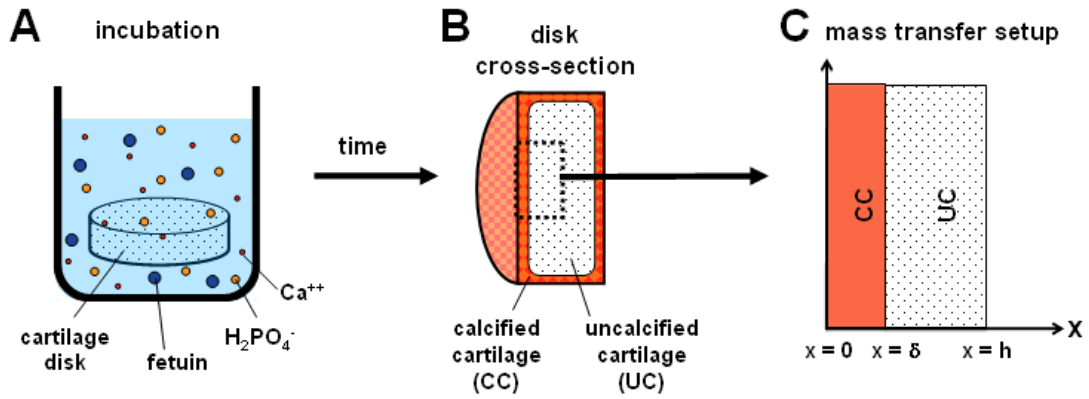

Figure 4.1: Schematic of model setup for mass transfer analysis of cartilage calcification. (**A**) Incubation of cartilage disk in media solution containing calcium ions (Ca^{++}), phosphate ions ($H_2PO_4^-$), and fetuin results in (**B**) calcification of cartilage that forms inwards from the cartilage surfaces. (**C**) Problem setup for one-dimensional diffusion of calcium from cartilage edge into tissue to form calcified cartilage (CC) of thickness δ.

Table 4.2: Key variables and parameters in the mass transfer analysis

variables	description	units
x	position within the cartilage	cm
t	time	s
$c_{Ca}(x, t)$	concentration of free (unbound) Ca^{++} in cartilage	mg / ml
$J_{Ca}(x, t)$	flux of free Ca^{++} ions	mg / ($cm^2 \cdot s$)
$\delta(t)$	thickness of CC layer	cm
$c_s(t)$	concentration of free Ca^{++} in solution	mg / ml
parameters	**description**	**units**
c_0	initial free Ca^{++} in solution	mg / ml
λ	decay constant for free Ca^{++} in solution	s^{-1}
λ_{fet}	decay constant for free Ca^{++} in solution with fetuin	s^{-1}
D_{Ca}	diffusivity of Ca^{++} in calcified cartilage	cm^2 / s
A	surface area of cartilage sample	cm^2
ρ_{HAP}	density of hydroxyapatite	g / cm^3
M_{HAP}	molecular weight of hydroxyapatite	g / mol

The expression for calcium flux, from Fick's law, is:

$$J_{Ca} = -D_{Ca}\frac{dc_{Ca}}{dx} \tag{2}$$

where J_{Ca} is the flux of free calcium across the cartilage surface, D_{Ca} is the diffusivity of free calcium in cartilage, and c_{Ca} is the concentration of free calcium in cartilage. At the disk surface boundary, the concentration of free calcium is equal to the calcium in solution. At the boundary of the CC-UC interface where the reaction occurs, the concentration of free calcium is zero.

$$\text{At } x = 0,\ c_{Ca} = c_s \tag{3}$$

$$\text{At } x = \delta,\ c_{Ca} = 0 \tag{4}$$

Using these boundary conditions and solving for J_{Ca} by integration,

$$\int_0^{\delta} J_{Ca}\,dx = -D_{Ca}\int_{c_s}^{0} dc_{Ca} \tag{5}$$

yields the solution:

$$J_{Ca} = \frac{D_{Ca}c_s}{\delta} \tag{6}$$

which describes the flux of calcium through the CC layer of thickness δ.

Given the stoichiometry of the reaction, one mole of HAP, $Ca_{10}(PO_4)_6(OH)_2$, is formed for every 10 moles of calcium consumed. Therefore,

$$\text{molar rate of HAPformation} = \frac{1}{10} \times (\text{molar rate of } Ca^{2+} \text{ consumption})$$

$$= \frac{J_{Ca}A}{10} \tag{7}$$

where A is the surface area of the cartilage.

Substituting in Equation (6) yields:

$$= \frac{D_{Ca} c_s}{10\delta} A \tag{8}$$

The molar rate of hydroxyapatite accumulation can be described as:

molar rate of accumulation of HAP = $\frac{d}{dt}$(moles of HAP)

$$= \frac{d}{dt}\left(\frac{\rho_{HAP} A \delta}{M_{HAP}}\right) \tag{9}$$

where ρ_{HAP} is the density of HAP and M_{HAP} is the molecular weight of HAP.

The mass balance of molar rate of formation of HAP and the molar rate of accumulation of HAP, or setting equations (8) and (9) equal yields:

$$\frac{\rho_{HAP}}{M_{HAP}} \frac{d\delta}{dt} = \frac{D_{Ca} c_s}{10\delta} \tag{10}$$

Solving by integration:

$$\int_0^{\delta} \delta d\delta = \frac{M_{HAP} D_{Ca}}{10\rho_{HAP}} \int_0^t c_s dt \tag{11}$$

The concentration of calcium in solution, c_s, was described using exponential decay with time:

$$c_s = c_0 e^{-\lambda t} \tag{12}$$

where c_0 is the initial calcium concentration in solution and λ is the decay constant for free calcium in solution. Substituting Equation (12) into (11) and solving for δ gives the expression for the change in CC thickness with time:

$$\delta = \sqrt{\frac{2M_{HAP}D_{Ca}c_0e^{-\lambda t}}{10\rho_{HAP}\lambda}} \tag{13}$$

The expression was used to estimate the change in CC wall thickness with time up to 3 days for the starting calcium concentrations, c_0 of 1.8 mM, 5.0 mM, 7.5 mM, and 10 mM. Values for decay constants λ and λ_{fet} were estimated from data by fitting the calcium supernatant concentration time course for the 5.0 mM, 7.5 mM, and 10 mM groups with an exponential curve using least summed square error analysis , with R^2 values in the range of ~0.94-0.97. Decay constants for solutions without fetuin, λ and with fetuin, λ_{fet} were estimated separately. Solutions with starting calcium concentration of 1.8 mM were fit to curves separately because they were below the critical concentration for mineral precipitate formation outside of cartilage, and thus did not exhibit exponential decay behavior. The value used for the diffusivity of calcium in CC, D_{CC}, was 9.5×10^{-9} cm^2/s, measured in a previous study for rhodamine B base (a small cationic molecule) through the native zone of calcified cartilage [2]. Established values were used for the theoretical density of HAP, 3.156 g/cm^3, and for the molecular weight of HAP, 1004.52 g/mol.

4.4 Results

Calcium supernatant concentration. Calcium supernatant concentration was dependent on time ($P<0.001$) and on fetuin ($P<0.001$), with an interactive effect ($P<0.001$) (Fig.4.2). Media starting at the physiological concentration, with 1.8 mM $CaCl_2$ and 2.0 mM NaH_2PO_4 remained relatively stable in calcium supernatant concentration over the 3 days, decreasing only slightly to 1.4 mM calcium for media without fetuin or 1.6 mM calcium for media with fetuin by the end of the 3 days. In contrast, the supersaturated media with the starting concentrations of 5 mM, 7.5 mM and 10 mM of $CaCl_2$ and NaH_2PO_4 without fetuin dropped precipitously, with all three solutions reaching ~0.4 mM or less by within first day (24 hours) (Fig. 4.2A). With fetuin, the media with 5 mM starting concentrations reached ~2mM by 1 day and hovered around that concentration until the end of the 3 days (Fig. 4.2B). Media starting at 7.5 mM concentrations with fetuin dropped to 4.4 mM calcium by 1 day, decreasing steadily until reachig 2.8 mM by 3 days. Media starting at 10 mM of $CaCl_2$ and NaH_2PO_4, with fetuin, exhibited a very similar trend as the 7.5 mM medium, reaching 3.9 mM by 1 day and 2.8 mM by 3 days. By the end of 3 days, the presence of fetuin had maintained calcium in the supernatant of supersaturated media at ~30-40% of the starting concentration of calcium in the supernatant, compared to a 97-99% loss of calcium in the supernatant without fetuin ($P<0.001$).

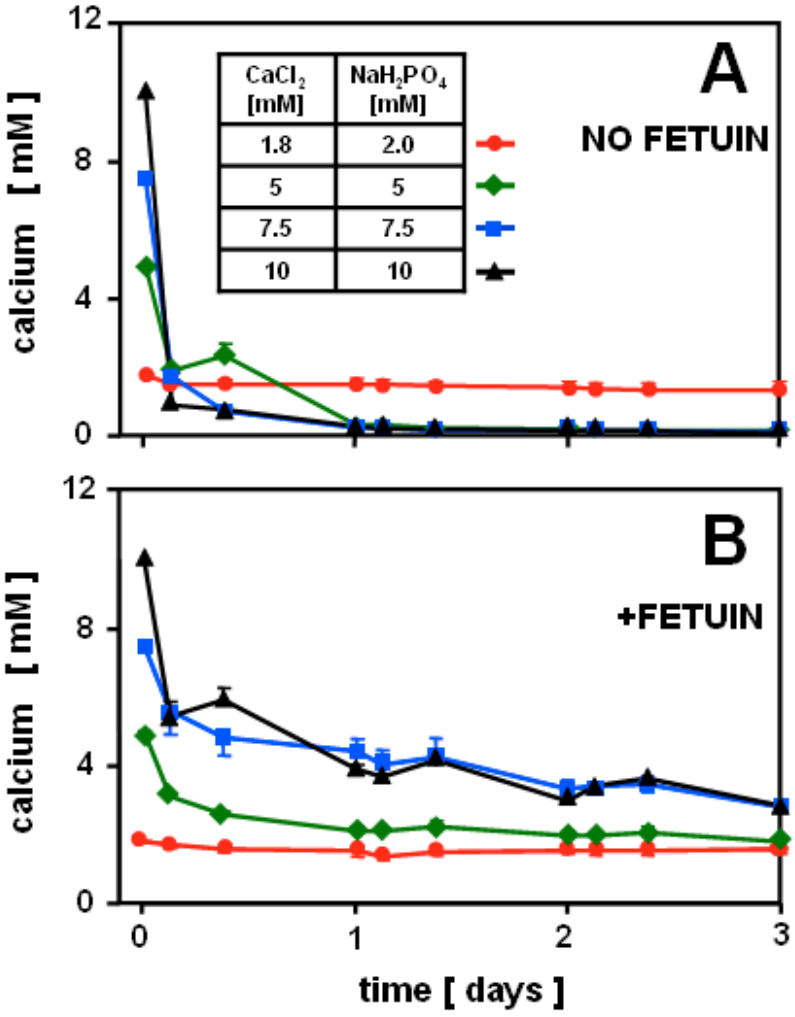

Figure 4.2: Calcium supernatant concentration for different starting concentrations without fetuin (**A**) or with fetuin (**B**) (n=5-6) Mean ± SE.

Macroscopic staining for calcification. In concentrations of 5.0 mM and above with fetuin, there was macroscopically visible Alizarin Red staining for calcification of cartilage. Cartilage quarter-disks stained positive for calcium on surfaces of samples incubated with fetuin in media with starting concentration of 5.0 mM, 7.5 mM, and 10 mM, while samples incubated without fetuin appeared light pink (Fig. 4.3). In the positively stained samples, the whole disk surface appeared red (Fig. 4.3L-N). In cross-sectional view, the edges of the cartilage appeared to stain darker than the middle of the tissue. (Fig. 4.3P-R). There was some positive staining around the rim of cartilage samples incubated without fetuin in 5.0 mM starting ion concentration media, but the positive stain did not extend into tissue surface (Fig. 4.3D, H).

Microscopic staining for calcification. Histochemical staining with Alizarin Red S revealed the thickness and patterns of calcification in cartilage region (Fig. 4.4). Alizarin Red did not stain cartilage from day 0, cartilage that was incubated without fetuin, or cartilage incubated in the 1.8 mM calcium concentration with fetuin (Fig. 4.4A-F). In the samples with 5 mM, 7.5 mM, and 10 mM starting calcium concentration with fetuin, there was positive dense band of staining at the top edge with thickness of ~30-100 μm (Fig. 4.4G-I). In the 7.5 and 10 mM media, samples calcified on both edges, with a different pattern of staining on each side. While one edge showed a dense band of calcification, the calcification on the other edge appeared more diffuse and scattered, with spots of calcification appearing to correspond with cell organization (Fig. 4.4H-I).

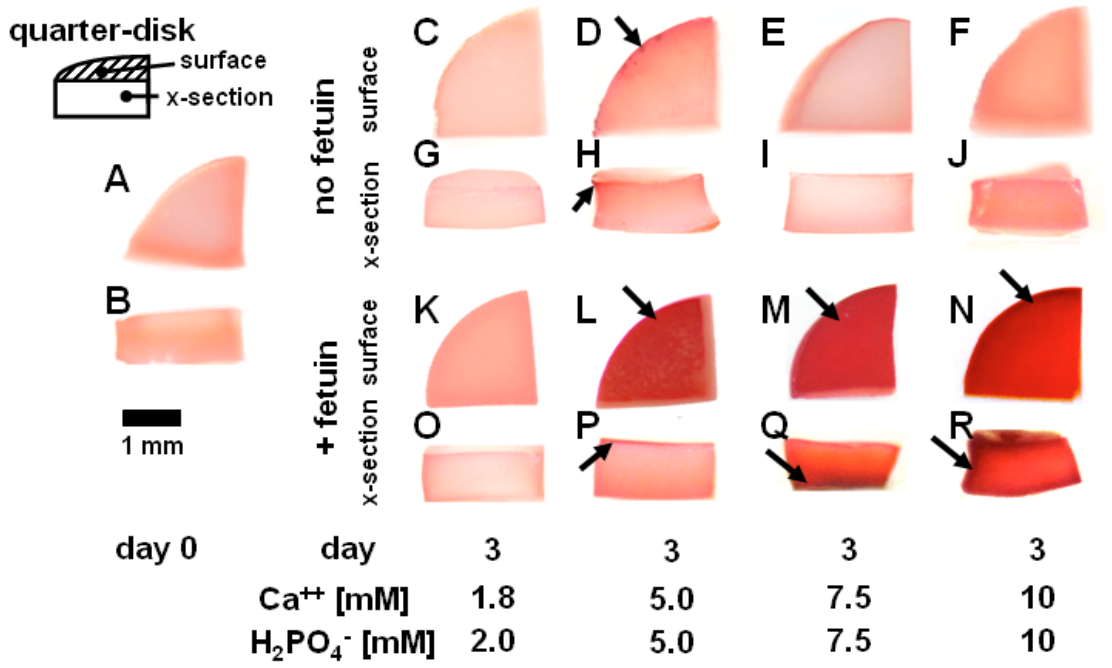

Figure 4.3: Macroscopic staining of calcification on cartilage quarter-disks by Alizarin Red S, including both a surface view and a cross-sectional view of day 0 samples (**A-B**) and samples incubated without fetuin (**C-J**) or with fetuin (**K-P**), at the different starting solution concentrations of 1.8 mM, 5.0 mM, 7.5 mM or 10 mM calcium.

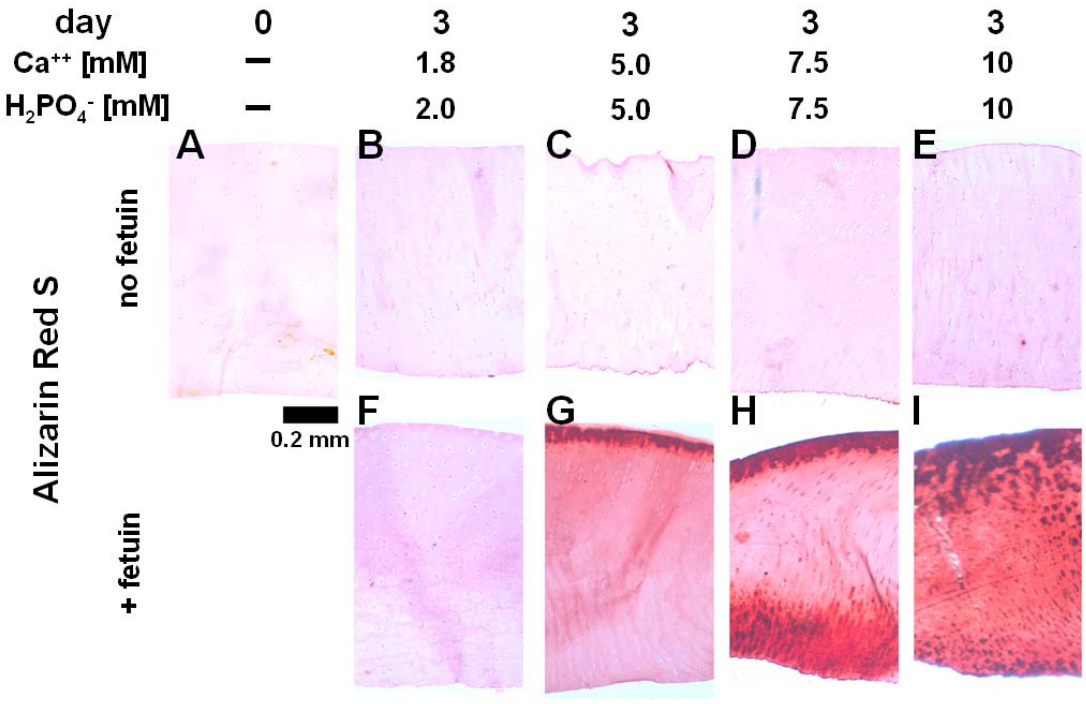

Figure 4.4: Alizarin Red histological staining of cartilage for calcium before culture (**A**) and after culture without fetuin (**B-E**) or with fetuin (**F-I**) in media with different starting calcium and phosphate concentrations.

Calcium content. Biochemical indices of calcium deposition in cartilage disks were consistent with macroscopic staining. Calcium content of the cartilage disks was dependent on medium initial calcium concentration ($P < 0.05$) and on fetuin ($P < 0.05$), with an interactive effect ($P < 0.05$). Calcium content was highest for samples that were incubated in 7.5 mM initial concentration media with fetuin, accumulating ~250 μg/cm^2 of calcium, 9-fold higher than samples incubated in the same starting media concentration without fetuin ($P < 0.05$) (Fig. 4.5A). Cartilage disks also exhibited calcification, to a lesser extent, in fetuin-containing media with 10 mM starting calcium concentration, accumulating 122 μg/cm^2 of calcium. Samples incubated in media with starting concentration of 5 mM accumulated ~53 μg/cm^2 calcium whether or not there was fetuin present, while samples incubated in the media with 1.8 mM starting calcium concentration had low calcium content of ~5 μg/cm^2 either with or without fetuin.

GAG removal and content. Trypsin digestion of cartilage disks at day 0 removed ~600 μg of sulfated GAG, or ~94% of total GAG content (Fig. 4.5B). There was no significant difference in the amount of GAG in the cartilage after incubation in media with different starting concentrations, and no difference from day zero. There was also no significant effect of fetuin. Histochemical staining with Toluidine Blue confirmed the depletion of proteoglycan throughout the cartilage (Fig. 4.6)

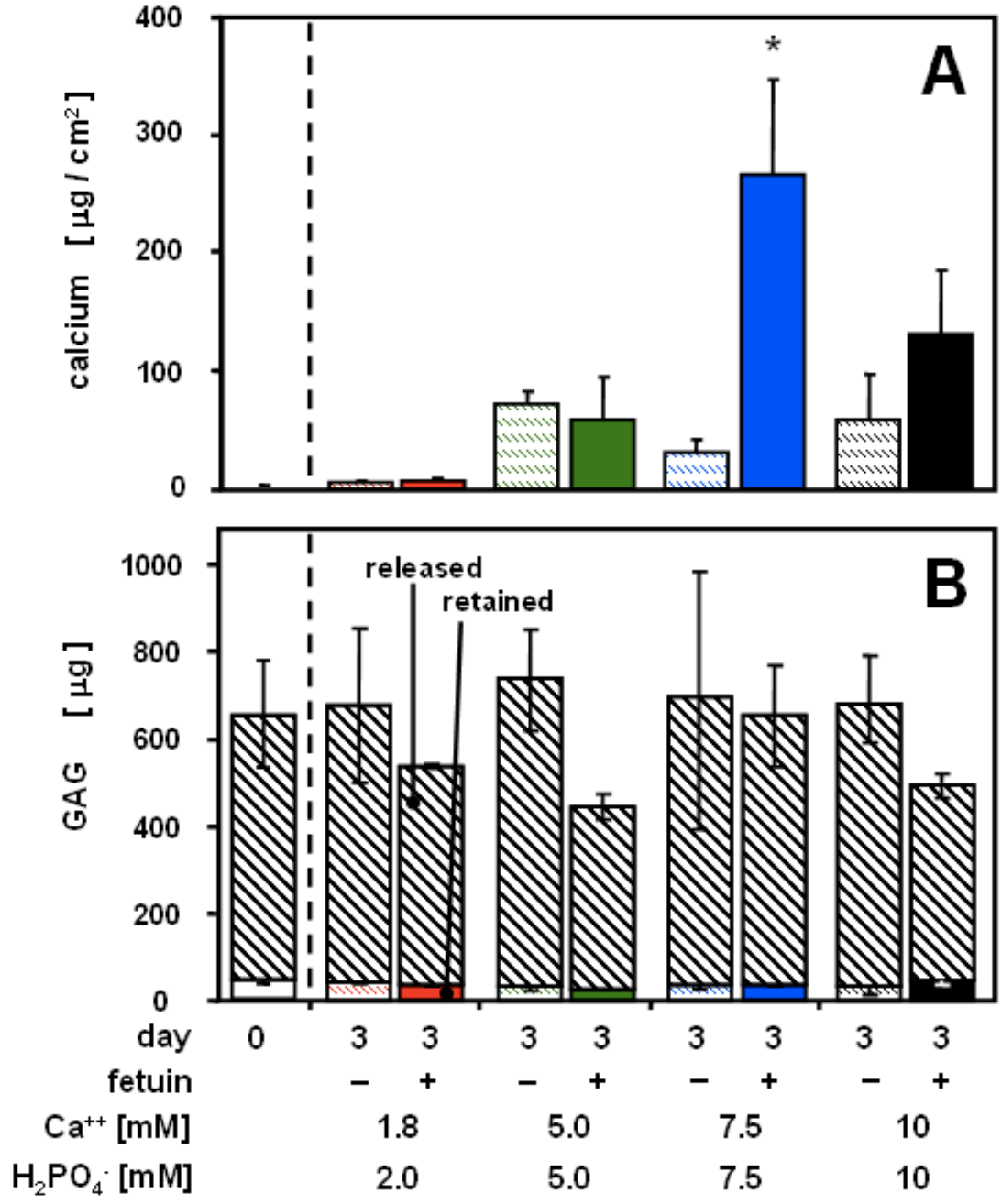

Figure 4.5: (**A**) Calcium content and (**B**) GAG released and retained within cartilage samples at day 0 and as a function of starting ion concentrations and addition of fetuin in the media Significant differences from group at corresponding concentration with no fetuin are indicated by *, $p < 0.05$.

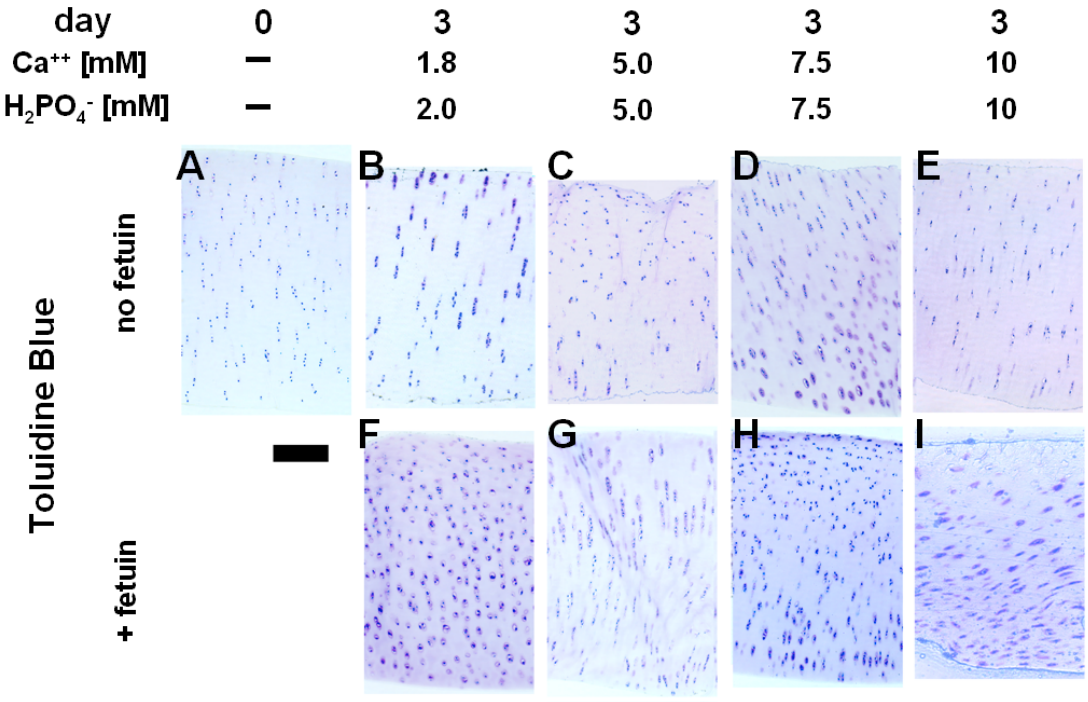

Figure 4.6: Toluidine Blue histological staining of cartilage for proteoglycan before culture (**A**) and after culture without fetuin (**B-E**) or with fetuin (**F-I**) in media with different starting calcium and phosphate concentrations.

Cell viability. Live/Dead vertical cross-sections showed that day 0 controls, after trypsin digestion, had primarily live cells, with a few dead cells (Fig. 4.7A, B). After incubation for 3 days, there was cell death throughout vertical cross-section (Fig. 4.7C-R). Quantitative analysis indicated that chondrocyte viability varied with fetuin ($P<0.001$) and with tissue region (middle vs. edge) ($P<0.001$) but not with medium starting concentration ($P=0.70$) (Fig. 4.8). There was a significant interactive effect between tissue region and fetuin ($P<0.05$). In the calcifying condition of 7.5 mM starting concentration with fetuin, there was a ~20% loss of viability at the top and bottom edges of tissue compared to the middle of the tissue ($P<0.05$) (Fig. 4.8). There was a corresponding loss of green staining of live cells and visible red staining of dead cells at the tissue edges (Fig. 4.7O, P). Samples incubated at 10 mM starting concentration followed a similar trend.

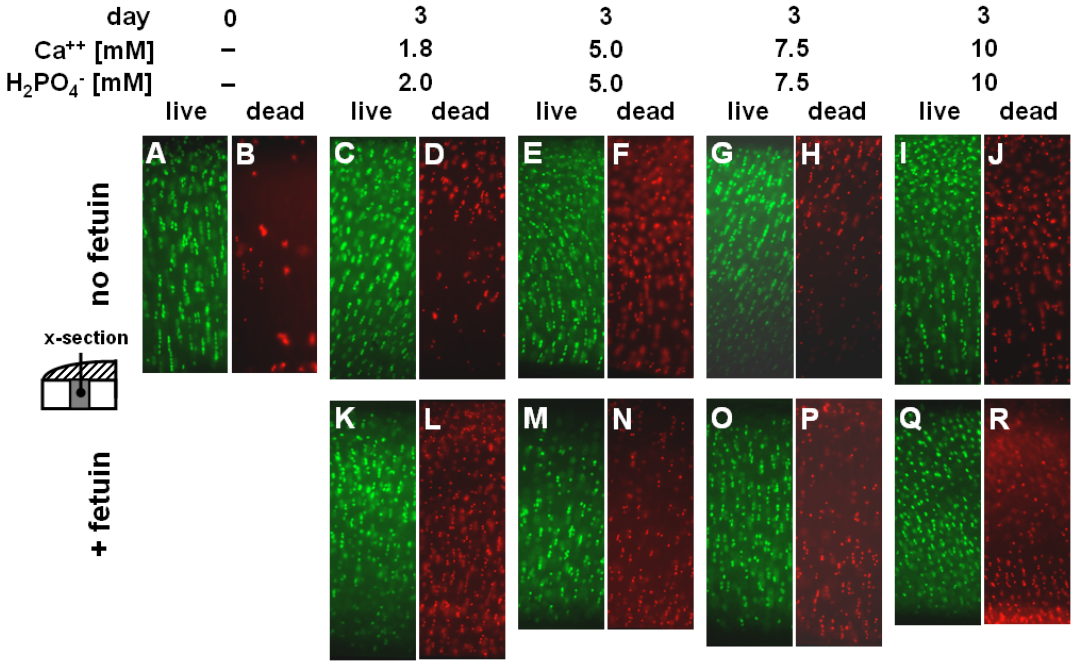

Figure 4.7: Live/Dead paired images of cartilage disk cross-sections before incubation (**A, B**) or after incubation in media without fetuin (**C-J**) or with fetuin (**K-R**) at different starting calcium and phosphate concentrations.

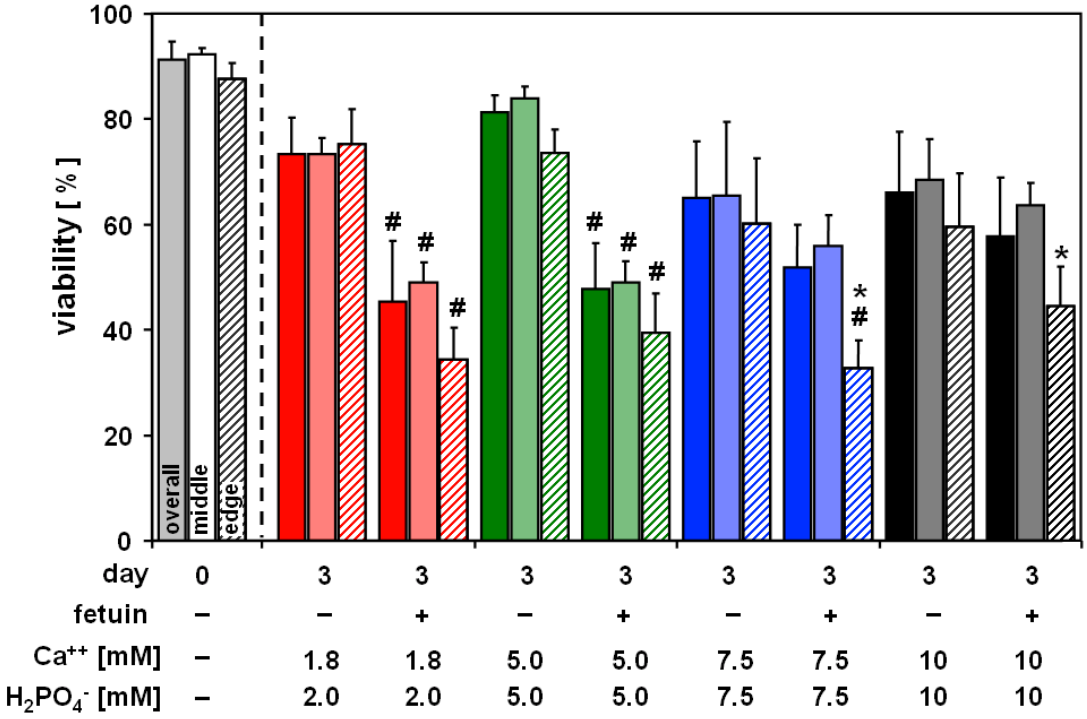

Figure 4.8: Percentage cell viability in cartilage samples as a function of media starting concentration, fetuin, and tissue region of the overall tissue cross-section, the middle bulk tissue, and the tissue edges t(op and bottom 15%). Significant difference from middle tissue region of the same culture condition is indicated by *, $p<0.05$. Significant difference from corresponding tissue region of samples in same media concentration without fetuin is indicated by #, $p<0.05$.

Mass Transfer Analysis of CC thickness. The mass transfer analysis was used to simulate the change in thickness of the calcified cartilage region for samples cultured in media with different starting calcium concentrations, without or with fetuin, over the 3-day culture. The best-fit exponential curves for calcium in solution had a decay constant of $\lambda = 0.55\ h^{-1}$ ($R^2 = 0.94$) for supersaturated solutions (5 mM, 7.5 mM, 10 mM) without fetuin, which resulted in a rapid decrease for all three groups to below 1 mM calcium in solution after 12 hours (Fig. 4.9A). With the addition of 5 mg/ml of fetuin, the best-fit decay constant for the calcium supernatant data was $\lambda_{fet} = 0.012\ h^{-1}$ ($R^2 = 0.97$) , for a gradual decrease in calcium to 86% of the starting concentration after 12 hours and to 42% after 3 days (Fig. 4.9B). For the control media with 1.8 mM starting concentration, the fits to calcium supernatant data were performed individually, since they were below the critical concentrations for precipitate formation and did not undergo the same decay behavior as the supersaturated concentrations. The decay constants for the 1.8 mM starting concentration media were $0.0049\ h^{-1}$ and $0.0034\ h^{-1}$ for without and with fetuin, respectively.

The thickness of calcified cartilage, δ, varied with the initial media calcium concentration and with fetuin (Fig. 4.9C, D). For supersaturated solutions (5 mM, 7.5 mM, and 10 mM) without fetuin, the calcified cartilage thickness remained close to zero. For supersaturated media with fetuin, the calcified cartilage thickness increased logarithmically, reaching 36 μm in 5 mM initial calcium medium, 45 μm in 7.5 mM medium, and 51 μm in 10 mM medium after 3 days. For the control media (1.8 mM initial calcium), the calcified cartilage thickness reached ~28 μm in 3 days with or without fetuin.

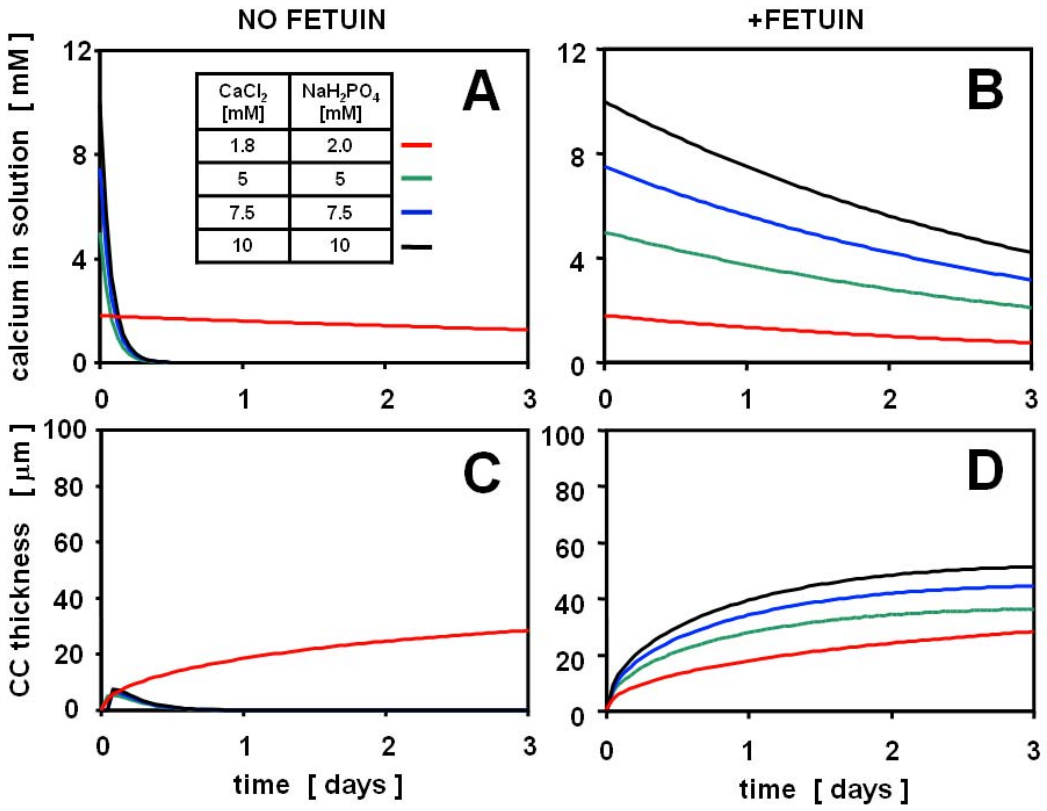

Figure 4.9: Mass transfer simulation results for the change in calcium concentration in supernatant (**A, B**) and in calcified cartilage thickness (**C, D**), as a function of time and starting calcium concentration.

4.5 Discussion

The results from this study indicate that fetuin-mediated chemical calcification of cartilage can be implemented to form a zone of calcified cartilage ~30-100 μm thick at the edge of live, adult cartilage within a few days. The extent of calcification is dependent on fetuin and on the concentration of calcium and phosphate in the medium. Cartilage depleted of proteglycan by enzymatic treatment with trypsin was able to undergo tissue calcification in media with 5 mM or higher of calcium and phosphate. Calcification was higher in 7.5 mM medium than in 5 mM or 10 mM, resulting in accumulation of 93 μg of calcium in 3 days. Fetuin helped to maintain high supernatant calcium concentration in the media , which decayed to about half of starting concentration by 3 days, whereas media without fetuin fell to <1 mM calcium within the first 24 h due to formation of mineral precipitate outside of cartilage. Cell viability was maintained in the bulk tissue for all concentrations, although at the tissue edges, there was loss of cell viability by ~20 % compared to the bulk for cartilages in calcifying media. Mass transfer analysis used to simulate the change in thickness of the calcified cartilage region, based on parameters of time and free calcium in solution, predicted logarithmic growth of the calcified cartilage zone and was consistent with experimental endpoint results.

The results indicate that although cartilage matrix does calcify in metastable supersaturated solutions, the precipitation of mineral in solution is the dominant process consuming free calcium and phosphate. In solution, calcium phosphate crystals form when the concentration of calcium and phosphate ions exceeds the critical supersaturation, which is a value close to the solubility product [5]. If these ions are at a high enough concentration and collide at a certain orientation, they nucleate a crystal, which can then grow with the addition of more component ions.

This crystal formation and growth depletes the solution of the ions unless the solution ion concentration is maintained by titration. In the body, where ion concentrations are generally regulated by homeostatic mechanisms, the concentration of calcium and phosphate does not change so dramatically. Body fluids are slightly supersaturated with respect to calcium and phosphates; but most tissues in the body do not calcify because of inhibitory factors that inhibit calcium phosphate formation and crystal growth, including proteoglycans and fetuin. Fetuin was used in the present study at a constant concentration across all groups to inhibit crystal growth in solution, but there is also a dose-dependence of fetuin, which has been previously demonstrated [39].

The formation of crystals in biological matrices is distinct from crystal formation in solution because the components of the extracellular matrix can act as nucleators and inhibitors of crystal formation. In bone, collagen I is the primary component of the organic matrix and organizes the formation of hydroxyapatite in an orderly pattern corresponding to the hole zone region within collagen fibrils [14]. However, in calcified cartilage in the epiphyseal growth plate, crystals are not associated with collagen fibrils [3], although collagen is still thought to support hydroxyapatite formation. In cartilage, proteoglycans are potent inhibitors of hydroxyapatite growth and formation, due partially to steric hindrance effects [8].

The depletion of proteoglycan from cartilage used in the present study may have enhanced tissue calcification. Proteoglycans normally protect cartilage from calcification by inhibiting the reaction between extracellular fluid components and collagen fibrils. Proteoglycans can bind calcium ions via their sulfate side chain groups, and also inhibit the diffusion of calcium and exclude phosphate ions. During calcification of cartilage in endochondral ossification, the removal and degradation of proteoglycan occurs to expose the collagen fibrils and allow them to calcify [7]. It has

also been demonstrated that collagen in native skin did not calcify *in vitro* in metastable solutions of calcium and phosphate, whereas skin that was pre-treated with hyaluronidase did mineralize [13]. In the present study, proteoglycan was removed throughout the full thickness of cartilage, but calcification still occurred primarily on tissue edges, likely due to mass transfer limitations associated with buildup of mineral. It may be possible to exert more control over the thickness of the zone of calcification using a partial trypsin digestion, such that only the tissue edge is depleted of proteoglycan and available for calcification.

The calcification of cartilage in a thin dense band at the tissue edge in the present study may reflect the mass transport properties of proteoglycan-depleted and of calcifying cartilage. Normal articular cartilage is highly hydrated, with fluid comprising ~75-80% of the tissue. Solute diffusion through cartilage depends on the composition and density of the extracellular matrix, with proteoglycan being primarily responsible for restricting solute mobility. Due to their high negative charge density, proteoglycans interact strongly with small ions and also with large molecules such as proteins due to steric hindrance. For albumin, which is about the same size as fetuin, diffusivity in cartilage is an order of magnitude lower than in free solution [31]. Removal of 93% proteoglycan from cartilage was found to increase the diffusivity of large macromolecules by ~1.6-2.0 times for uncharged solutes with molecular weight of 5000-70,000 Da [42]. During tissue calcification, water volume in the tissue is replaced with mineral, which would decrease the diffusivity to ions even further. The diffusivity of a small cationic solute, rhodamine B base (MW 443), and a highly anionic solute, fluorescein sodium salt, had diffusivities ~5-fold lower in calcified cartilage than in uncalcified cartilage [2]. In the present study, the diffusion of ions occurred into the cartilage from the edge and nucleated into mineral crystals, which

grew into a continuous zone of calcification. This may have effectively formed a "wall" to act as a barrier to diffusive transport, which may have limited the calcification from spreading farther towards the center of the tissue and maintained a thin, dense zone of calcification at the tissue edge.

The different patterns of calcification in the cartilage suggest different mechanisms of calcification, a chemical mechanism and a cell-mediated mechanism. The chemical mechanism based on the spontaneous nucleation of mineral due to diffusion of calcium and phosphate into the matrix has been modeled in the present study and resulted in a thin, dense band of calcification at the tissue edge. The cell-dependent mechanism takes place at higher concentrations (7.5 mM and 10 mM in the present study) and results in more diffuse calcification with nucleation coinciding with cell organization, suggesting a cell-mediated mechanism. Deep zone chondrocytes are able to mineralize their surrounding matrix but may undergo apoptosis as part of terminal differentiation. It is unknown whether the cells surrounded by mineral in the present study are viable, although the loss of cell viability at the tissue edges is suggestive that calcification was associated with cell death. Although apoptosis of chondrocytes is not required for mineralization [37], there is a link between mineralization and cell death [16]. Inorganic phosphate has been shown to be a potent apoptogen [30], whose effects are dependent on extracellular calcium concentration [29]. High concentrations of calcium have also been implicated in plasma membrane injury and possible alterations in intracellular calcium homeostasis [9]. It is uncertain whether the cells died before or after calcification and what the local concentration of free calcium and phosphate was the tissue edge versus in the bulk.

The mass transfer analysis used in the present study demonstrated that diffusion to a reacting boundary in a pseudo-steady state could be used to describe the

chemical calcification of cartilage in a system with supersaturated calcium and phosphate. For chemical calcification of cartilage, the simulation showed calcified cartilage thickness increasing logarithmically with time, reaching ~30-60 μm in 3 days. The wall thickness found in the mass transfer analysis was consistent with experimental data, within the same order of magnitude, and showed slight increases in calcified cartilage thickness with higher initial calcium concentration in the medium, which was also consistent with experimental results. However, the model did not take into account any cell-mediated calcification, so it did not describe the formation of a thick, diffuse zone of calcification occurring at higher concentrations (7.5 mM and 10 mM) in the present study and would underestimate the amount of calcification in the cartilage. In addition, since the model only took into account calcium and not the phosphate counterion, it was assumed that the solution was metastable and would undergo exponential decay due to precipitation of mineral within 3 days. The fit of exponential curves to the calcium supernatant data was a simplification for the kinetics of calcium phosphate precipitation in solution and may not accurately represent the kinetics of the system. For example, the exponential decay was not a good fit for the behavior of the control solution with 1.8 mM initial calcium and 2.0 mM initial phosphate, where the concentrations remained relatively constant.

Improvements to this mass transfer model to increase its accuracy and utility would be to include a kinetic analysis of the reaction to form hydroxyapatite based on the supersaturation level of the media. Such an analysis could be used to find the change in free calcium and phosphate concentrations in the supernatant associated with precipitation in solution, and the rate of buildup of mineral mass within the cartilage itself. Another improvement would be a time-dependent diffusivity to take into the account the decrease in diffusivity of calcium through the calcified zone as the

calcification becomes denser. It would also be useful to incorporate a reaction term throughout the calcified zone, rather than just at the boundary with uncalcified cartilage. Finally, the model assumes that the precipitation reaction between calcium and phosphate always forms hydroxyapatite, which is the most thermodynamically stable phase, but several other phases of calcium phosphate precipitate could be formed, as a precursor to hydroxyapatite. With refinements to the model and determination of parameters, this model could be useful to determine the conditions needed to form a desired thickness of calcification in a dense band at the edge of cartilage, similar to the native zone of calcified cartilage.

This study has demonstrated that *in vitro* calcification of live, adult articular cartilage can occur within 3 days using fetuin in metastable supersaturated calcium and phosphate, with the extent of calcification of cartilage dependent on fetuin and on the concentrations of calcium and phosphate in the media. Greater control may be exerted over the calcification by using partial proteoglycan depletion of a defined zone of cartilage, prior to calcification culture. The ability to calcify a zone of cartilage with defined thickness at the tissue edge within short time scales may be applicable to calcify cartilaginous tissues in osteochondral tissue engineering. It may useful to tissue engineer a biomimetic zone of calcified cartilage using the fetuin-mediated method at the interface between cartilage and bone, to perform a similar mechanical function to the native zone of calcified cartilage. Engineering a zone of calcified cartilage at the interface of cartilage and bone within an osteochondral graft may help the graft to withstand shear loading, and potentially, physiological joint articulation soon after implantation.

4.6 Acknowledgments

We would like to thank Andrea Pallante and Drs. Paul A Price and Robert L Sah for their contributions to this work. This work was supported by the National Institute of Health and Howard Hughes Medical Institute through the Professors Program Grant to UCSD for Dr. Robert L Sah.

4.7 References

1. Anderson HC: Molecular biology of matrix vesicles. *Clin Orthop Rel Res* 314:266-80, 1995.

2. Arkill KP, Winlove CP: Solute transport in the deep and calcified zones of articular cartilage. *Osteoarthritis Cartilage* 16:708-14, 2008.

3. Arsenault AL, Grynpas MD: Crystals in calcified epiphyseal cartilage and cortical bone of the rat. *Calcif Tissue Int* 43:219-25, 1988.

4. Blumenthal NC, Posner AS, Silverman LD, Rosenberg LC: Effect of proteoglycans on in vitro hydroxyapatite formation. *Calcif Tissue Int* 27:75-82, 1979.

5. Boskey AL: Pathogenesis of cartilage calcification: mechanisms of crystal deposition in cartilage. *Curr Rheumatol Rep* 4:245-51, 2002.

6. Brown RA, Blunn GW, Salisbury JR, Byers PD: Two patterns of calcification in primary (physeal) and secondary (epiphyseal) growth cartilage. *Clin Orthop Relat Res* 294:318-24, 1993.

7. Buckwalter JA: Proteoglycan structure in calcifying cartilage. *Clin Orthop Relat Res*:207-32, 1983.

8. Chen CC, Boskey AL: Mechanisms of proteoglycan inhibition of hydroxyapatite growth. *Calcif Tissue Int* 37:395-400, 1985.

9. Farber JL: The role of calcium ions in toxic cell injury. *Environ Health Perspect* 84:107-11, 1990.

10. Farndale RW, Buttle DJ, Barrett AJ: Improved quantitation and discrimination of sulphated glycosaminoglycans by use of dimethylmethylene blue. *Biochim Biophys Acta* 883:173-7, 1986.

11. Ferguson VL, Bushby AJ, Boyde A: Nanomechanical properties and mineral concentration in articular calcified cartilage and subchondral bone. *J Anat* 203:191-202, 2003.

12. Gannon JM, Walker G, Fischer M, Carpenter R, Thompson RC, Jr., Oegema TR, Jr.: Localization of type X collagen in canine growth plate and adult canine articular cartilage. *J Orthop Res* 9:485-94, 1991.

13. Glimcher MJ: Molecular biology of mineralized tissues with particular reference to bone. *Rev Mod Phrs* 31:359-93, 1959.

14. Glimcher MJ: The nature of the mineral component of bone and the mechanism of calcification. *Instr Course Lect* 36:49-69, 1987.

15. Gupta HS, Schratter S, Tesch W, Roschger P, Berzlanovich A, Schoeberl T, Klaushofer K, Fratzl P: Two different correlations between nanoindentation modulus and mineral content in the bone-cartilage interface. *J Struct Biol* 149:138-48, 2005.

16. Huitema LF, Vaandrager AB: What triggers cell-mediated mineralization? *Front Biosci* 12:2631-45, 2007.

17. Hunziker EB: Articular cartilage structure in humans and experimental animals. In: *Articular Cartilage and Osteoarthritis,* ed. by KE Kuettner, Schleyerbach R, Peyron JG, Hascall VC, Raven Press, New York, 1992, 183-99.

18. Hunziker EB, Quinn TM, Hauselmann HJ: Quantitative structural organization of normal adult human articular cartilage. *Osteoarthritis Cartilage* 10:564-72, 2002.

19. Hwang J, Kyubwa EM, Bae WC, Bugbee WD, Masuda K, Sah RL: *In vitro* calcification of immature bovine articular cartilage: formation of a functional zone of calcified cartilage. *Cartilage*, 2010.

20. Inskeep WP, Silvertooth JC: Kinetics of hydroxyapatite precipitation at pH 7.4 to 8.4. *Geochimica et Cosmochimica Acta* 52:1883-93, 1988.

21. Kandel RA, Boyle J, Gibson G, Cruz T, Speagle M: In vitro formation of mineralized cartilagenous tissue by articular chondrocytes. *In Vitro Cell Dev Biol Anim* 33:174-81, 1997.

22. Koutsoukos P, Amjad Z, Tomson MB, Nancollas GH: Crystallization of calcium phosphates. A constant composition study. *J Am Chem Soc* 102:1553-7, 1980.

23. Lane LB, Bullough PG: Age-related changes in the thickness of the calcified zone and the number of tidemarks in adult human articular cartilage. *J Bone Joint Surg Br* 62:372-5, 1980.

24. Lei C, Liao Y, Feng Z: Kinetic model for hydroxyapatite precipitation on human enamel surface by electrolytic deposition. *Biomed Mater* 4:035010, 2009.

25. Li KW, Ahsan T, Sah RL: Effect of trypsin treatment on integrative cartilage repair *in vitro*. *Trans Orthop Res Soc,* 21:101, 1996.

26. Lohmander S, Hjerpe A: Proteoglycans of mineralizing rib and epiphyseal cartilage. *Biochim Biophys Acta* 404:93-109, 1975.

27. Lovell T, Eyre D: Unique biochemical characteristics of the calcified cartilage zone of articular cartilage. *Trans Orthop Res Soc,* Atlanta, GA, 1988.

28. Mankin HJ: Localization of tritiated thymidine in articular cartilage of rabbits. I. growth in immature cartilage. *J Bone Joint Surg Am* 44-A:682-98, 1962.

29. Mansfield K, Pucci B, Adams CS, Shapiro IM: Induction of apoptosis in skeletal tissues: phosphate-mediated chick chondrocyte apoptosis is calcium dependent. *Calcif Tissue Int* 73:161-72, 2003.

30. Mansfield K, Rajpurohit R, Shapiro IM: Extracellular phosphate ions cause apoptosis of terminally differentiated epiphyseal chondrocytes. *J Cell Physiol* 179:276-86, 1999.

31. Maroudas A: Transport of solutes through cartilage: permeability to large molecules. *J Anat* 122:335-47, 1976.

32. Martin B: Mathematical model for the mineralization of bone. *J Orthop Res* 12:375-83, 1994.

33. McGee-Russell S: Histochemical methods for calcium. *J Histochem Cytochem* 6:22-42, 1958.

34. Oegema T, Jr., Carpenter R, Hofmeister F, Thompson RC, Jr.: The interaction of the zone of calcified cartilage and subchondral bone in osteoarthritis. *Microsc Res Tech* 37:324-32, 1997.

35. Oegema T, Jr., Thompson RC, Jr.: The zone of calcified cartilage: its role in osteoarthritis. In: *Articular Cartilage and Osteoarthritis,* ed. by K Kuettner, Raven Press, Ltd., New York, 1992, 319-31.

36. Pallante AL, Bae WC, Chen AC, Görtz S, Bugbee WD, Sah RL: Effects of storage at 4°C and 37°C on chondrocyte viability in fresh goat osteochondral grafts. *Am J Sports Med* 37:24S-32S, 2009.

37. Pourmand EP, Binderman I, Doty SB, Kudryashov V, Boskey AL: Chondrocyte apoptosis is not essential for cartilage calcification: evidence from an in vitro avian model. *J Cell Biochem* 100:43-57, 2007.

38. Price PA, Lim JE: The inhibition of calcium phosphate precipitation by fetuin is accompanied by the formation of a fetuin-mineral complex. *J Biol Chem* 278:22144-52, 2003.

39. Price PA, Toroian D, Lim JE: Mineralization by inhibitor exclusion: the calcification of collagen with fetuin. *J Biol Chem* 284:17092-101, 2009.

40. Schenk RK, Eggli PS, Hunziker EB: Articular cartilage morphology. In: *Articular Cartilage Biochemistry,* ed. by K Kuettner, Schleyerbach R, Hascall VC, Raven Press, New York, 1986, 3-22.

41. Schinke T, Amendt C, Trindl A, Poschke O, Muller-Esterl W, Jahnen-Dechent W: The serum protein alpha2-HS glycoprotein/fetuin inhibits apatite formation in vitro and in mineralizing calvaria cells. A possible role in mineralization and calcium homeostasis. *J Biol Chem* 271:20789-96, 1996.

42. Torzilli PA, Arduino JM, Gregory JD, Bansal M: Effect of proteoglycan removal on solute mobility in articular cartilage. *J Biomech* 30:895-902, 1997.

43. Zizak I, Roschger P, Paris O, Misof BM, Berzlanovich A, Bernstorff S, Amenitsch H, Klaushofer K, Fratzl P: Characteristics of mineral particles in the human bone/cartilage interface. *J Struct Biol* 141:208-17, 2003.

CHAPTER 5

FETUIN-MEDIATED CALCIFICATION FOR INTEGRATION OF ARTICULAR CARTILAGE TO BONE TO FORM A FUNCTIONAL OSTEOCHONDRAL GRAFT

5.1 Abstract

Objective: To attach articular cartilage to bone *in vitro* using fetuin-mediated calcification to calcify across the cartilage-bone interface to form a functional osteochondral (OC) graft and determine if calcification increases integration strength.

Methods: Immature and mature bovine articular cartilage disks with proteoglycan depleted from the deep surface were incubated dead or live, in apposition with devitalized trabecular bone for 5 days, with application of intermittent compressive loading cycles. OC constructs were incubated in control medium or in calcifying media of supersaturated calcium and phosphate, with or without fetuin. Osteochondral constructs were tested by a lap-shear pull-to-failure test to measure integration strength, and cartilage was analyzed for calcification and viability.

Results: Immature and mature cartilage integrated to devitalized bone with integration strengths of 400-500 kPa, independent of chondrocyte viability and dependent on

fetuin. Integration strengths attained *in vitro* were in the same range as those for cartilage and bone of immature native OC tissue. Constructs incubated with fetuin exhibited calcification on the cartilage surface adjacent to bone and had ~7-25-fold higher calcium content than cartilage incubated without fetuin. In OC constructs with live cartilage, viability remained high in the bulk cartilage, with some cell death occurred in the proteoglycan-depleted zone of cartilage adjacent to bone.

Discussion: Fetuin-mediated calcification may act as a cement for biological fixation of cartilaginous grafts to bony substrate through a biomimetic zone of calcified cartilage. Integration through calcification of the cartilage-bone interface may enable the fabrication of large osteochondral grafts that can withstand physiological joint articulation and loading soon after implantation.

5.2 Introduction

At the native osteochondral junction is the zone of calcified cartilage (ZCC), a transition zone of intermediate stiffness which is ~100-300μm in thickness [21] and anchors articular cartilage to underlying subchondral bone. The ZCC is bound on one side by the tidemark, the gently undulating interface with deep zone articular cartilage, and on the other side by the cement line, the highly interdigitated interface with bone. The intermediate stiffness of the ZCC may serve to reduce stress concentrations that would otherwise occur at the osteochondral interface due to the discontinuity in material stiffness of cartilage and bone [4, 20]. At the tidemark, the undulating geometric pattern and the collagen II fibrils crossing the interface may provide some resistance to shear loads [23]. High levels of shear stress occurring at the tidemark and cement line interfaces with joint loading are implicated in joint failure during fracture in the osteochondral region [6, 19]. The mature osteochondral junction, with a fully developed ZCC, has higher fracture toughness than immature tissue [6], suggesting that the ZCC structure at the osteochondral interface helps to resist crack propagation.

Osteochondral treatments are currently in common use as a surgical technique for the repair of articular cartilage defects. If left untreated, cartilage defects may enlarge and progress to osteoarthritis. In surgical treatments for cartilage repair, it is difficult to attach a cartilage graft onto the bony defect base. Sufficient attachment and graft stability in the early period are essential for the successful outcome of a technique. The insufficient fixation of the graft may facilitate detachment of the transplanted biomaterial and may lead to treatment failure [15]. The transplantation of

osteochondral grafts offers advantages of transplanting structurally intact osteochondral tissue to restore the architecture and characteristics of native tissue at the defect site [5, 9]. The chondrocytes within the cartilage of the graft are viable, while the graft bone provides a stable method of graft fixation through bone interlocking and osseous healing by creeping substitution [7].. Fresh osteochondral grafting has a long and successful clinical history but limitations related to tissue availability have restricted its widespread use. The *in vitro* fabrication of osteochondral constructs using tissue engineering has the potential to overcome these limitations.

Osteochondral tissue engineering aims to create a composite graft with distinct but integrated cartilaginous and osseous components with structural, functional, and remodeling properties suitable for surgical transplantation for repair of articular defects [18]. Approaches to the fabrication of engineered osteochondral grafts include both scaffold-free and scaffold-based designs for the cartilaginous layer and cell-free or cell-seeded for the bony layer, as well as biphasic scaffolds [2, 10, 11, 14, 25, 27, 29, 30, 32]. Integration between the cartilaginous and bony layers may be critical to the function of an engineered osteochondral graft, particularly for withstanding the shear forces of joint articulation after graft implantation. Bonding between the cartilaginous and osseous layers of the graft may provide initial fixation strength as well as allow for biological remodeling to provide long-term integration *in vivo* at the osteochondral interface.

Integration of cartilaginous and osseous components of an engineered osteochondral graft into a single functionally integrated unit often involves initial

mechanical fixation followed by biological remodeling. Initial fixation may be attained through sutures [25], adhesives such as fibrin glue [10, 26], novel bioadhesives that bridge tissues with covalent chemical bonds [31], or mechanical interlocking formed by hydrogel penetration into a porous substrate [8, 11, 13]. Alternatively, cells have been seeded directly onto a porous substrate without any additional mechanical fixation [30]. Following initial assembly, the composite may be cultured *in vitro* to enhance biologically-mediated fixation between the cartilaginous and osseous components [25, 28]

Calcification of cartilage at the interface between cartilage and bone to form a biomimetic zone of calcified cartilage may help improve the interfacial shear properties of the osteochondral graft. Strategies for calcification of cartilaginous tissue may involve cell-mediated or chemical methods to form hydroxyapatite mineral similar to the mineral of the *in vivo* ZCC. Cell-mediated methods rely on specific cellular phenotypes, such as the ability of deep zone chondrocytes to calcify their surrounding matrix, to facilitate the formation of a biomimetic zone of calcified cartilage [3, 12]. The mineral formed by deep zone chondrocytes has been characterized as poorly crystalline hydroxyapatite. For shorter time scales, chemical methods for calcification may be employed, such as mineralization by inhibitor exclusion using fetuin in supersaturated solutions of calcium chloride and sodium phosphate. Fetuin is a 48 kDa glycoprotein that is present in high concentrations in serum and inhibits mineralization by binding small crystals and not allowing them to grow. Calcification using fetuin has been performed on many types of matrices, including collagen-I-based tissues like bone and tendon, as well as Sephadex beads

and acrylamide gels [22]. The calcification mechanism is based on spontaneous precipitation of calcium and phosphate ions from a metastable solution into a calcium-phosphate mineral precipitate, so a matrix is calcifiable by fetuin if it can exclude fetuin based on size, but will allow the calcium and phosphate ions in to form mineral crystals and propagate throughout the matrix. Previous work (Chapter 4) has demonstrated that cartilage which has been depleted of proteoglycan is vulnerable to fetuin-mediated calcificatiosn in supersaturated solutions, which occurs within a few days.

The hypothesis of this study was that cartilage can be attached to bone *in vitro* in a calcifying medium with fetuin to form an integrated osteochondral construct, with calcification across the cartilage-bone interface. The objectives of this study were to determine (1) if cartilage properties of tissue maturity and viability affect the strength of integration with bone, and (2) whether calcification at the cartilage-bone interface is associated with integration strength.

5.3 Materials and Methods

Experimental Design. (Table 5.1) Experiment 1. The effects of fetuin calcifying solution and duration of trypsin pre-treatment of cartilage on the integration of immature and mature cartilage explants to bone under intermittent compression were assessed. Cartilage disks were pre-treated with trypsin for 1 or 2 hours and killed by freeze-thaw prior to incubation atop devitalized bone in custom loading chambers in phosphate buffered saline or in a supersaturated calcifying solution with fetuin. Resulting osteochondral constructs were assessed for integration by a lap shear pull-to-failure test, and post-failure cartilage was assessed for calcification by Alizarin Red staining and by calcium content. Native calf osteochondral tissue was harvested in the same geometry and assessed similarly for comparison. Exp. 2. The effect of fetuin in the calcification medium on the integration of live immature and mature cartilage explants to bone under intermittent compression was assessed. Live, trypsin-treated cartilage disks were cultured atop devitalized bone in custom loading chambers in control medium (DMEM) or in supersaturated calcifying media with or without fetuin. Osteochondral constructs were analyzed for structure by microcomputed tomography (mCT) and for integration by lap shear pull-to-failure, and post-failure cartilage was assessed for viability by Live/Dead and for calcification by Alizarin Red staining and calcium content.

Table 5.1: Experimental groups with varying cartilage viability, maturity, trypsin digestion time, and media components.

expt #	viability	tissue	trypsin [hr]	media	Ca^{++} $H_2PO_4^-$	fetuin
1	dead	calf	1	HEPES	–	–
					+	+
			2		–	–
					+	+
		adult	1		–	–
					+	+
			2		–	–
					+	+
2	live	calf	1	DMEM	–	–
					+	–
					+	+
		adult	1		–	–
					+	–
					+	+

Cartilage harvest and trypsin digestion. Osteochondral blocks were harvested from the patellofemoral groove of calf knee (3 animals) and from the patella of adult bovine knee (2 animals). From each block, the superficial slice (0.5mm thick for calf, 0.2mm thick for adult) was removed, and the next slice (1mm thick) was harvested as middle zone tissue. Cartilage disks were punched using disposable dermal punches with 4mm diameter. The deep surface of the disks was nicked using a scalpel blade to track orientation. Calf cartilage disks were incubated for 1 or 2 hours, at 37°C and 5% CO2 on a nutator, in 20 tissue volumes of complete medium DMEM+ (DMEM, 10mM HEPES, 0.1 mM nonessential amino acids, 0.4 mM L-proline, 2 mM L-glutamine, 100 U/ml penicillin, 100 μg/ml streptomycin, 0.25 μg/ml amphotericin), with 10 μg/ml trypsin. For adult cartilage disks, to limit trypsin digestion to the deep surface, filter paper was placed on the deep surface of each disk and wetted with trypsin digestion solution. To stop the digestion, samples were rinsed with DMEM+ with 20% FBS for 10 minutes each. To kill cells, some disks were frozen at -80°C overnight, while others were incubated overnight in DMEM+, before assembly into composite culture. Loss of viability from freeze/thaw was confirmed by Live/Dead.

Bone substrate harvest and preparation. Osteochondral cores (6.4 mm diameter) with a flat cartilage-bone interface parallel to the articular surface.were harvested from the patellofemoral groove of adult bovine knees using a drill press. The cartilage and top 2mm of bone was removed, and the next 2 mm segment was harvested as native trabecular bone (TB) substrate, using a low speed saw (Buehler, Lake Bluff, Illinois). Marrow and lipid debris were removed by ultrasonication and rinsing. For Experiment 2, TB substrates were sterilized using a bone allograft cleansing procedure (LifeNet

Health, Virginia Beach, VA) involving a series of washes in cell lysis and disinfecting solutions.

Assembly of cartilage and bone components into compression bioreactor and incubation (Fig. 5.1A). Cartilage disks were placed on top of bone substrates with the deep (nicked) surface of cartilage adjacent to bone and placed into custom polysulfone sample chambers to fit into custom spring-loaded bioreactors. A porous polysulfone block was placed on top of the cartilage (applying small load of ~0.1 kPa), and a compressive stress of ~20kPa was applied to this block using a spring-loaded post. The magnitude of load was calculated using the spring constant and the difference between the initial and final spring length, and the load could be released by lifting the post off of the loading block and sample during free-swelling (FS) phases. Samples were subjected to alternating phases of free-swelling and loading in a daily cycle of 3hr FS - 3hr load - 3hr FS - 15hr load for 5 days. Samples were nutated during the loaded phases. In Experiment 1, samples were incubated in either PBS or a fetuin calcifying solution comprised of 5mM $CaCl_2$, 5mM $NaH_2PO_4^-$, 5 mg/ml fetuin, and 200 mM HEPES in water at pH 7.4. In Experiment 2, samples were incubated in either DMEM+, DMEM+ with 7.5 mM $CaCl_2$ and 7.5 mM $NaH_2PO_4^-$, or DMEM+ with 7.5 mM $CaCl_2$ and 7.5 mM $NaH_2PO_4^-$ and 0.1 mM (5 mg/ml) fetuin. Media was changed daily, with supersaturated calcifying solutions made fresh each day.

Micro-computed Tomography (mCT). Osteochondral constructs were scanned by mCT (SkyScan) to visualize the composite structure and to detect calcification of cartilage at the cartilage-bone interface. Three-dimensional image datasets were

obtained at $(9\ \mu m)^3$ voxel resolution and data were viewed using SkyScan DataViewer.

Lap Shear Pull-to-Failure (Fig. 5.1B). To determine the adhesive integrative strength of the interface region, osteochondral constructs were tested using a modification of American Society for Testing and Materials (ASTM) Standard D 3983 (CITE). Each construct was fixed with cyanoacrylate to wooden adapters on the bottom surface of the bone and on the top surface of the cartilage. The adapters were clamped into the mechanical test setup and samples were tested to failure by application of a uniaxial displacement at a rate of 0.5 mm/min while measuring load as described previously [24]. The adhesive integration strength was calculated as the peak load divided by area of the interface, which was taken as the area of the cartilage sample. Samples that did not adhere during the incubation period were assigned an adhesive integration strength of zero. Average load-displacement curves were generated by aligning the start of the test and the peak (ultimate) load at failure, normalizing the displacement distance between the start and peak load and averaging the load values.

Alizarin Red S staining. For macroscopic visualization of calcification, cartilage disks were removed from the wooden adapter and incubated at room temperature in a staining solution of 0.0015% wt:vol Alizarin Red S in 0.5% KOH for 24 h. Samples were destained in 0.05% KOH for 24 h, and photographed, as described previously [22].

Live/Dead staining. To assess cell viability, cartilage disks were cut in half and incubated in a solution of calcein AM and ethidium homodimer-1 for 20 minutes at

room termperature. Images of live cells and dead cells were obtained for the vertical profile of the disk cross-section by fluorescence photomicroscopy.

Histology. Cartilage disk halves were fixed in 4% paraformaldehyde in PBS overnight, embedded in OCT, and tissue cross-sections at 5 μm thickness were obtained using a cryostat. Sections were stained with 0.04% Toluidine blue in acetate buffer at pH 4.0 for 10 minutes to localize proteglycan or with 2% Alizarin Red S at pH 4.2 for 2 minutes to localize calcium [17].

Calcium content. Cartilage disk halves were incubated in 1 N HCl for 24 h at 110°C to extract calcium. The acid was evaporated and samples were reconstituted in deionized water before colorimetrically assaying for calcium content using cresolphthalein complexone, as described previously [22]. For native calf osteochondral tissue, calcium content was measured for post-fracture cartilage disk halves.

Statistics. For Experiment 1, ANOVA was used to assess effects with fixed factors of incubation solution (PBS or calcifying solution) and duration of trypsin digestion (1 or 2 hours). For Experiment 2, ANOVA was used to assess effects with a fixed factor of media type (DMEM, DMEM + CaP, DMEM +CaP + fetuin). Tukey's post-hoc comparisons were used, with P values less than 0.05 considered significant. The relationship between integrative adhesive strength and calcium was analyzed using linear regression. Data are presented as mean ± SEM.

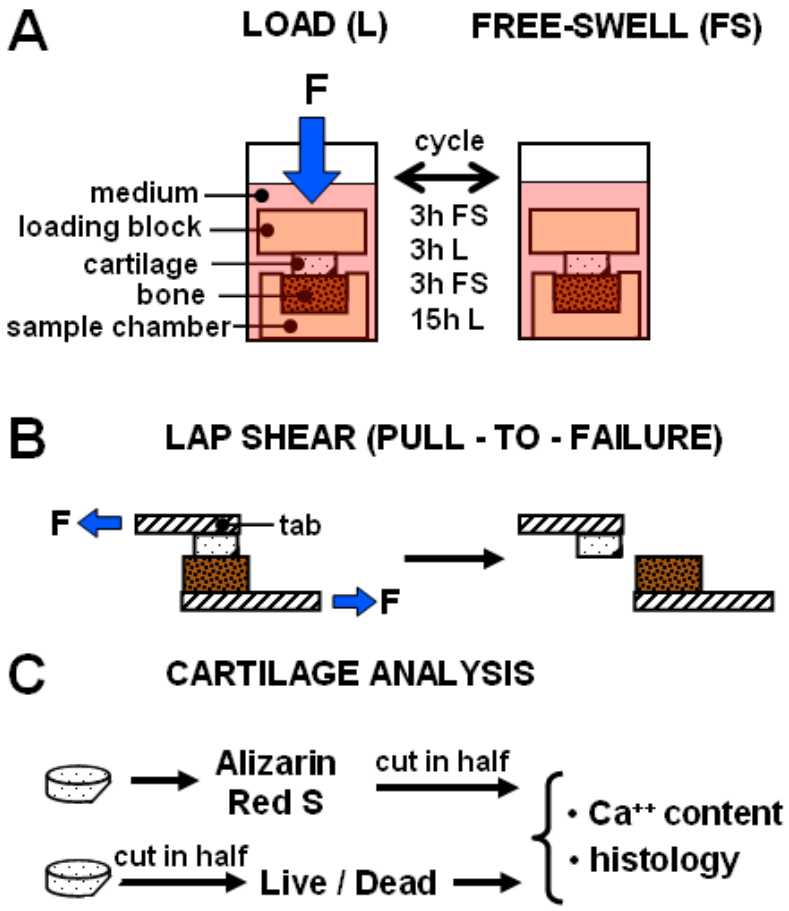

Figure 5.1: Schematic of experimental methods and cartilage analysis. (**A**) Configuration of composite culture with cartilage atop bone in a custom-built bioreactor, with application of compressive load to form osteochondral constructs. (**B**) Configuration of lap shear pull-to-failure test to determine integrative adhesive strength between cartilage and bone layers of osteochondral constructs. (**C**) Work-flow diagram of methods used for cartilage analysis after detachment from bone during lap shear testing.

5.4 Results

Adhesive integrative strength. Load-displacement curves from lap shear tests of native and engineered OC constructs showed increased load with displacement until the maximum load, after which the load dropped suddenly (Fig. 5.2). For some constructs, the load dropped to zero, while for others, the load would drop and plateau at nonzero values before dropping suddenly again and eventually decreasing to zero. In all cases, fracture and separation occurred at the interface between the cartilage and bone. Average load-displacements curves looked similar for native calf osteochondral tissue (Fig. 5.2A) and for engineered osteochondral tissue made with calf and adult cartilage (Fig. 5.2B, C), with peak loads around 6 N.

Adhesive integrative strength between cartilage and bone layers of engineered OC constructs was dependent on fetuin calcifying media for both dead and live cartilage. Exp 1. Adhesive integrative strength of engineered OC constructs formed using non-viable cartilage was dependent on the incubation solution ($P < 0.001$) (Fig. 5.3A). OC constructs (with cartilage trypsin digested for 1 hour) incubated in fetuin calcification solution had an adhesive integrative strength of 107 kPa for constructs with calf cartilage and 274 kPa for constructs with adult cartilage, ~100 times higher than samples incubated in PBS, which had adhesive integrative strengths of 1.3 kPa for calf cartilage and 31 kPa .for adult cartilage. There was a trend for higher integration strength for longer trypsin digestion ($P = 0.12$). Adhesive integrative strengths of engineered OC constructs were close to native calf OC tissue, which had an integrative adhesive strength of 466 kPa. Exp 2. Integrative adhesive strength of

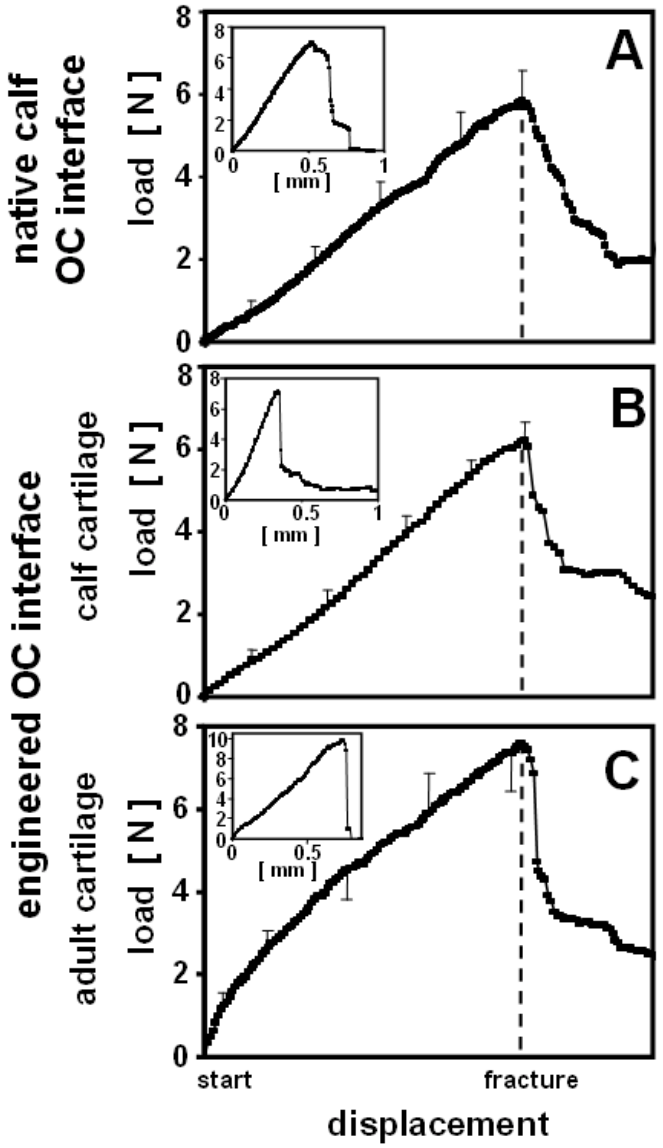

Figure 5.2: Average load-displacement curves from lap shear testing of (**A**) native calf osteochondral tissue (n=6) (**B**) engineered osteochondral constructs formed with calf cartilage on trabecular bone in media containing fetuin (n=4), and (**C**) engineered osteochondral constructs formed with adult cartilage on trabecular bone in media containing fetuin (n=4). Insets show sample load-displacement curves of an individual sample from each group.

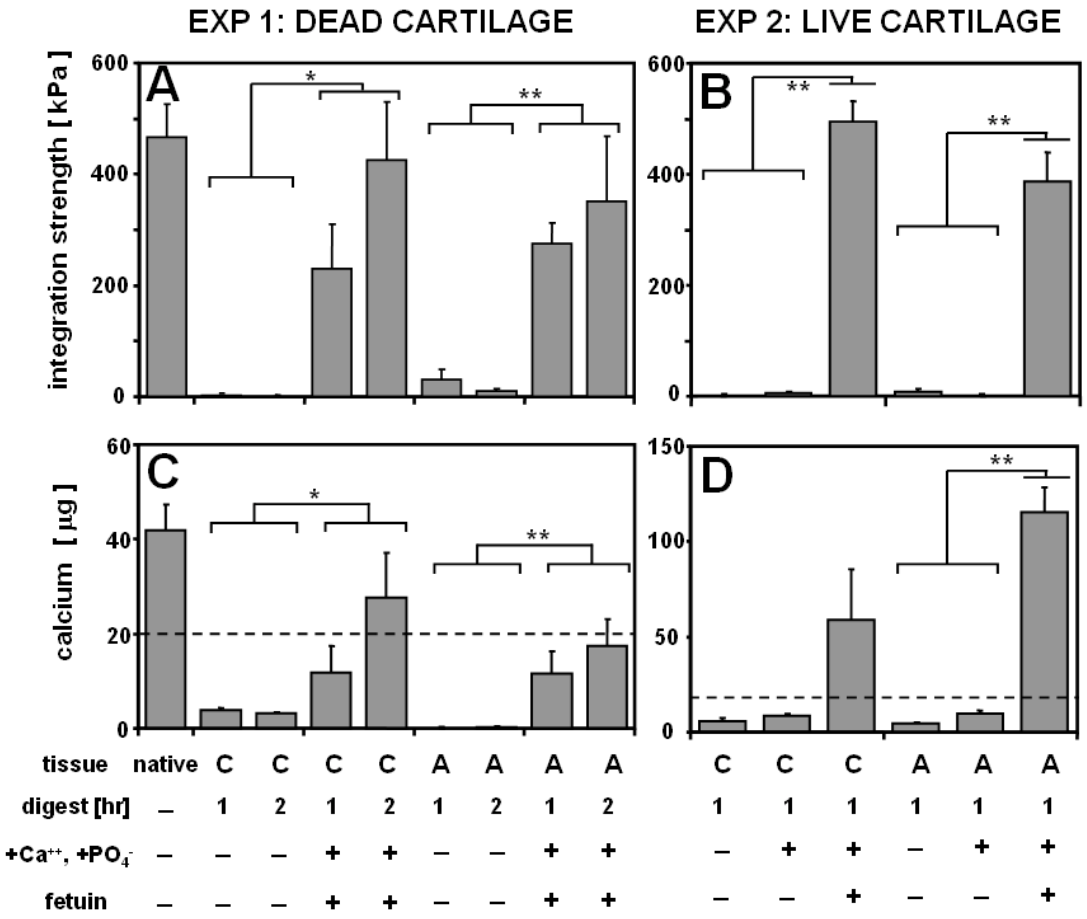

Figure 5.3: Adhesive integrative strength of osteochondral constructs (**A, B**) and calcium content of the cartilage component (**C, D**) as a function of cartilage viability, maturity (with calf denoted by "C" and adult denoted by "A"), duration of trypsin digestion, and components of incubation solution including supersaturated calcium and phosphate and fetuin. Significant differences are indicated by *, $p<0.05$ and **, $p<0.001$.

engineered OC constructs formed using live cartilage was dependent on presence of fetuin in the medium ($P < 0.001$) (Fig. 5.3B). OC constructs formed using live calf cartilage in calcification medium with fetuin had adhesive integrative strength of 495 kPa, 2 orders of magnitude higher than constructs formed in medium without fetuin ($P < 0.001$). OC constructs formed using live adult cartilage in calcification medium exhibited the same trend, with constructs formed in the presence of fetuin having adhesive integrative strength of 388 kPa, ~50-fold higher than constructs formed in control medium ($P < 0.001$). There was no significant effect of cartilage maturity on integrative adhesive strength ($P = 0.14$).

Calcium content. Calcium content of the cartilage portion of the OC construct was dependent on fetuin calcifying media for both dead and live cartilage Exp 1. The calcium content of dead cartilage from engineered osteochondral constructs was dependent on incubation solution ($P<0.001$) (Fig. 5.3C). Calf cartilage from OC constructs incubated in fetuin calcifying solution had 12 μg of calcium, 4-fold higher than calf cartilage from constructs incubated in PBS. Adult cartilage followed a similar trend. Exp 2. The calcium content of live cartilage from engineered OC constructs was dependent on fetuin in the medium ($P < 0.001$) (Fig. 5.3D) OC constructs formed in medium with fetuin using live adult cartilage had 116 mg of calcium, 12-fold higher than adult cartilage from constructs in calcifying media without fetuin, and 25-fold higher than adult cartilage from constructs in control media ($P < 0.001$). Calf cartilage exhibited similar trend. Calcium content of cartilage correlated positively with adhesive integrative strength with bone for both dead cartilage ($P < 0.001$, $R^2 = 0.89$) and for live cartilage ($P < 0.001$, $R^2 = 0.67$).

Micro CT. MicroCT images of intact OC constructs revealed differences in the shape of the cartilage for calf and adult bovine, as well as calcification of cartilage incubated with fetuin (Fig. 5.4). Calf cartilage stayed on top of the trabecular bone, in contact with bone but not entering trabecular pores (Fig. 5.4A, B, E, F). Adult cartilage had decreased thickness and larger diameter compared to the starting dimensions and appeared to enter or bulge into some trabecular pores (Fig. 5.4C, D, H). Calcification was evident in cartilage incubated with fetuin, in the outer circumference of the cartilage disk and small portions of the top cartilage surface (Fig. 5.4B, D), and in cartilage at the interface with bone (Fig. 5.4F, H).

Macroscopic staining for calcification of cartilage. Alizarin Red staining of cartilage revealed patterns of calcification on the surface adjacent to bone for OC constructs incubated with fetuin (Fig. 5.5). Cartilage from native OC calf tissue stained for calcium in a continuous pattern completely covering the deep surface (Fig. 5.5A). Cartilage samples that were incubated without fetuin did not show positive stain for calcification (Fig. 5.5B, D, F, H) Exp 1. The deep surface of dead cartilage incubated with fetuin stained for calcification in a distinct web-like pattern appearing to correspond to trabecular struts of the underlying bone (Fig. 5.5C, G). Exp 2. The deep surface of live cartilage samples incubated with fetuin stained for calcification in a spotted pattern appearing to correspond to trabecular pores (Fig. 5.5E, I).

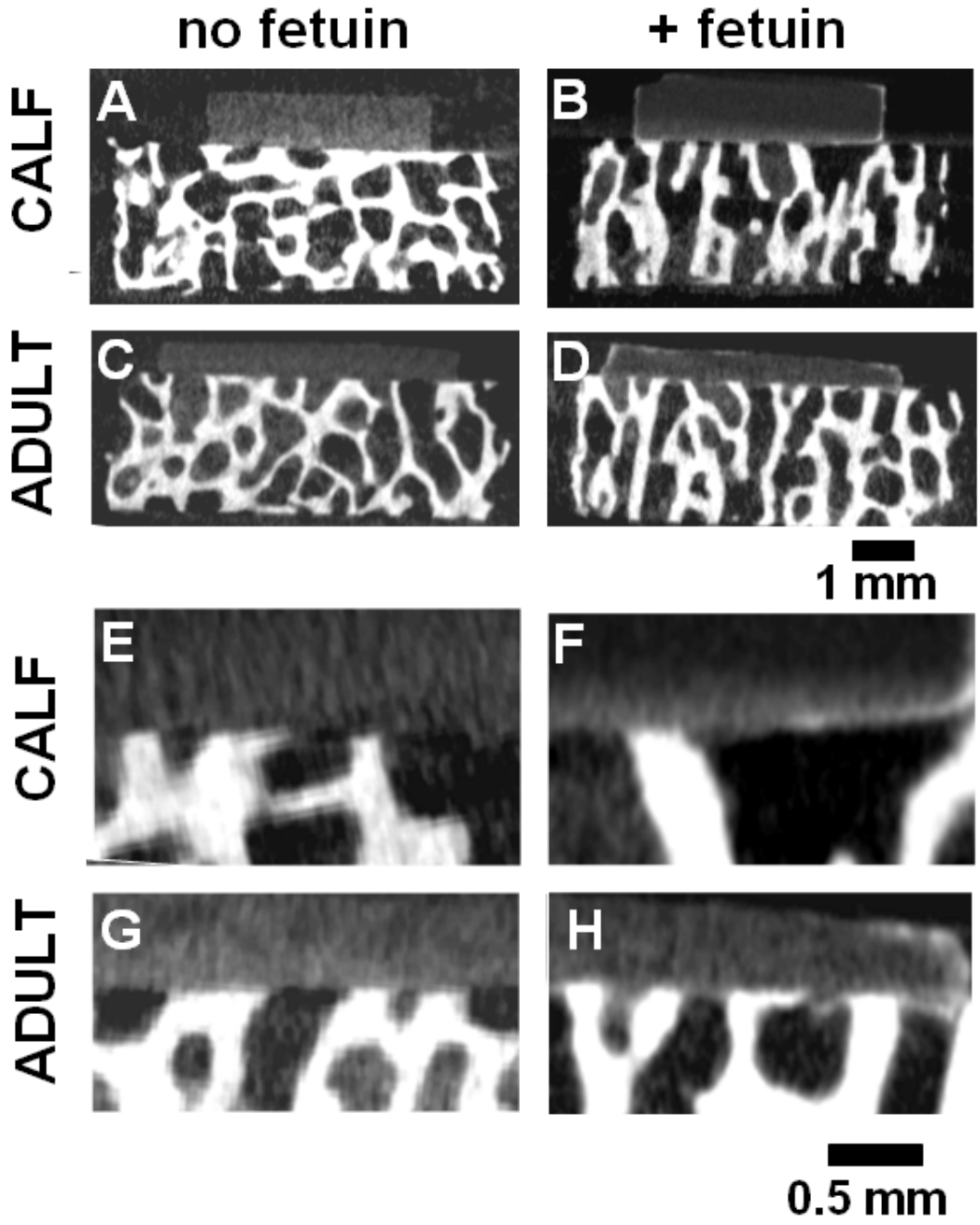

Figure 5.4: MicroCT vertical cross-sections of intact osteochondral constructs and interface for calf (**A, B, E, F**) and adult (**C, D, G, H**) cartilage incubated without fetuin (**A, C, E, G**) or with fetuin (**B, D, F, H**).

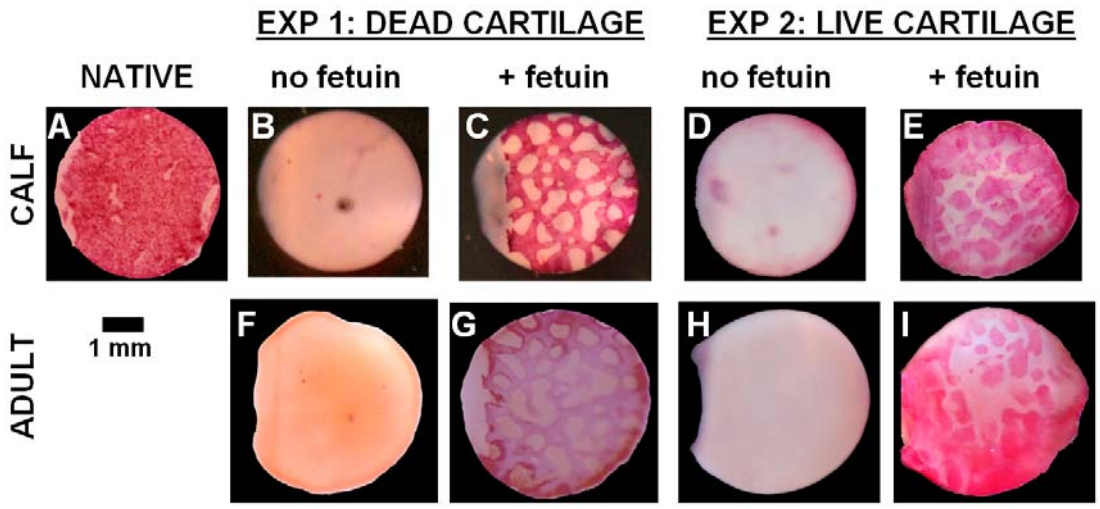

Figure 5.5: Alizarin Red S staining for calcium on fractured cartilage surface for native (**A**) and engineered (**B-I**) osteochondral constructs, as a function of cartilage viability, maturity, and presence of fetuin in the medium.

Histochemical staining for calcium. Histological staining with Alizarin Red S revealed the thickness of the calcified cartilage region. Cartilage samples incubated without fetuin did not stain positively by Alizarin Red for calcium in the cartilage tissue (Fig. 5.6A, B, E, F), while cartilage incubated with fetuin showed calcification on the deep cartilage surface (Fig. 5.6C, D, G, H). Calcification occurred in thin disconnected bands ~30 μm thick along the cartilage deep surface. Results appeared similar for dead cartilage (Fig. 5.6 A, C, E, G) and for live cartilage (Fig. 5.6 B, D, F, H).

Histochemical staining for proteoglycan removal. Toluidine Blue revealed the thickness of the proteoglycan-depleted zone due to trypin digestion (Fig. 5.7). Toluidine Blue staining indicated a consistent zone of proteoglycan depletion in the deep ~200 mm of calf cartilage (Fig. 5.7A-C). Adult cartilage had fainter staining with Toluidine Blue in the deep region but exhibited a less distinct region of proteoglycan depletion (Fig. 5.7D-F).

Live/Dead. Cell viability remained high in the cartilage bulk tissue for all groups (Fig. 5.8). There was a zone of cell death in the deep ~200 um of cartilage for both calf and adult bovine cartilage in all medium conditions. The live tissue bulk and zone of cell death were demarcated by a gently undulating border visible in the live cell images (Fig. 5.8A-C, G-I).

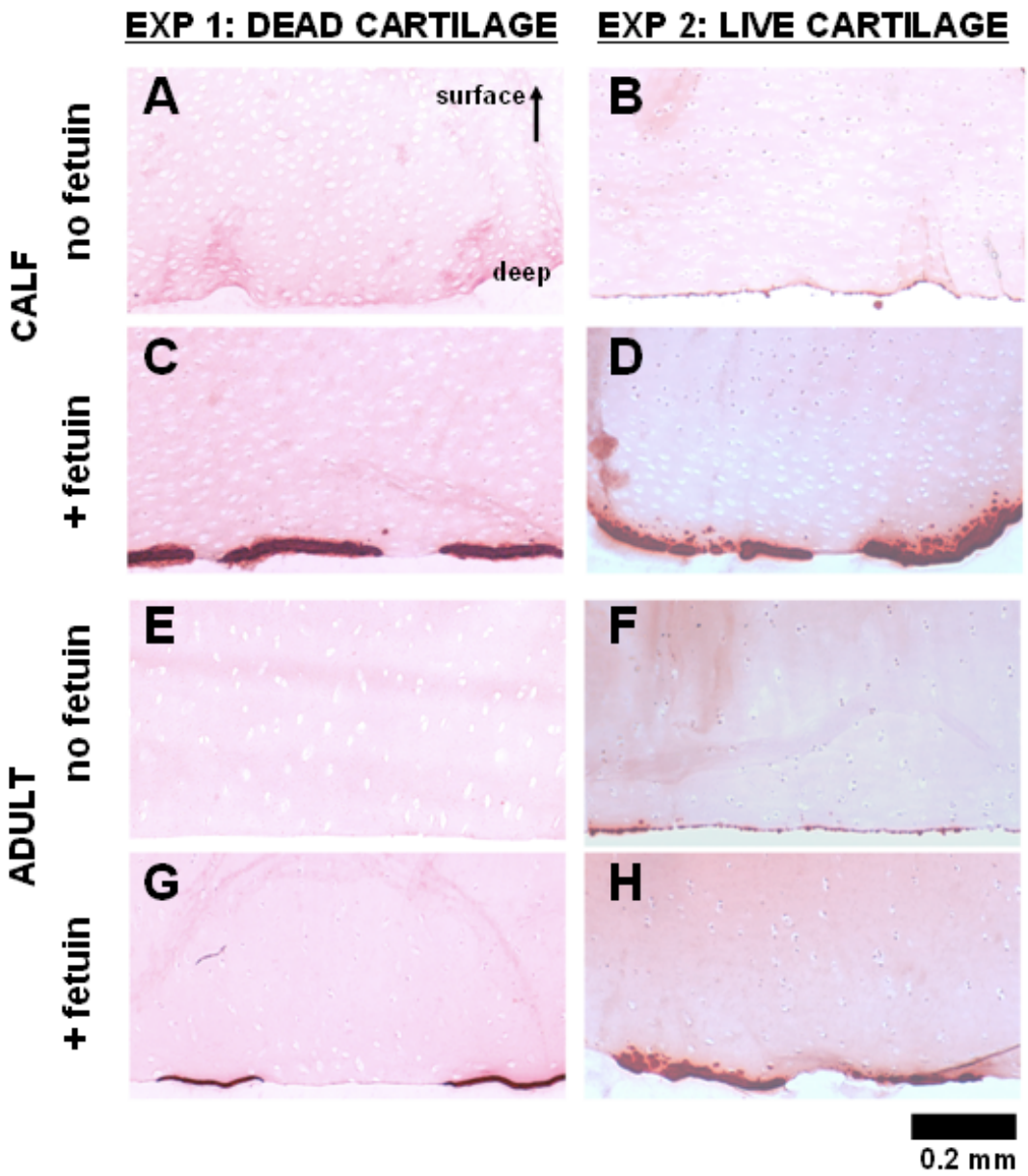

Figure 5.6: Histological staining of cartilage for calcification with Alizarin Red S of calf cartilage (**A-D**) and adult bovine cartilage (**E-H**) samples after composite culture with bone, for dead cartilage (**A, C, E, G**) or live cartilage (**B, D, F, H**) in medium without fetuin (**A, B, E, F)**, or with fetuin and supersaturated calcium and phosphate (**C, D, G, H**).

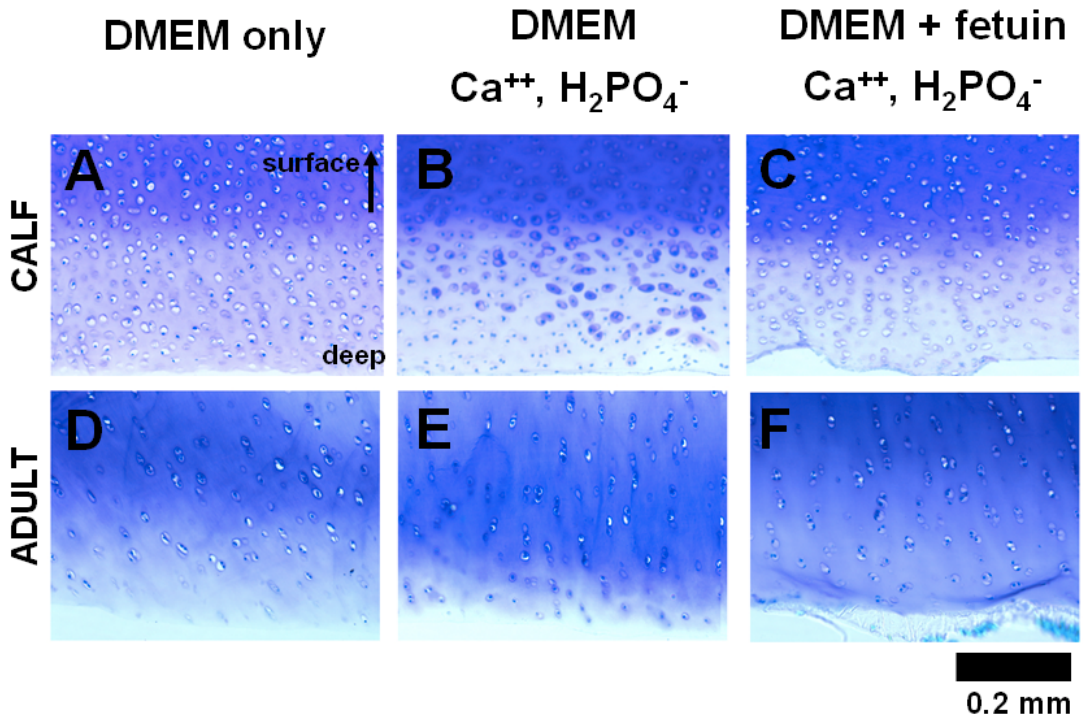

Figure 5.7: Histological staining of cartilage with Toluidine Blue of calf cartilage (**A-C**) and adult bovine cartilage (**D-F**) samples after composite culture with bone, in medium of DMEM (**A, D)**, DMEM with supersaturated calcium and phosphate concentrations (**B, E**), or DMEM with supersaturated calcium and phosphate and fetuin (**C, F**).

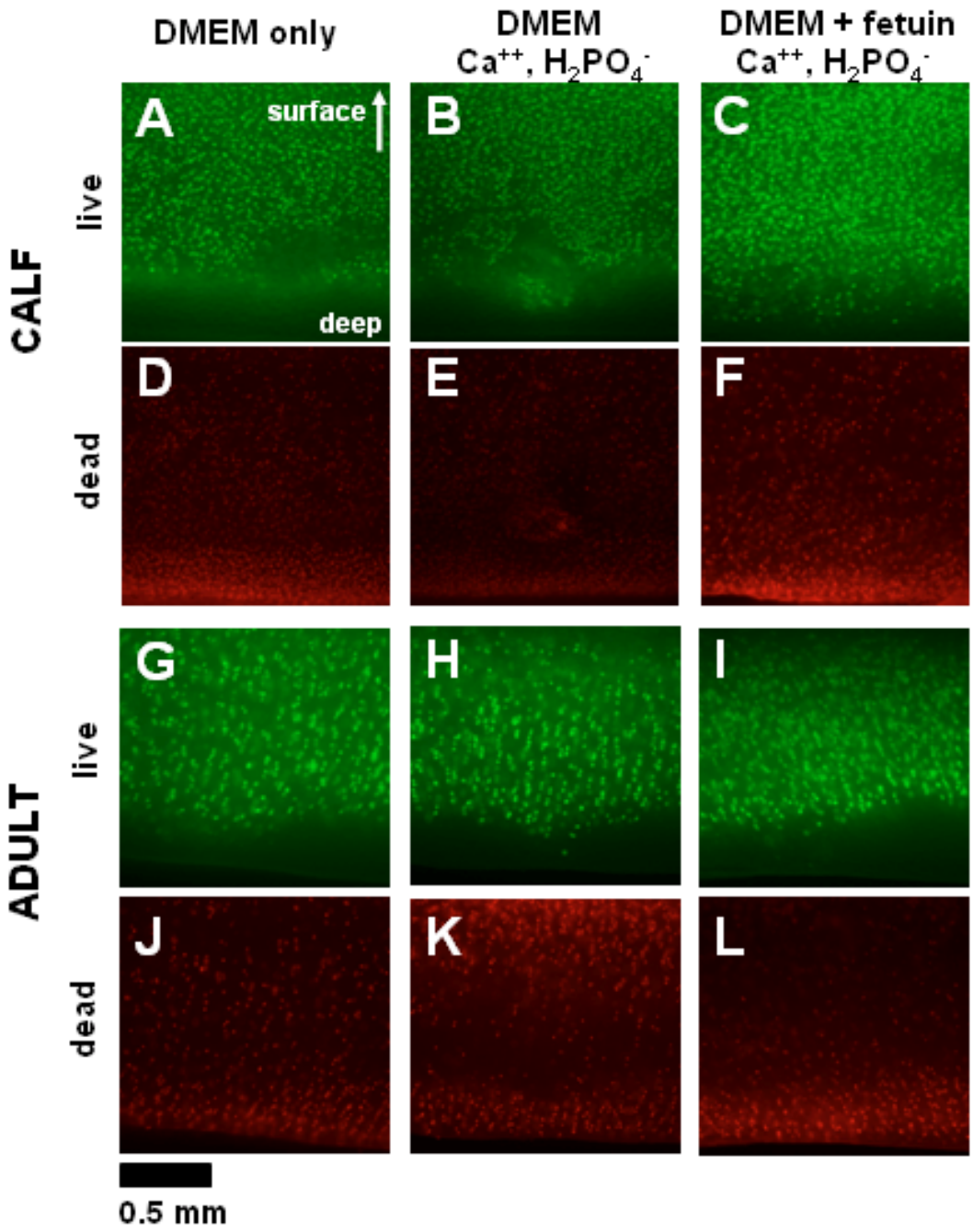

Figure 5.8: Live/Dead of cartilage after composite culture for calf (**A-C, G-I**) and adult bovine cartilage (**D-F, J-L**) which were cultured in medium of DMEM (**A, D, G, J)**, DMEM with supersaturated calcium and phosphate concentrations (**B, E, H, K**), or DMEM with supersaturated calcium and phosphate and fetuin (**C, F, I, L**)

5.5 Discussion

The results presented here describe a novel strategy to integrate cartilage tissue to bone through an interfacial zone of calcified cartilage, which develops substantial adhesive integrative strength of ~400 kPa between cartilage and bone, attaining integration strength comparable to native immature osteochondral tissue *in vitro* within 5 days. Composite culture of cartilage explants atop devitalized trabecular bone, with phases of compressive loading alternated with free-swelling, resulted in the mechanical integration of cartilage to bone through calcification of cartilage at the interface, which was dependent on fetuin. Adhesive integrative strength formed between cartilage and bone reached similar values whether the cartilage was immature or mature and whether cells were dead or alive. For dead cartilage integrated to bone, calcification of cartilage occurred in a web-like pattern corresponding to regions of direct contact with bone, whereas for live cartilage integrated to bone, calcification occurred in a spotted pattern corresponding to regions in the trabecular pores. Strong mechanical integration of cartilage explants and bone through a biological interface formed by fetuin-mediated calcification has implications for strategies in osteochondral tissue engineering and fixation of cartilage grafts for defect repair.

In the present study, integration between cartilage and bone was assessed using a lap-shear pull-to-failure mechanical test, which was used to test the integrative strength in the mode of likely shear interface failure for engineered osteochondral implants. Fracture modes between integrated tissues can be tested in Mode I, which occurs as an opening or peeling motion, Mode II, which is in-plane shear like the

configuration used in the present study, or Mode III, out-of-plane shear [1]. Mechanical tests to assess integrative strength between two tissue phases can measure different properties depending on the mode of loading and the testing configuration. Due to different sample geometries and types, there is currently not a standard mechanical test for osteochondral integration. Previous studies have used a wide variety of testing configuration, including peel-off tests where one edge of cartilaginous tissue is clamped and pulled perpendicular or parallel to the interface [26], push-out tests of disk-ring constructs [28], interface shear tests where a shearing block just above the OC interface pushes the cartilaginous tissue off the bone substrate [3], and others. In many integration tests, the configuration of the test relies on the weakness of the OC interface to fail before tearing of the cartilaginous tissue occurs. Strong osteochondral interfaces like the mature native OC interface have been assessed by initiating a crack at the interface and hitting the cartilage off at a high displacement rate to estimate a fracture toughness [6]. Different sample types and testing configurations make it difficult to compare integration strengths across different strategies for osteochondral integration.

The dependence of adhesive integrative strength on the presence of fetuin in the media may reflect the importance of calcification for the integration of cartilage to bone in the current study. The region of calcification formed in the tissue was thin and did not extend upwards into the cartilage to surround cells and was not continusou across the entire deep surface. The pattern of calcification by Alizarin Red staining on dead cartilage tissue being different from the pattern found on live tissue suggests that they may follow different modes of calcification. In the dead cartilage, calcification

may have to initiate in the bone, after which small crystals may move into the cartilage in regions of direct contact with the bone. In the live cartilage, the transport of ions into the tissue may be the dominating factor. It is unknown whether longer culture duration or different cycle times between loading and free-swelling phases would modulate the thickness and extent of cartilage calcification, and thereby affect tissue shear properties or interface integration strength

The maintenance of high cell viability in the bulk of the tissue indicates that the bulk cartilage was able to tolerate the compressive loading and calcifying medium composite culture conditions used to facilitate integration between the cartilage and bone. Loss of cell viability at the deep cartilage surface was likely due to the depletion of GAG in the deep ~200 um of cartilage, leading to high tissue strains and cell death during compression. It is unknown what strains the cartilage tissue was experiencing, but based on an equilibrium modulus of 0.3 MPa for calf cartilage [12], and the application of 20 kPa of load, it would be expected that the bulk cartilage would experience 6-7% compressive strain at equilibrium, which is well within physiological levels.

The use of devitalized native trabecular bone as a substrate for the formation of an osteochondral graft has advantages and potential disadvantages for osteochondral tissue engineering. Native adult trabecular bone is a natural scaffold with appropriate osteoinductive and mechanical properties to match the defect site, as well as an interconnected porosity suitable for integration. However, some studies using chondrocyte-seeded agarose seeded atop devitalized trabecular bone have shown inhibition of cartilage matrix production due to the presence of the bone [16]

However, since integration occurred through a chemical reaction involving precipitation of calcium and phosphate ions, it is likely that the strategy presented in the present study could also be used to integrate cartilage or a cartilaginous material with a synthetic mineralized bone scaffold.

This study developed a novel method to integrate cartilage to bone through fetuin-mediated local calcification of cartilage at the osteochondral interface, forming a functional osteochondral construct with an engineered interface of calcified cartilage. These findings have implications for the development of osteochondral constructs and for fixation of chondral grafts to bone for the repair of articular defects. Fetuin-mediated calcification can be used as a biological "cement" to enable the attachment of cartilage and bone layers through a calcified cartilage interface to form an osteochondral graft capable of withstanding joint articulation soon after implantation. The engineered transition zone of calcified cartilage that is formed between cartilage and bone may mimic the function of the native zone of calcified cartilage to help resist fracture and delamination of cartilage from bone, particularly during shear loading. Such methods may be useful for integration of large, pre-shaped cartilage grafts to bone for the formation of shaped osteochondral grafts suitable for treatment of large defects, or ultimately, for resurfacing large areas of damaged joints.

5.6 Acknowledgments

We would like to thank Esther Cory for her help with micro-computed tomography and Drs. Paul A Price and Robert L Sah for their contributions to this work. This work was supported by the National Institute of Health and Howard Hughes Medical Institute through the Professors Program Grant to UCSD for Dr. Robert L Sah.

5.7 References

1. Ahsan T, Sah RL: Biomechanics of integrative cartilage repair. *Osteoarthritis Cartilage* 7:29-40, 1999.

2. Alhadlaq A, Elisseeff JH, Hong L, Williams CG, Caplan AI, Sharma B, Kopher RA, Tomkoria S, Lennon DP, Lopez A, Mao JJ: Adult stem cell driven genesis of human-shaped articular condyle. *Ann Biomed Eng* 32:911-23, 2004.

3. Allan KS, Pilliar RM, Wang J, Grynpas MD, Kandel RA: Formation of biphasic constructs containing cartilage with a calcified zone interface. *Tissue Eng* 13:167-77, 2007.

4. Anderson DD, Brown TD, Radin EL: The influence of basal cartilage calcification on dynamic juxtaarticular stress transmission. *Clin Orthop Rel Res* 286:298-307, 1993.

5. Bobic V: Current methods of treating articular cartilage defects in the knee: an update on arthroscopic osteochondral autograft transplantation. *Arthroscopy* S10:14, 1998.

6. Broom ND, Oloyede A, Flachsmann R, Hows M: Dynamic fracture characteristics of the osteochondral junction undergoing shear deformation. *Med Eng Phys* 18:396-404, 1996.

7. Bugbee WD: Fresh osteochondral allografts. *J Knee Surg* 15:191-5, 2002.

8. Chang CH, Lin FH, Lin CC, Chou CH, Liu HC: Cartilage tissue engineering on the surface of a novel gelatin-calcium-phosphate biphasic scaffold in a double-chamber bioreactor. *J Biomed Mater Res B Appl Biomater* 71B:313-21, 2004.

9. Czitrom AA, Langer F, McKee N, Gross AE: Bone and cartilage allotransplantation. A review of 14 years of research and clinical studies. *Clin Orthop Relat Res*:141-5, 1986.

10. Gao J, Dennis JE, Solchaga LA, Awadallah AS, Goldberg VM, Caplan AI: Tissue-engineered fabrication of an osteochondral composite graft using rat bone marrow-derived mesenchymal stem cells. *Tissue Eng* 7:363-71, 2001.

11. Hung CT, Lima EG, Mauck RL, Taki E, LeRoux MA, Lu HH, Stark RG, Guo XE, Ateshian GA: Anatomically shaped osteochondral constructs for articular cartilage repair. *J Biomech* 36:1853-64, 2003.

12. Hwang J, Kyubwa EM, Bae WC, Bugbee WD, Masuda K, Sah RL: *In vitro* calcification of immature bovine articular cartilage: formation of a functional zone of calcified cartilage. *Cartilage*, 2010.

13. Jiang J, Tang A, Ateshian GA, Guo XE, Hung CT, Lu HH: Bioactive Stratified Polymer Ceramic-Hydrogel Scaffold for Integrative Osteochondral Repair. *Ann Biomed Eng*, 2010.

14. Kandel RA, Grynpas M, Pilliar R, Lee J, Wang J, Waldman S, Zalzal P, Hurtig M: Repair of osteochondral defects with biphasic cartilage-calcium polyphosphate constructs in a sheep model. *Biomaterials* 27:4120-31, 2006.

15. Kon E, Delcogliano M, Filardo G, Pressato D, Busacca M, Grigolo B, Desando G, Marcacci M: A novel nano-composite multi-layered biomaterial for treatment of osteochondral lesions: Technique note and an early stability pilot clinical trial. *Injury*, 2009.

16. Lima EG, Grace Chao PH, Ateshian GA, Bal BS, Cook JL, Vunjak-Novakovic G, Hung CT: The effect of devitalized trabecular bone on the formation of osteochondral tissue-engineered constructs. *Biomaterials* 29:4292-9, 2008.

17. McGee-Russell S: Histochemical methods for calcium. *J Histochem Cytochem* 6:22-42, 1958.

18. McMahon LA, O'Brien FJ, Prendergast PJ: Biomechanics and mechanobiology in osteochondral tissues. *Regen Med* 3:743-59, 2008.

19. Meachim G, Bentley G: Horizontal splitting in patellar articular cartilage. *Arthritis Rheum* 21:669-74, 1978.

20. Muller-Gerbl M, Schulte E, Putz R: The thickness of the calcified layer of articular cartilage: a function of the load supported? *J Anat* 154:103-11, 1987.

21. Oegema T, Jr., Carpenter R, Hofmeister F, Thompson RC, Jr.: The interaction of the zone of calcified cartilage and subchondral bone in osteoarthritis. *Microsc Res Tech* 37:324-32, 1997.

22. Price PA, Toroian D, Lim JE: Mineralization by inhibitor exclusion: the calcification of collagen with fetuin. *J Biol Chem* 284:17092-101, 2009.

23. Redler I, Mow VC, Zimny ML, Mansell J: The ultrastructure and biomechanical significance of the tidemark of articular cartilage. *Clin Orthop Rel Res* 112:357-62, 1975.

24. Reindel ES, Ayroso AM, Chen AC, Chun DM, Schinagl RM, Sah RL: Integrative repair of articular cartilage *in vitro*: adhesive strength of the interface region. *J Orthop Res* 13:751-60, 1995.

25. Schaefer D, Martin I, Shastri P, Padera RF, Langer R, Freed LE, Vunjak-Novakovic G: In vitro generation of osteochondral composites. *Biomaterials* 21:2599-606, 2000.

26. Scotti C, Wirz D, Wolf F, Schaefer DJ, Burgin V, Daniels AU, Valderrabano V, Candrian C, Jakob M, Martin I, Barbero A: Engineering human cell-based, functionally integrated osteochondral grafts by biological bonding of engineered cartilage tissues to bony scaffolds. *Biomaterials* 31:2252-9, 2010.

27. Sherwood J, Riley S, Palazzolo R, Brown S, Monkhouse D, Coates M, Griffith L, Landeen L, Ratcliffe A: A three-dimensional osteochondral composite scaffold for articular cartilage repair. *Biomaterials* 23:4739-51, 2002.

28. Tognana E, Chen F, Padera RF, Leddy HA, Christensen SE, Guilak F, Vunjak-Novakovic G, Freed LE: Adjacent tissues (cartilage, bone) affect the functional integration of engineered calf cartilage in vitro. *Osteoarthritis Cartilage* 13:129-38, 2005.

29. Tuli R, Nandi S, Li WJ, Tuli S, Huang X, Manner PA, Laquerriere P, Noth U, Hall DJ, Tuan RS: Human Mesenchymal Progenitor Cell-Based Tissue Engineering of a Single-Unit Osteochondral Construct. *Tissue Eng* 10:1169-79, 2004.

30. Waldman SD, Grynpas MD, Pilliar RM, Kandel RA: Characterization of cartilagenous tissue formed on calcium polyphosphate substrates in vitro. *J Biomed Mater Res* 62:323-30, 2002.

31. Wang DA, Varghese S, Sharma B, Strehin I, Fermanian S, Gorham J, Fairbrother DH, Cascio B, Elisseeff JH: Multifunctional chondroitin sulphate for cartilage tissue-biomaterial integration. *Nat Mater* 6:385-92, 2007.

32. Wang X, Grogan SP, Rieser F, Winkelmann V, Maquet V, LaBerge M, Mainil-Varlet P: Tissue engineering of biphasic cartilage constructs using various biodegradable scaffolds: an in vitro study. *Biomaterials* 25:3681-8, 2004.

CHAPTER 6

CONCLUSIONS

6.1 Summary of Findings

This dissertation examined the native osteochondral interface and developed a novel i*n vitro* approach for calcification of cartilage apposed to bone to achieve the overall objective of this work: *To form a functional osteochondral tissue graft with a biomimetic transitional zone of calcified cartilage at the interface of cartilage and bone, and to further the understanding of the function of a specialized ZCC interface structure in native and engineered osteochondral tissues.*

The zone of calcified cartilage was examined in terms of fluid transport and structure in normal and osteoarthritic human osteochondral tissue, and the formation of engineered zones of calcified cartilage *in vitro* were investigated for calcification of immature cartilage with an organic phosphate source, and for calcification of mature cartilage with fetuin-mediated chemical calcification. Using local *in vitro* calcification of cartilage at the interface with bone, cartilage was integrated to bone within 5 days to form a functional osteochondral construct with integration strengths similar to native immature tissue. The major findings of this dissertation were:

1. With increasing stages of osteoarthritis, the native human osteochondral interface increases in hydraulic conductance (ease of fluid transport), and undergoes

corresponding structural changes in thickness and vascularity of the zone of calcified cartilage.

a. The hydraulic conductances of native osteochondral tissue and subchondral bone plate were higher (2700- and 3-fold respectively) in osteoarthritic samples with full erosion of cartilage than in normal osteochondral tissue.
b. The calcified cartilage layer was 1.5-fold thicker in osteoarthritic tissue with partial erosion of cartilage than in normal tissue, but thinner and incomplete in tissue with full erosion of cartilage to bone.
c. Vascularity at the osteochondral interface was altered with increasing stages of OA, with larger vascular canals and increasing density of vascular canals penetrating into the zone of calcified cartilage.

2. The deep zone of immature articular cartilage (AC) can undergo calcification within 3 weeks of *in vitro* explant culture in medium supplemented with β–glycerophosphate (ßGP) as an organic phosphate source, resulting in an increase in tissue stiffness related to the extent of calcification.
   a. The deep zone (bottom 20%) of AC exhibited a compressive modulus of 0.53 MPa after calcification in medium supplemented with ßGP, ~4-fold stiffer than AC incubated without ßGP.
   b. Calcification in medium with ßGP was specific to tissue zone, with the surface and middle regions of AC resisting mineralization, and was dependent on cell viability.
   c. Calcification in AC had a distinct pattern of mineral organization deposited around cells, whereas calcification in growth plate cartilage was deposited primarily between cell columns, consistent with their expected *in vivo* phenotypes.

3. Adult AC can undergo fetuin-mediated chemical calcification to form a zone of calcified cartilage ~30-100 μm thick at the edge of tissue within 3 days, with calcification dependent on fetuin and on medium concentrations of calcium and phosphate.
    a. Proteoglycan-depleted live adult AC calcified in media supplemented with fetuin and 5 mM or higher each of calcium and phosphate, with formation of a dense band of calcification at the cartilage edge.
    b. Cell viability was maintained in the bulk tissue for calcium and phosphate concentrations up to 10 mM each, although there was loss of cell viability by ~20 % at tissue edges compared to the bulk for cartilage incubated in calcifying conditions.
    c. Mass transfer analysis demonstrated that diffusion of calcium to a reacting boundary between calcified cartilage and uncalcified cartilage could be used to describe the increasing thickness of the calcified cartilage layer based on parameters of time and free calcium in solution.
4. Fetuin-mediated calcification of cartilage while apposed to bone in composite *in vitro* culture can attach cartilage to bone through an interface zone of calcified cartilage. Such a calcified interface provides substantial integrative strength of ~400 kPa, comparable to native immature osteochondral tissue.
    a. Both immature and mature articular cartilage, live or dead, were attached through fetuin-mediated calcification to devitalized trabecular bone with integration strengths of 400-500 kPa.
    b. Osteochondral constructs incubated with fetuin exhibited calcification on the cartilage surface adjacent to bone and had ~7-25-fold higher calcium content than cartilage incubated without fetuin.

c. Calcification of the cartilage surface adjacent to bone occurred in different patterns for dead and live cartilage, with dead cartilage calcifying in a web-like pattern corresponding to regions of contact with bone, whereas live cartilage calcified in a spotted pattern corresponding to regions of trabecular pores.
d. In OC constructs with live cartilage, cell viability remained high in the bulk cartilage during the culture, with some cell death in the proteoglycan-depleted zone of cartilage adjacent to bone.

6.2 Discussion

Structural changes in thickness and vascularity of the zone of calcified cartilage and the increase in the ease of fluid transport through the osteochondral interface with progression of osteoarthritis suggest that the zone of calcified cartilage, even in mature adults, is a dynamic structure that can become disrupted with imbalances between cartilage and bone [6]. The CC layer may play a critical role in OA pathogenesis by mediating interactions between cartilage and bone. Calcified cartilage becomes "activated" in OA, increasing in thickness with the formation of new zones of CC, duplications of the tidemark, and vascular invasion into the tidemark [4, 14, 15].This suggests that the ZCC structure is important in the function of normal osteochondral tissue, not only as a zone of intermediate stiffness, but also as a biologically active area of remodeling and repair [14]. This provides motivation for the formation of a zone of calcified cartilage in repair strategies involving the implantation of osteochondral grafts.

Calcification of cartilage *in vitro*, with local calcification occurring within a zone at the edge of cartilage, was investigated using two different mechanisms in this

dissertation work. For immature bovine cartilage cultured with βGP as an organic phosphate source, the likely mechanism for local calcification to occur only in the deep zone was for matrix calcification to be mediated by mineralization-competent cells which were localized to the deep zone of immature cartilage [6, 8]. The deep zone chondrocytes may secrete alkaline phosphatase to cleave the βGP into inorganic phosphate, making it available for use, and also prepare their surrounding matrix for mineralization [3 , 11]. Additionally, the lack of calcification in the superficial and middle zones under the same *in vitro* conditions may reflect an inhibitory mechanism normally in place to prevent the unwanted calcification of soft tissue [7]. For mature cartilage cultured in metastable supersaturated calcium and phosphate with fetuin for calcification by the mechanism of inhibitor exclusion, the dominant mechanism limiting cartilage calcification to tissue edges was likely the hindrance of diffusive transport of calcium and phosphate ions into the tissue. As the calcification of cartilage developed at the tissue edge, the diffusivity of the calcified zone may have decreased to a point where it acted as a transport barrier. Thus, the calcification zone was maintained as a thin, dense zone of calcification with a slowly advancing calcification front at the tissue edge.

The use of immature cartilage and mature cartilage each have advantages and potential drawbacks for use in interface calcification for tissue engineering. Immature tissue was used as an explant model for tissue-engineered cartilaginous tissues, which could have similar matrix composition and content [9], and possibly respond similarly to calcifying stimuli. However, immature tissue is not a readily available source for tissue engineering or repair strategies, and thus is not directly applicable to clinical repair strategies. Mature cartilage is often used in clinical procedures involving autografting or allografting of mature osteochondral plugs for defect repair. Thus,

calcification of mature articular cartilage may be useful and was investigated using a chemical method for rapid calcification. It is uncertain if mature articular cartilage would undergo *in vitro* calcification to the extent that immature articular cartilage did in the 10 mM βGP condition, or whether it would limit calcification to the deep zone. In the fetuin calcifying media, the diffuse areas of adult cartilage calcification with mineral coinciding with cells suggest that deep zone cells in the mature articular cartilage may still be able to nucleate mineral crystals and calcify their surrounding matrix under stimulatory conditions.

Integration of cartilage to bone was achieved in this dissertation by using rapid chemical calcification of the interface by exclusion of fetuin; however a cell-mediated calcification of the interface to integrate cartilage and bone may be feasible, especially over longer time scales of culture. It may be possible to form an interdigitating zone of calcified cartilage *in vitro* between cartilage and bone through the proliferation of cells and secretion of matrix molecules from the cartilaginous tissue into the top layer of bone substrate, followed by calcification of the newly secreted matrix. Previous work investigating integration of cartilage to bone through biologically mediated integration by the secretion of matrix into the interface region has resulted in integration strength on the order of tens of kilopascals [17], so the effect of calcification of the interface region on integration strength could be investigated.

The formation of a transitional interface structure through interface calcification may potentially be applied to the formation and repair of other soft-hard tissue interfaces, particularly orthopedic interfaces which involve a calcified connection with bone. These interfaces include the ligament-bone interface, tendon-bone interface, and meniscus-bone interface, as well as the endplate interface between the intervertebral disk and the vertebral body [12, 16, 18]. Such interfaces involve

gradations in matrix composition, interdigitation of tissue zones, and interconnecting collagen fibers to enable load transfer between disparate tissues [13, 21]. Integration of soft tissue to bone through fetuin-mediated calcification may provide strong initial fixation strength for composite grafts to withstand implantation and initial loading, while biological remodeling *in vivo* by cells in the cartilage and ingrowth of bone may be needed for long-term incorporation and success of the graft.

Collectively, this dissertation work has contributed to the field of osteochondral tissue engineering by developing a novel method to integrate cartilage to bone through local calcification of cartilage at the osteochondral interface, forming a functional osteochondral construct. The findings of this work have implications for the development of osteochondral constructs and for fixation of chondral grafts to bone for the repair of articular defects. The engineered transition zone of calcified cartilage that is formed between cartilage and bone may mimic the function of the native zone of calcified cartilage to help resist fracture and delamination of cartilage from bone, particularly during shear loading. These studies demonstrate that calcification can be used as biological "cement" for fixation of cartilage to bone, or cartilaginous tissue to a calcified osseous substrate, in a time scale of days, to form a mechanically functional osteochondral graft. Such methods may be useful for integration of large, pre-shaped cartilage grafts to bone for the formation of shaped osteochondral grafts suitable for treatment of large defects, or ultimately, for resurfacing large areas of damaged joints.

6.3 Future Work

The current work can be expanded upon in a number of ways, including a more detailed analysis of the mechanics of the calcified cartilage interface under shear loading and articulation, and the assessment of osteochondral graft performance mechanically in a defect model *in vitro* and biologically after *in vivo* implantation.

In the current work, the assessment of integration between cartilage and bone using a lap-shear pull-to-failure was useful for osteochondral samples where the interface region is relatively weak [1], but as the osteochondral integration becomes stronger, using a fracture mechanics approach to characterize the strength of the interface may be more appropriate. In previous studies of immature and mature native osteochondral tissue, an impact fracture test was used to measure fracture toughness of the osteochondral junction, which was found to increase with tissue maturity [2]. A cyclic shear fracture test has been developed to study the intrinsic fracture toughness of the osteochondral interface, taking into account the viscoelastic energy dissipation [10]. Testing immature and mature osteochondral tissue using such a test resulted in markedly lower shear fracture toughness values than those estimated in impact fracture, as well as gradual fracture propagation that would likely be similar to the type of failure that would be experienced by an osteochondral graft, shear fracture by gradual crack propagation. Testing the intrinsic shear fracture toughness of engineered osteochondral constructs formed by the fetuin-mediated calcification of their interface may provide a useful measure of how the constructs would perform in an osteochondral defect.

Another potential future direction for this work is to evaluate the integration between cartilage and bone using a shear micromechanics approach to determine how tissue calcification and an integrated interface affects intra-tissue strains while

undergoing shear articulation. A mechanical testing system has been developed in which apposing osteochondral blocks are compressed and cartilage surfaces are slid relative to each other to mimic shear articulation during joint movement, while being recorded by video microscopy. Tissue deformations are determined by tracking cell nuclei as fiducial markers [20]. Osteochondral constructs formed by integration of cartilage to bone in the present work could be placed into such a setup to determine the strain maps through the full thickness of the cartilage tissue, including the calcified cartilage zone, and to find the corresponding shear moduli for uncalcified and calcified regions. Such an analysis could provide a greater understanding of how calcification affects mechanical properties of cartilage.

Furthermore, it would be useful to determine the cartilage-bone integration strength that is needed for an osteochondral graft to sustain a certain level of compression and shear within a focal defect. With the presence of a focal defect, the cartilage geometry is different, resulting in elevated contact stress and stress gradients during compression, particularly in the tissue near the edges of the defect, which experience increased tissue deformation and local strains [5]. The implantation of an osteochondral graft into the focal defect could help to partially restore normal cartilage mechanics. It would be useful to assess whether the graft fixation at the cartilage-bone interface has an effect on the restoration of normal cartilage mechanics during articulation, using the shear video microscopy setup described above.

Besides mechanical analysis of the calcified interface, another potential future direction could be to apply the integration by calcification method to integrate cartilage to bone to form large shaped osteochondral grafts for large defect repair. Cartilage explant shape can be modulated via mechanical load *in vitro* [19]. Applying compressive load to a cartilage explant or cartilaginous tissue with a negative mold of

appropriate anatomical shape could potentially be used simultaneously or sequentially with the intermittent compression used for cartilage calcification atop bone in the current work, to shape the cartilage surface while calcifying the cartilage base to attach it to either a shaped or flat bone substrate.

Finally, the ultimate evaluation of the success of the osteochondral graft and the effect of a calcified cartilage interface on graft performance must be assessed *in vivo.* The *in vivo* performance of a large osteochondral graft with an interface zone of calcified cartilage could be assessed at early times, around 2 weeks after implantation, for graft fixation and any cartilage delamination. At later times, the remodeling of the engineered zone of calcified cartilage within an osteochondral graft and its effects on cartilage tissue quality and graft incorporation at the graft-host interfaces, could be evaluated. Including an engineered zone of calcified cartilage to provide strong fixation between cartilage and bone may be helpful for restoring normal cartilage mechanics to the site of a defect immediately after implantation, and thereby increase long-term graft remodeling and functional performance.

6.4 References

1. Ahsan T, Sah RL: Biomechanics of integrative cartilage repair. *Osteoarthritis Cartilage* 7:29-40, 1999.

2. Broom ND, Oloyede A, Flachsmann R, Hows M: Dynamic fracture characteristics of the osteochondral junction undergoing shear deformation. *Med Eng Phys* 18:396-404, 1996.

3. Chung CH, Golub EE, Forbes E, Tokuoka T, Shapiro IM: Mechanism of action of beta-glycerophosphate on bone cell mineralization. *Calcif Tissue Int* 51:305-11, 1992.

4. Dequeker J, Mokassa L, Aerssens J, Boonen S: Bone density and local growth factors in generalized osteoarthritis. *Microsc Res Tech* 37:358-71, 1997.

5. Gratz KR, Wong BL, Bae WC, Sah RL: The effects of focal articular defects on cartilage contact mechanics. *J Orthop Res* 27:584-92, 2009.

6. Hwang J, Bae WC, Shieu W, Lewis CW, Bugbee WD, Sah RL: Increased hydraulic conductance of human articular cartilage and subchondral bone plate with progression of osteoarthritis. *Arthritis Rheum* 58:3831-42, 2008.

7. Jiang J, Leong NL, Mung JC, Hidaka C, Lu HH: Interaction between zonal populations of articular chondrocytes suppresses chondrocyte mineralization and this process is mediated by PTHrP. *Osteoarthritis Cartilage* 16:70-82, 2008.

8. Kandel RA, Boyle J, Gibson G, Cruz T, Speagle M: In vitro formation of mineralized cartilagenous tissue by articular chondrocytes. *In Vitro Cell Dev Biol Anim* 33:174-81, 1997.

9. Klein TJ, Chaudhry M, Bae WC, Sah RL: Depth-dependent biomechanical and biochemical properties of fetal, newborn, and tissue-engineered articular cartilage. *J Biomech* 40:182-90, 2007.

10. Kyubwa EM, Hwang J, Masuda K, Chen AC, Sah RL: Maturation-associated increase in the intrinsic fracture toughness of the osteochondral interface. *Trans Orthop Res Soc,* 35:1727, 2010.

11. Miao D, Scutt A: Histochemical localization of alkaline phosphatase activity in decalcified bone and cartilage. *J Histochem Cytochem* 50:333-40, 2002.

12. Moffat KL, Kwei AS, Spalazzi JP, Doty SB, Levine WN, Lu HH: Novel Nanofiber-Based Scaffold for Rotator Cuff Repair and Augmentation. *Tissue Eng Part A*, 2008.

13. Moffat KL, Wang IN, Rodeo SA, Lu HH: Orthopedic interface tissue engineering for the biological fixation of soft tissue grafts. *Clin Sports Med* 28:157-76, 2009.

14. Oegema T, Jr., Carpenter R, Hofmeister F, Thompson RC, Jr.: The interaction of the zone of calcified cartilage and subchondral bone in osteoarthritis. *Microsc Res Tech* 37:324-32, 1997.

15. Oettmeier R, Arokoski J, Roth AJ, Helminen HJ, Tammi M, Abendroth K: Quantitative study of articular cartilage and subchondral bone remodeling in the knee joint of dogs after strenuous running training. *J Bone Miner Res* 7 Suppl 2:S419-24, 1992.

16. Schoenfeld AJ, Landis WJ, Kay DB: Tissue-engineered meniscal constructs. *Am J Orthop (Belle Mead NJ)* 36:614-20, 2007.

17. Scotti C, Wirz D, Wolf F, Schaefer DJ, Burgin V, Daniels AU, Valderrabano V, Candrian C, Jakob M, Martin I, Barbero A: Engineering human cell-based, functionally integrated osteochondral grafts by biological bonding of engineered cartilage tissues to bony scaffolds. *Biomaterials* 31:2252-9, 2010.

18. Spalazzi JP, Dagher E, Doty SB, Guo XE, Rodeo SA, Lu HH: In vivo evaluation of a multiphased scaffold designed for orthopaedic interface tissue engineering and soft tissue-to-bone integration. *J Biomed Mater Res A* 86:1-12, 2008.

19. Williams GM, Lin JW, Sah RL: Cartilage reshaping via in vitro mechanical loading. *Tissue Eng* 13:2903-11, 2007.

20. Wong BL, Bae WC, Chun J, Gratz KR, Lotz M, Sah RL: Biomechanics of cartilage articulation: effects of lubrication and degeneration on shear deformation. *Arthritis Rheum* 58:2065-74, 2008.

21. Yang PJ, Temenoff JS: Engineering Orthopedic Tissue Interfaces. *Tissue Eng Part B Rev*, 2009.